SAINT-PETERSBURG STATE UNIVERSITY

As the manuscript

Kharullina Evgeniia Musaevna

Laser-induced synthesis of metallic nanostructured electrodes for non-enzymatic sensors

Scientific specialty 1.4.15. Solid-State Chemistry

Dissertation for the degree of candidate of chemical sciences

Translation from Russian

Supervisor:
Doctor of Chemical Sciences,
Professor
Manshina Alina Anvyarovna

Saint-Petersburg
2024

CONTENTS

INTRODUCTION

In the field of modern solid-state chemistry, the development of new methods for the synthesis of solid-phase materials is a central area of research, driving advances in numerous applied technological fields. Among the myriad of techniques for producing solid-phase materials, laser-assisted synthesis is emerging as a particularly innovative and promising approach that has yet to realize its full potential. The unique properties of lasers, including their high monochromaticity and precise directionality, enable selective interactions with reaction media. This allows the localized laser-induced photo- and thermo-processes upon absorption of radiation, which is difficult to achieve with traditional synthesis methods. Laser irradiation enables micro- and nanoscale modification of materials by precisely controlling the power, duration and area of exposure. This capability paves the way for the fabrication of materials with tailored properties. The study of how laser irradiation conditions affect the physicochemical properties of solid-phase materials not only addresses practical challenges in functional materials synthesis, but also enriches the fundamental understanding of laser-induced materials synthesis and modification processes.

The production of materials with high electrochemical activity, especially highly sensitive electrochemical sensors for the detection of important analytes, deserves a special focus within laser synthesis research. One of the major challenge in fabrication of electrochemical sensors, which affects their functionality, is achieving optimal adhesion of the electrochemical active material to its substrate. Poor adhesion can critically undermine the analytical and operational performance of advanced nanomaterials, leading to reduced reproducibility, reliability and sensitivity. Laser radiation offers a unique solution, serving both as a synthesis tool for a wide range of materials with controlled composition, structure and properties, and as a means of substrate modification. This dual capability is key to synthesizing new materials with high adhesion to substrate, achieved by controlled modification of the interface between the substrate and the synthesized materials. The synthesis medium plays a crucial role in the effect of the laser radiation on the substrate-reaction system interface. Interactions can occur across several interfaces, including substrate-air, substrate-liquid, and substrate-solid, each presenting a unique set of variables that influence the final properties and adhesion of the synthesized materials.

This study focuses on the potential of fabricating metallic nanostructured electrode materials for electrochemical sensors via the laser-induced synthesis (LIS) approach. It examines three LIS scenarios characterized by different states of the reaction system: at the substrate-air interface, enabling local substrate morphology modification for subsequent selective chemical metallization; at the substrate-liquid interface, facilitating simultaneous substrate activation and solid metallic phase formation from a

liquid precursor under focused laser irradiation; and at the substrate-solid interface, using oxide nanoparticles as precursors reduced by laser action to form conductive metallic structures.

This combination of approaches allow for a thorough investigation of how laser exposure conditions influence material adhesion properties, providing a comprehensive assessment of their efficacy for new sensor materials development. A notable aspect of this work is the use of both rigid and flexible polymeric materials as substrates for LIS, highlighting the research's practical importance for developing flexible electrochemical sensors.

Relevance of the topic

One of the most pressing research directions in modern materials science and solid-state chemistry is the synthesis of nanostructured materials with unique and controllable functional properties. This problem is actively discussed, among others, in the development of electrochemical sensors, since the demand for efficient sensors poses a number of scientific and technological challenges. These include the need for novel materials and deposition methods that ensure strong adhesion of functional layers to both flexible and rigid substrates.

The importance of investigation of the laser-induced synthesis (LIS) process is underscored by its versatility. LIS can be applied to fabricate wide spectra of materials, allowing controlled modification of their properties at the micro- and nanoscale. In addition, LIS offers unique advantages in substrate modification to improve properties such as adhesion - a feat that remains challenging with conventional material deposition techniques such as spin coating and drop casting.

Despite the advances in LIS, the literature still lacks a systematic review and deep understanding of the processes involved in the synthesis of electrode materials for electrochemical sensors. For example, there is no unified framework describing how laser processes at the interface affect the properties of the resulting nanostructured electrode materials. To unlock the full potential and ensure the successful implementation of advanced technological applications of LIS, it is necessary to provide a deep and comprehensive understanding of the physical and chemical processes occurring during the interaction of laser radiation with matter. Studying the laser-induced processes that lead to the formation of new phases and changes in their physical and chemical properties will enable the fabrication of unique functional materials for a wide range of applications.

It is also important to note that the interaction between laser radiation and matter can vary significantly, depending on the characteristics of both the radiation and the material being irradiated. This variability requires complex experimental studies to optimize the processes.

Therefore, a thorough study of the laser-induced processes at the substrate-reaction medium interface will reveal the key patterns in the formation of electrochemically active nanostructured

materials with strong adhesion. This understanding highlights the importance of this dissertation study and highlights its relevance in the field.

The aim of this work was to investigate laser-induced processes at the substrate-reaction medium interface for the synthesis of electrochemically active nanostructured materials.

In order to accomplish this, the following tasks have been addressed:

1. Laser-induced synthesis of electrochemically active materials at the different substrate-reaction medium interfaces;

2. Development of surface modification methods for the synthesized electrodes;

3. Comprehensive characterization of the synthesized nanomaterials;

4. Investigation of the sensory properties of the obtained materials in relation to glucose, hydrogen peroxide and dopamine.

Scientific novelty

In this work, laser-induced synthesis of materials for non-enzymatic electrochemical sensors at the substrate-reaction medium interface have been described for the first time from a unified perspective. Particular attention was paid to the study of the reduction of transition metal ions at the substrate-reaction medium interface leading to the formation of conductive metallic structures, as well as to the investigation of how the functional properties of the synthesized materials are affected by the laser irradiation of on the substrate where the metallic phase formation takes place. It has been shown that each case of the LIS possesses distinct features that significantly distinguish it from others, both in terms of experimental realization and fundamental mechanisms, as well as in the functional properties of the fabricated materials.

As a result of this work, the scope of LIS has been significantly broadened with the development of methods for the synthesis of mono- and polymetallic nanostructured electrodes based on transition metals, and the list of available substrates for LIS realization, including flexible polymers, has been greatly expanded. Direct exposure of the substrate to laser radiation, either in air or through a layer of low-absorbing liquid precursor, has been shown to yield materials that maintain stable contact with the surface under glucose and hydrogen peroxide electrochemical detection conditions. Optimization of the surface laser-assisted activation of the substrate in air was found to allow the achievement of high scanning speeds (~2-6 m/s), contributing to a significant increase in synthesis productivity.

Furthermore, original approaches based on colloidal, laser-induced and electrochemical synthesis have been developed for the surface modification of electrodes with nanostructures. The modification of transition metal-based electrodes with noble metal nanostructures, such as gold and platinum, has been shown to significantly improve the analytical performance of sensors, including an increase in

sensitivity and a reduction in detection limits. In addition, it has been experimentally demonstrated that by varying the analytical conditions and the method of surface modification of the synthesized electrodes, it is possible to create sensors with high electrochemical activity towards different analytes based on the same initial electrode.

Through the analysis and systematization of the data obtained from the study of laser-induced processes at different substrate-reaction medium interfaces, the critical role of the laser radiation effect on the substrate in the formation process of electrode materials with high adhesion and electrochemical activity was highlighted.

Practical significance of the work

Laser-induced synthesis have led to the development of methods for fabricating both rigid and flexible electrochemical sensors capable of addressing a wide range of practically important analytical problems. It's worth noting that flexible sensors are emerging as a particularly fast growing category due to their mechanical flexibility. This allows them to withstand various deformations without losing functionality or electrochemical stability. Investigations into the electrocatalytic properties of the synthesized electrodes have demonstrated their potential for the electrochemical detection of a wide range of biologically relevant substances, such as glucose, hydrogen peroxide and dopamine. The enhancement of the electrodes with gold nanostructures has significantly improved the analytical performance of the sensors, including an eightfold increase in the sensitivity of glucose analysis. Moreover, the addition of a CuO layer on the surface of copper electrodes has expanded the range of detectable substances, facilitating the detection of dopamine under neutral pH conditions.

The proposed method allows spatial localization of the synthesis based on additive principles, along with precise control of the electrode fabrication conditions. This results in the creation of materials with the desired functional properties. These properties include not only analytical aspects such as sensitivity and linear range, but also mechanical properties such as adhesion to the substrate and mechanical stability.

Methodology

The primary technique used to address the aforementioned challenges was laser-induced synthesis (LIS) at the interface between the substrate and the reaction medium. LIS was applied to fabricate metal nanostructured electrodes for sensor platforms. To further modify these electrodes with nanostructures of different compositions, complementary wet chemistry methods such as colloidal and electrochemical synthesis were also applied.

Special emphasis was placed on the systematic analysis of the relationship between composition, structure and functional properties of the sensor materials. To achieve this, a thorough characterization

of the materials at different stages of synthesis was performed using advanced characterization techniques. These included X-ray diffraction, scanning electron microscopy, energy-dispersive X-ray spectroscopy, X-ray XPS spectroscopy, and others. The electrochemical properties of the resulting structures were studied using techniques such as impedance spectroscopy, cyclic voltammetry, and chronoamperometry.

The structure of the dissertation

The thesis consists of 138 pages of typed text, including an introduction, a literature review, a discussion of the results, a conclusion, and a bibliography. The thesis contains 85 figures, 21 tables, and 263 references.

Conferences

The main results of the research were presented at 10 international conferences:

1. XI International Conference on Chemistry for Young Scientists Mendeleev 2019, St. Petersburg, Russia, 2019;

2. International Symposium Fundamentals of Laser Assisted Micro- and Nanotechnologies FLAMN 2019, St. Petersburg, Russia, 2019;

3. 102nd Canadian Chemistry Conference and Exhibition, Québec, Канада, 2019;

4. International Student Conference Science and Progress 2020, St. Petersburg, Russia, 2020;

5. V International Conference on Ultrafast Optical Science UltrafastLight-2021, Moscow, Russia, 2021;

6. International Youth Scientific Forum Lomonosov 2021, Moscow, Russia, 2021;

7. 20th Asia-Pacific Conference on Fundamental Problems of Opto and Microelectronics APCOM-2022, Vladivostok, Russia, 2022;

8. International Symposium Fundamentals of Laser Assisted Micro- and Nanotechnologies FLAMN 2022, St. Petersburg, Russia, 2022;

9. International Conference on Advanced Laser Technologies ALT'23, Samara, Russia, 2023;

10. XXV International scientific and practical conference of students and young scientists Chemistry and chemical technology in the XXI century, Tomsk, Russia, 2023.

Articles

The results of the dissertation have been published in 5 articles in international peer-reviewed journals:

1. **Evgeniia Khairullina,** Maxim Panov, Vladimir Andriianov, Karolis Ratautas, Ilya Tumkin, Gediminas Račiukaitis, High rate fabrication of copper and copper–gold electrodes by laser-

induced selective electroless plating for enzyme-free glucose sensing, RSC advances, 11, 32, 19521-19530, 2021, DOI: 10.1039/D1RA01565F

2. **Evgeniia Khairullina,** Karolis Ratautas, Maxim Panov, Vladimir Andriianov, Sarunas Mickus, Alina Manshina, Gediminas Račiukaitis, Ilya Tumkin, Laser-assisted surface activation for fabrication of flexible non-enzymatic Cu-based sensors, Microchimica Acta, 189, 7, 259, 2022, DOI 10.1007/s00604-022-05347-w
3. **Evgeniia Khairullina,** Ilya Tumkin, Daniil Stupin, Alexandra Smikhovskaia, Andrey Mereshchenko, Alexey Lihachev, Andrey Vasin, Mikhail Ryazantsev, Maxim Panov, Laser-assisted surface modification of Ni microstructures with Au and Pt toward cell biocompatibility and high enzyme-free glucose sensing, ACS omega, 6 ,28 ,18099-18109, 2021, DOI 10.1021/acsomega.1c01880
4. Ilya Tumkin, **Evgeniia Khairullina,** Maxim Panov, Kyohei Yoshidomi, Mizue Mizoshiri, Copper and nickel microsensors produced by selective laser reductive sintering for non-enzymatic glucose detection, Materials, 14, 10, 2493, 2021, DOI: 10.3390/ma14102493
5. **Evgeniia Khairullina**, Kseniia Mosina, Rachelle Choueiri, Andre Philippe Paradis, Ariel Alcides Petruk, German Sciaini, Elena Krivoshapkina, Anna Lee, Aftab Ahmed, Anna Klinkova; An aligned octahedral core in a nanocage: synthesis, plasmonic, and catalytic properties, Nanoscale, 11, 7, 3138-3144, 2019, DOI 10.1039/C8NR09731C

Statements for the defense

1. Fabrication of non-enzymatic electrochemical sensors on the surfaces of flexible substrates such as polyimide, polyethylene terephthalate, and polyethylene naphthalate by laser-induced surface modification followed by chemical metallization.
2. Synthesis and subsequent surface modification of electrochemically active nanostructured materials by laser irradiation of the interface between the substrate and the liquid reaction medium.
3. Laser irradiation of the substrate during the formation of electrode materials influences their adhesion. Local changes in substrate morphology at the substrate-liquid reaction medium and substrate-air interfaces caused by laser irradiation lead to the formation of metallic structures with stable adhesion to the substrate.
4. Laser-induced synthesis at the substrate-air/liquid/solid reaction medium interfaces enables the fabrication of non-enzymatic electrochemical sensors for detection glucose, hydrogen peroxide, and dopamine.

Main scientific results

1. Evgeniia Khairullina, Maxim Panov, Vladimir Andriianov, Karolis Ratautas, Ilya Tumkin, Gediminas Račiukaitis, High rate fabrication of copper and copper–gold electrodes by laser-induced selective electroless plating for enzyme-free glucose sensing, RSC advances, 11, 32, 19521-19530, 2021, DOI: 10.1039/D1RA01565F

In this study, a laser-assisted technique was developed for the synthesis of copper-based non-enzymatic electrochemical sensors on the surface of flexible polymers, including polyethylene terephthalate, polyethylene naphthalate, and polyimide. Optimization of laser modification parameters of polymer surfaces in air by picosecond laser was performed. This optimization allowed the selective metallization of the modified regions. Furthermore, composite systems based on copper and gold were fabricated. It was shown that these composites have improved electrocatalytic properties compared to copper electrodes and exhibit higher sensitivity in the enzyme-free detection of glucose, hydrogen peroxide and dopamine.

The Ph.D. candidate contributed significantly to this study by collecting and analyzing literature data related to the research topic. The candidate was also heavily involved in the development of techniques for laser-induced surface modification of polymeric materials, followed by copper plating, and the subsequent investigation of the physicochemical and electrocatalytic properties of the synthesized structures. In addition, the candidate played an active role in the preparation of the article, which included data processing and analysis, as well as manuscript writing.

2. Khairullina, Evgeniia M; Panov, Maxim S; Andriianov, Vladimir S; Ratautas, Karolis; Tumkin, Ilya I; Račiukaitis, Gediminas; High rate fabrication of copper and copper–gold electrodes by laser-induced selective electroless plating for enzyme-free glucose sensing, RSC advances, 11, 32, 19521-19530, 2021, DOI: 10.1039/D1RA01565F

In this study, the laser-induced synthesis of copper-based non-enzymatic electrochemical sensors on the surfaces of glass and glass-ceramics was proposed. The developed sensors were used for the electrochemical detection of glucose. In particular, the gold-modified copper structures synthesized on the glass-ceramic surface showed particularly high sensitivity to glucose values. In addition, the developed electrodes were characterized by high selectivity and long-term stability.

The PhD candidate contributed significantly to this study by collecting and analyzing literature data related to the research topic. In addition, the candidate was actively involved in the development of techniques for laser-induced modification of glass and glass-ceramic surfaces, followed by copper plating, and further investigation of the physicochemical and electrocatalytic properties of the synthesized materials. . In addition, the candidate played an active role in the preparation of the article, which included data processing and analysis, as well as manuscript writing.

3. Khairullina, Evgeniia M; Tumkin, Ilya I; Stupin, Daniil D; Smikhovskaia, Alexandra V; Mereshchenko, Andrey S; Lihachev, Alexey I; Vasin, Andrey V; Ryazantsev, Mikhail N; Panov, Maxim S; Laser-assisted surface modification of Ni microstructures with Au and Pt toward cell biocompatibility and high enzyme-free glucose sensing, ACS omega, 6 ,28 ,18099-18109, 2021, DOI 10.1021/acsomega.1c01880

In this work, laser-induced synthesis at the interface between the substrate and the liquid reaction medium leading to the formation of nickel-based non-enzymatic electrochemical sensors was investigated. The influence of morphology and composition of Ni structures modified with Au and Pt on cell biocompatibility and electrocatalytic activity in enzyme-free glucose determination was studied. It was found that Ni-Au electrodes provided better cell adhesion compared to Ni-Pt electrodes. Conversely, porous Ni and Ni-Pt electrodes, which have a more developed surface area than Ni-Au, exhibited superior electrocatalytic properties in glucose detection, demonstrating high sensitivity, selectivity, and stability.

The Ph.D. candidate contributed significantly to this study by collecting and analyzing literature data related to the research topic. In addition, the candidate was actively involved in the laser-induced synthesis at the substrate-liquid reaction medium interface and the subsequent investigation of the physicochemical and electrocatalytic properties of the synthesized structures. The candidate also played a major role in the preparation of the scientific publication, which included the processing and analysis of the data, as well as manuscript writing.

4. Tumkin, Ilya I; Khairullina, Evgeniia M; Panov, Maxim S; Yoshidomi, Kyohei; Mizoshiri, Mizue; Copper and nickel microsensors produced by selective laser reductive sintering for non-enzymatic glucose detection, Materials, 14, 10, 2493, 2021, DOI: 10.3390/ma14102493

In this study, non-enzymatic electrochemical sensors based on copper and nickel were prepared by a laser-induced synthesis at the interface between the substrate and the solid reaction medium. The activity of these proposed materials in the enzyme-free electrochemical detection of glucose was investigated. It was also demonstrated that the developed materials possess high selectivity, long-term stability and reproducibility of analisys results.

The Ph.D. candidate contributed significantly to this study by collecting and analyzing literature data related to the research topic. In addition, the candidate participated in the development of laser-induced synthesis methods at the interface between the substrate and the liquid reaction medium, as well as in the further investigation of the physicochemical and electrocatalytic properties of the synthesized structures. The candidate also played an active role in the preparation of the scientific publication, which included data processing and analysis, as well as manuscript writing.

5. Evgeniia Khairullina, Kseniia Mosina, Rachelle M. Choueiri, Andre Philippe Paradis, Ariel Alcides Petruk, German Sciaini, Elena Krivoshapkina, Anna Lee, Aftab Ahmed, Anna Klinkova; An

aligned octahedral core in a nanocage: synthesis, plasmonic, and catalytic properties, Nanoscale, 11, 7, 3138-3144, 2019, DOI 10.1039/C8NR09731C

In this work, a methodology for the synthesis of metallic nanoparticles characterized by a unique core-cell-like structure is described and their plasmonic and catalytic properties are investigated. The results of this study confirm the potential of bottom-up synthesis for complex plasmonic nanostructures, opening wide prospects for their application in areas such as sensing, catalysis, and beyond.

The PhD candidate contributed significantly to this study by collecting and analyzing literature data related to the research topic. In addition, the candidate was directly involved in the development of procedure for the colloidal synthesis of gold nanoparticles and the subsequent investigation of their physicochemical and electrocatalytic properties.

CHAPTER 1. LITERATURE REVIEW

1.1 Laser-induced processes at the interface substrate - reaction media

Laser radiation has revolutionized chemical synthesis including the fabrication of nanostructures, making it possible to produce nanomaterials with outstanding properties [1–5]. The main advantage of lasers in the synthesis of nanomaterials is their ability to create specific conditions within the irradiated area. Consequently, the focal region of the laser beam can be considered as a special kind of chemical reactor with precisely controlled conditions [6].

Irradiation of a chemical system can lead to the laser-induced thermal and/or photoprocesses [7]. Photoprocesses can be described as molecules absorbing photons of specific wavelengths, which can lead to electronic transitions and the formation of excited states, which can result in the rearrangement of chemical bonds. Lasers have a number of advantages over broad-spectrum lamps for studying photoprocesses due to the monochromaticity and coherence of the radiation and the ability to generate short pulses. These characteristics of laser radiation allow for targeted interaction with specific chemical bonds and molecules, in contrast to the broad-spectrum approach of lamps. Purely photoinduced processes do not result in a temperature change within the system under laser irradiation. In contrast, thermal processes cause a local temperature increase due to the thermalization of absorbed radiation. Both photochemical and thermochemical processes often occur simultaneously in chemical systems exposed to laser radiation. The intensity of the laser radiation is a critical parameter and can be used to some extent to control the processes taking place in the reaction system. At relatively low power, especially for short wavelength lasers, photochemical processes tend to dominate. However, as the laser power increases, thermal effects become more pronounced. This can lead not only to thermal activation of chemical reactions, but also to evaporation of precursors, substrate destruction, and degradation of synthesized materials when critically high energy densities are reached [8].

This work focuses on laser-induced thermal processes occurring at various substrate-reaction media interfaces. High power laser sources are primarily used to induce thermal processes and provide stable heating of the reaction media. Laser radiation provides precise control of temperature and exposure time, allowing localized heating without affecting the entire volume of the reaction medium. The mechanisms behind thermally induced reactions are highly specific to different precursor compositions and irradiation conditions. In general, the chemical reaction results from overcoming the energy activation barrier, e.g., by changing the redox potential due to a localized temperature increase or by the formation of an active intermediate [9].

Laser irradiation of the interface between a substrate and a reaction medium results in a localized temperature increase. This temperature increase causes several key processes:

- The chemical reactions,
- Substrate modification,
- Mass transfer driven by temperature and concentration gradients within the reaction medium.

All of the processes described above depend on the composition of the reaction medium and the temperatures reached. Therefore, precise adjustment of the laser irradiation parameters is essential to synthesize materials with the required functional properties. In addition, these processes are significantly influenced by the substrate-reaction medium interface. The properties of the resulting material are determined not only by the reaction medium, but also by the substrate properties and the nature of the interface. When synthesizing a new phase on the substrate, three types of interfaces can be identified: substrate-air, substrate-liquid reaction medium, and substrate-solid reaction medium. LIS at different interfaces can reveal the relationships between laser treatment conditions and the properties of the synthesized nanostructured materials, including adhesion and electrochemical performance. This study focuses on LIS processes in which the metal phase precursor defines the nature of the interface between the substrate and the reaction medium (Figure 1a). This approach contrasts with methods where the metal phase is directly derived from the substrate itself (Figure 1b) [8]. An example of a technique from the latter category is the laser-induced synthesis of metal nanoparticles within specially prepared glass or polymer substrates [10,11].

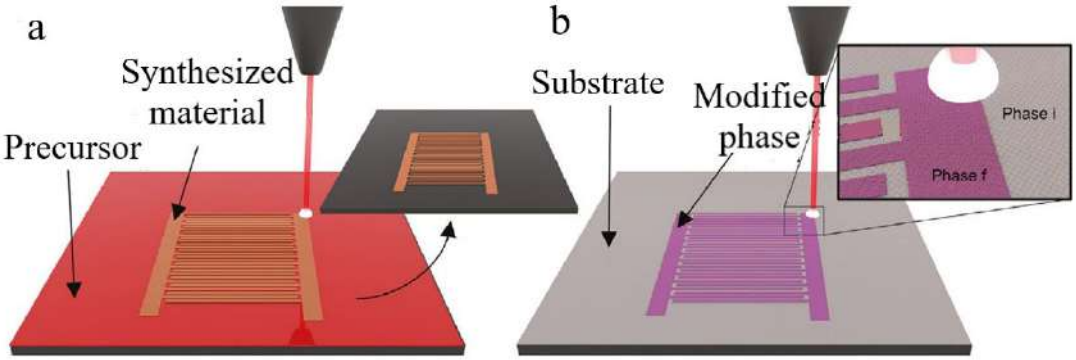

Figure 1 - Schematic comparison of LIS approaches [8]

During LIS at interfaces, a new metallic phase can be formed by reduction reactions involving both liquid and solid phase precursors (Figure 2). It is noteworthy that in our case laser irradiation of the substrate-air interface results in modification of the substrate, where the formation of metallic structures occurs in the absence of direct laser irradiation. However, since this process takes place without laser assistance and has been extensively studied [12], the focus shifts primarily to the surface modification process. LIS can also be performed at the substrate-gas reaction medium interface using gaseous precursors such as metal carbonyls [13,14]. In this scenario, LIS is performed in a single step by laser-induced decomposition of the gaseous precursor. Despite the obvious advantages of this single-step

method, it has been extensively studied and found to be inefficient due to the need to use gas reactors, the stringent requirements for precursors-which are often highly toxic-and the critically low deposition rates that do not address practical issues. Given these challenges, the scientific community has focused its main efforts on studying LIS for the fabrication of metallic structures at the substrate-liquid/solid reaction medium or substrate-air/inert gas interfaces. These approaches have shown greater promise for the efficient synthesis of metallic structures with potential applications in various fields, including electrochemical sensing.

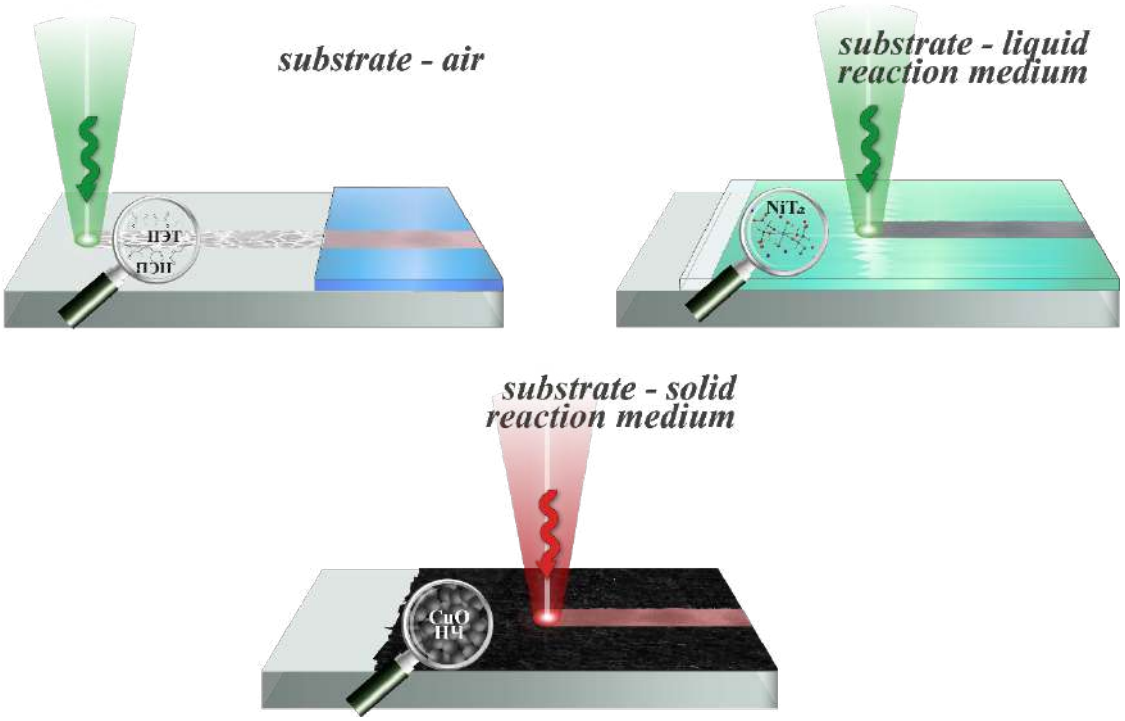

Figure 2 - LIS at the substrate reaction medium interfaces

Liquid phase precursors may include solutions of salts and complexes in suitable solvents, while solid phase precursors may consist of metal oxide nanoparticles, insoluble salts and complexes that are reduced under the influence of laser radiation [15,16]. Since LIS involves the laser-induced chemical reaction, the use of metal nanoparticles for sintering without chemical transformation is excluded from this discussion. A critical difference in the process of new metal phase formation during laser heating between solid and liquid phase precursors lies in the heterogeneous crystallization following the reduction of metal ions in the latter case [7]. In view of this, changing the thermal influence on the liquid phase precursor by modifying the laser irradiation conditions can significantly affect the morphology of the synthesized material [17]. In contrast, when solid phase precursors based on metal oxide nanoparticles are used, the morphology of the final structure is largely determined by the size of the initial particles. For example, it has been shown that the presence of large particle agglomerates (> 1

μm) in the initial mixture leads to the formation of defective structures characterized by the presence of discontinuities leading to the loss of electrical conductivity (Figure 3) [18].

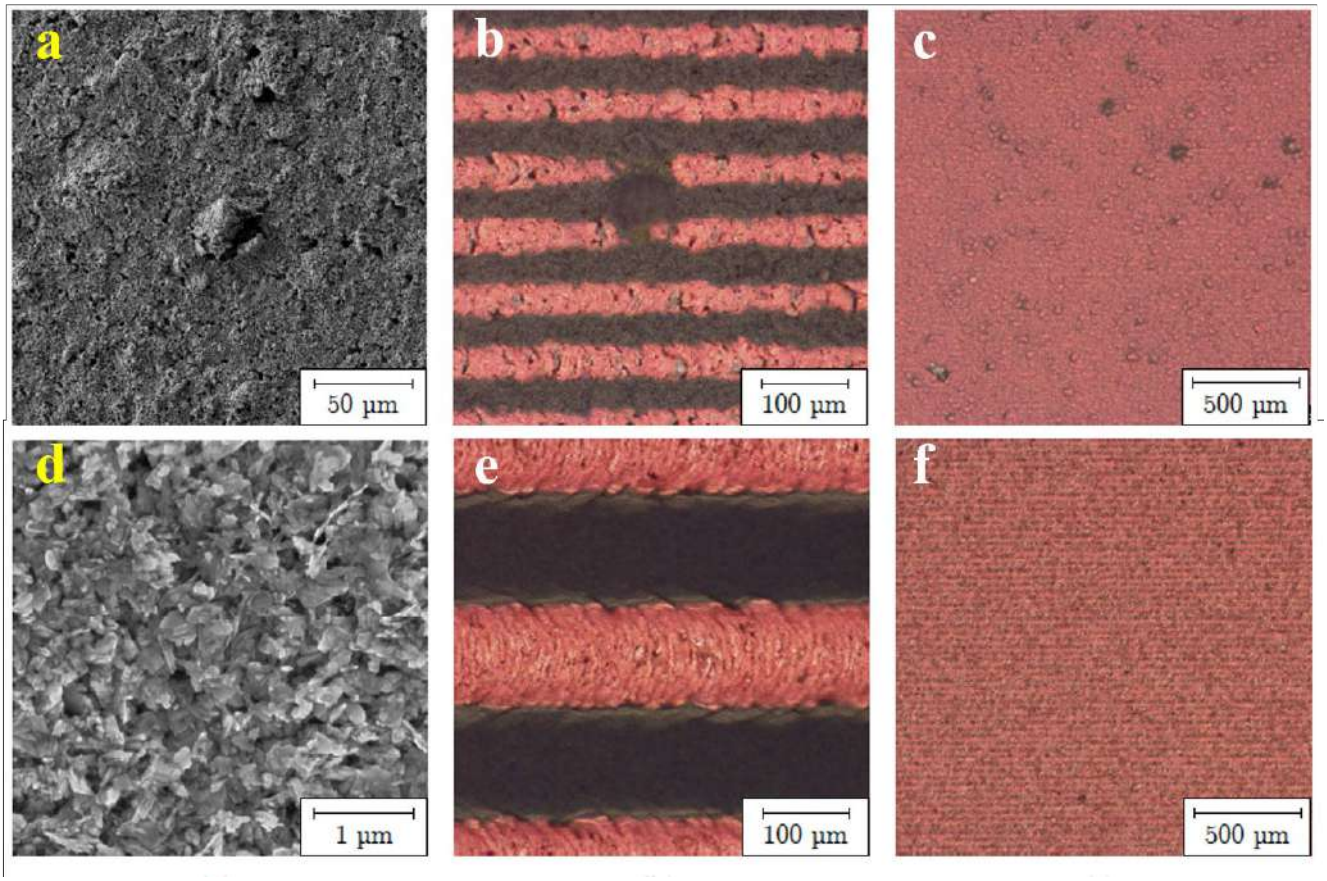

Figure 3 - SEM images of precursor film (a) with particle agglomerates, (b) without particle agglomerates, optical microscopy of materials obtained from solid phase precursor (b, c) with particle agglomerates, (e, f) without particle agglomerates [18]

In addition to laser-induced the chemical reaction for metal reduction leading to the formation of solid phase materials, laser irradiation also triggers processes that modify the surface layer of the substrate. In this study, irradiation of the substrate-air interface was used for local surface modification of polymeric and glass-ceramic materials, setting the stage for their subsequent spatially selective metallization in these regions. Possible processes include the formation of defects in the near-surface layer of the material and the induction of chemical reactions with surrounding air molecules. In addition, the temperature increase enhances the diffusion of atoms within the near-surface layer, facilitating the penetration of gas molecules deeper into the substrate material [19–21].

One of the pioneers in the field of laser surface modification for selective metallization is G.A. Shafeev, the works of his group made a significant contribution to the development of the field. However, their primary focus was on the metallization of wide-gap crystalline and amorphous dielectrics

(Al_2O_3, SiC, CeO_2, ZrO_2) [22,23]. G.A. Shafeev proposed a two-step process involving activation of the dielectric surface by laser radiation followed by a subsequent metallization step by immersion in a solution of the liquid phase precursor. It has been shown that laser treatment of such dielectrics in air under certain conditions leads to the formation of catalytic centers capable of reducing metals from solutions of their salts and complexes. The appearance of catalytic activity on the surface after laser treatment is related to the modification of the band gap of the dielectric, resulting in the creation of a non-zero density of electronic states near the potential for chemical reduction of the metal. These electronic states may arise either from the formation of point defects (F-centers for Al_2O_3, CeO_2, ZrO_2) or from the bending of the dielectric bands caused by residual mechanical stresses in the material post-laser ablation (SiC, diamond) [24].

When the interface between the substrate and the liquid reaction medium is irradiated, the primary process observed in the surface degradation of the substrate is likely to involve the formation of defects and active centers by mechanisms similar to those described above. These defects and centers later facilitate the growth of metallic structures [7,25]. Laser-induced synthesis (LIS) at the substrate-liquid reaction medium interface is a method that combines the activation steps of LIS at the substrate-air interface with metallization into a single process. Consequently, LIS in the solution of metal complexes enables the direct formation of conductive structures on the substrate under laser irradiation.

In scenarios where the substrate, solid reaction medium, and air interface are irradiated, the effect of laser irradiation on the substrate is indirect, mediated through the precursor film layer [26,27]. The new phase is formed by the reduction of oxide nanoparticles to their metallic counterparts, with the conductivity of the system facilitated by the fusion of these reduced nanoparticles due to laser-induced heating [16,28]. Similar to the direct laser irradiation of the substrate, the formation of defects on the substrate is also possible. Here, the magnitude of the thermal effect of laser irradiation at a fixed power is significantly influenced not only by the properties of the substrate material itself, but also by the absorption coefficient and thickness of the precursor film [28,29]. The precursor film can significantly mitigate the thermal effect of the laser at the substrate-solid reaction medium interface. This attenuation makes it more difficult to modify the interface to improve contact with the synthesized material, but it also allows the use of less temperature-resistant materials as substrates, including flexible polymers [30,31]. In [32], the possibility of synthesizing conductive copper structures as a result of laser-induced reduction of a solid phase precursor on the surface of polydimethylsiloxane (PDMS) was demonstrated (Figure 4 a,b); the formation of metallic copper on a substrate with three-dimensional morphology should be highlighted separately (Figure 4 c,d).

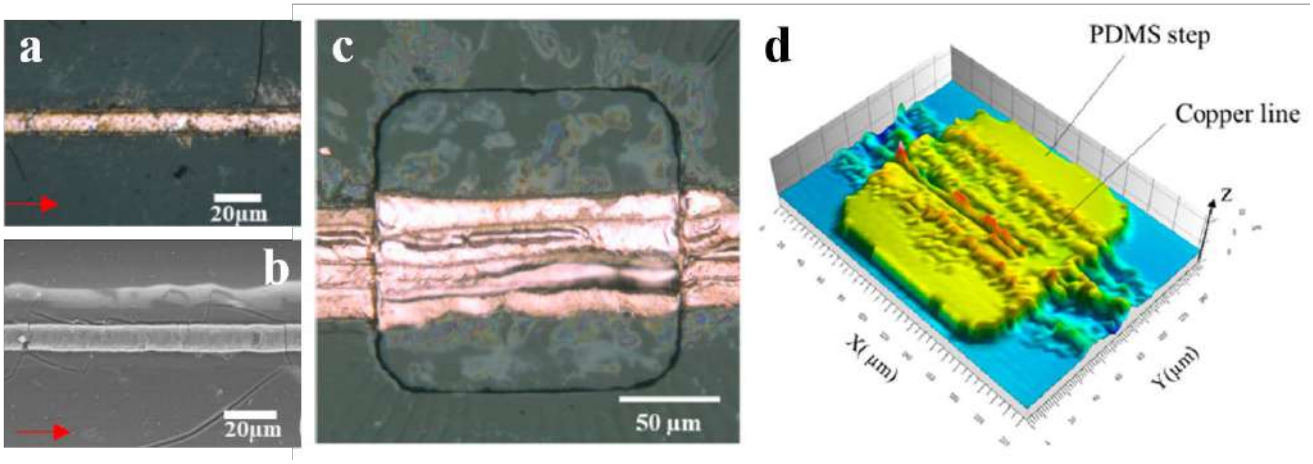

Figure 4 - Optical microscopy (a) and SEM image (b) of copper structure on PDMS surface; optical microscopy (c) and profile (d) of copper structure on substrate with three-dimensional morphology [32]

The study of the processes occurring at the interface between the substrate and the reaction medium under laser irradiation represents an important area of research. This is because it allows the synthesis of solid-phase materials with unique functional properties. These properties can be extensively modulated by varying not only the parameters of the laser radiation itself, but also the characteristics of the medium in which the induced processes take place.

Despite the high relevance and considerable potential of this field, there is a notable lack of systematic studies exploring the interaction between laser radiation and the reaction medium and substrate. Such interactions are crucial for the formation of solid-phase materials with enhanced electrocatalytic properties. A unified description of laser-induced synthesis (LIS) processes at the substrate-reaction medium interface could help to fill the existing knowledge gaps. It would also pave the way for new methods to control the properties of the synthesized materials, offering promising avenues for future research and applications.

1.2 Adhesion of electrochemical sensors to the substrate

In addition to the electrocatalytic activity of the material with respect to the target analyte, the adhesion of the electrocatalytic layer to the substrate is a property that determines its practical application. Regardless of the chosen methods of synthesis of electrochemical sensors and technologies of their deposition on the substrate, high adhesion between the substrate and the sensor layer is a critical requirement in the development of sensor platforms.

A number of methods exist to improve the adhesion of sensor layers to the substrate, among which the following main directions can be emphasized:

Surface cleaning: a preliminary surface preparation that includes mechanical and/or ultrasonic cleaning in organo-aqueous solutions to remove contaminants that adversely affect the adhesion properties of the structures. Surface cleaning is an integral step in most methods of applying sensing materials to a substrate. In most cases, this step is considered a routine preparatory step and the conditions of this process are rarely studied in detail, as the effect of this method on the final adhesion of the material is extremely limited [33–35].

Substrate Modification: This area includes methods such as plasma treatment, etching, laser structuring. These approaches can increase surface roughness and/or form surface functional groups that improve adhesion.

Changing the morphology of the substrate has a significant impact on the adhesion properties of the coating, affecting the micromechanical bond and the contact area between the metal layer and the surface [36,37]. A rough surface can provide high adhesion due to the increased substrate-metal layer interface. Surfaces with greater roughness have more microroughness to anchor metal phase nuclei, whose growth fills the roughness to form a continuous conductive metal film. However, in some cases, an increase in roughness can lead to the formation of air pockets, resulting in a decrease in the effective contact area and the possible formation of defects in the structure of the synthesized materials. Therefore, optimization of the surface structuring process is an important part of the synthesis of materials with high adhesive properties [38].

In addition, surface cleaning is particularly important in the case of surface structuring, since a developed surface can promote the retention of contaminants, which prevents the formation of high-adhesion structures. For this reason, the aforementioned surface cleaning is a complementary method to more effective approaches.

Use of Bonding Agents (Promoters):

The use of adhesion promoters in the deposition of metal coatings on various substrates is one of the effective approaches to improve adhesion [39–43]. In general, promoters can form chemical bonds with the substrate and the deposited layer, with silane-based promoters being the most prominent example of the realization of this principle. They are particularly effective at the interface between inorganic (glass, metal) and organic (polymer) materials [44], among the promoters of this class we can mention the widely studied and effective aminopropyltrimethoxysilane [45].

It should be noted that spatially selective surface modification by adhesion promoters is a very challenging task. Despite its proven efficiency, this approach has very limited applicability in the case of spatially selective laser-induced synthesis methods. In addition, the use of promoters significantly complicates the synthesis procedure and requires the development of agents for different metal/substrate combinations. Therefore, this work focused on laser-induced processes for local changes in the

composition and morphology of the surface as the most promising way to increase the adhesion of materials while preserving the spatial localization of the processes.

Adhesion refers to properties that are difficult to measure in absolute terms. There are examples of measuring the adhesion of metallic coatings using different variants of tests based on measuring the tensile force required to peel the coating from the substrate (Figure 5), where an mating substrate is bonded to the sample under test [36,46]. However, this approach is most commonly used to study coatings of sufficiently large area.

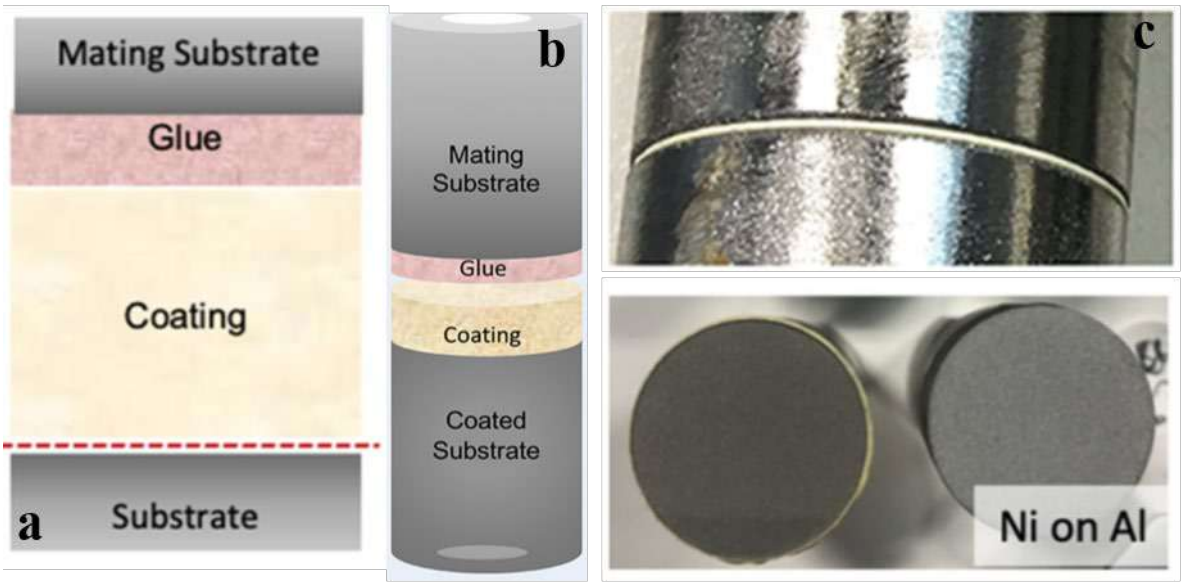

Figure 5 - (a) General principle of adhesion measurement, (b) the most common study design using a rod, (c) photographs of samples [46]

For laboratory studies of nanostructured coatings, the most commonly used, simple and effective method for assessing the adhesion of metal coatings to the substrate is the scotch test, which can be considered as a variation of the above approach, where adhesive tape acts as an auxiliary substrate and adhesive layer. This approach is widely used in laboratory practice to study the adhesion of LIS materials [47–49]. Most authors use ASTM D3359 Standard Test Methods for Rating Adhesion by Tape Test as a methodological basis, but in some cases this approach is adapted to take into account the special features of the samples, including the size of the synthesized structures. The essence of the method consists in sticking the tape on the sample to be examined and then tearing it off. Based on the analysis of the sample surface after the tape is removed and of the tape itself, it is possible to draw conclusions about the adhesion strength of the film to the substrate. If, according to the visual evaluation data, particles of metallic structure remain on the tape after it is torn off, this is an indicator of insufficient adhesion. If the metallic structure remains intact and there are no coating elements on the tape, the

adhesion is considered satisfactory. The scotch test is a universal approach that allows evaluating the adhesion of materials to the substrate regardless of their functional purpose.

However, the study of adhesion by indirect methods, which allow evaluating the effectiveness of materials for specific applications, provides more relevant data in the context of further promising research in the chosen direction. Since this work focuses on the synthesis of electrocatalytically active materials, indirect adhesion assessment of metallic structures was also carried out by investigating the functional properties using cyclic voltammetry (CV). The main idea of using CV for adhesion assessment is to study the stability of electrochemical behavior of electrodes during repeated potential sweep cycles. In case of high adhesion of the electrode material to the substrate, the CV shape should remain constant from cycle to cycle, otherwise, if the adhesion is insufficient, a change in the electrochemical signal indicating electrode exfoliation from the substrate can be observed. For instance, significant changes in the magnitude of the currents and/or oxidation/reduction potentials may indicate a change in the adhesion of the electrodes to the substrate. That said, changes in CV shape can occur due to a variety of causes other than just those related to insufficient adhesion, so this approach is indirect. However, the combination of different adhesion assessment methods, taking into account the functional properties of the materials, allows a fairly complete characterization of the adhesion properties of the systems under study.

1.3 Laser-induced synthesis of metal electrodes

Laser-induced synthesis refers to additive methods of material synthesis [27,50]. The main advantage of additive approaches is the possibility to obtain complex two- and three-dimensional structures with minimal precursor consumption. In contrast to subtractive approaches, where the processes of stencil-assisted etching the pre-deposited film are used to obtain electrodes of a given shape, additive approaches allow direct localized synthesis of the structure of the desired geometry and composition on the substrate. Among the additive approaches, laser technologies can be singled out, whose possibilities of high performance material processing have attracted great attention of researchers for many years. A unique feature of laser systems is their potential use in many technological processes, including synthesis, alloying, polymerization simultaneously with the formation of the required geometry of the structure [8]. Thus, the controlled action of the laser on the reaction medium allows to simultaneously realize both the tasks of synthesis of unique materials and methods of their deposition on a given substrate in the form of a given pattern. Thanks to the use of laser sources, it is possible to apply materials based on the selected geometry, which is optimal for a particular application and provides excellent functional properties. The process of laser-induced synthesis can also be realized on a substrate of any shape, including those with a large radius of curvature. Gaseous, liquid, and solid

systems can serve as the reaction medium, which is directly irradiated and serves as a precursor for the formation of a new phase, ensuring the versatility of the laser-induced synthesis approach. Because of these broad capabilities, laser synthesis has found wide application in the creation of advanced materials in energy storage and delivery systems, microelectronics, sensing, etc., where high spatial accuracy of deposition and optimization of the shape of functional elements are required to effectively solve the task at hand (Figure 6) [8,51].

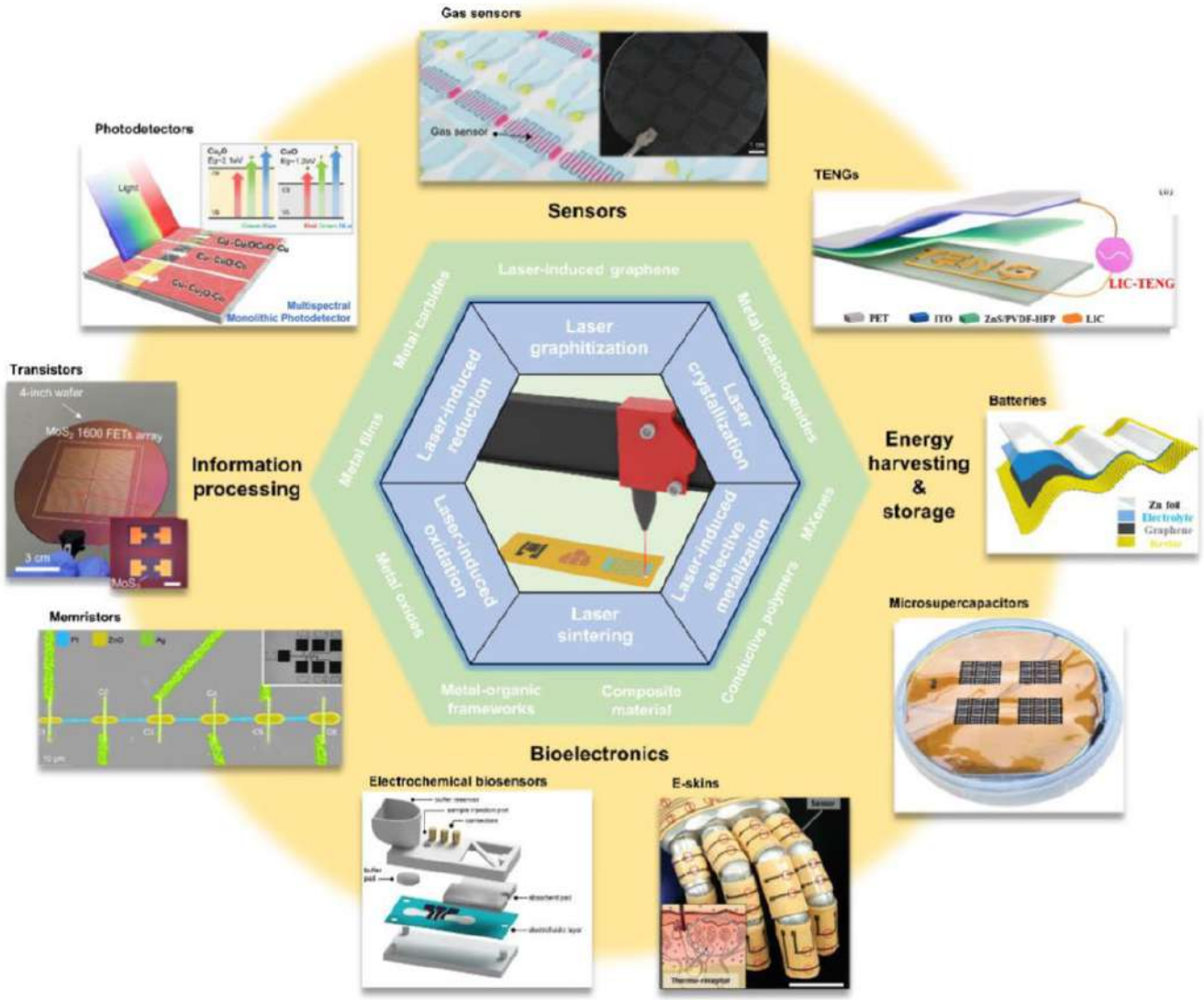

Figure 6 – Laser synthesis of materials and applications [8]

Since the invention of laser sources in the 1960s, laser radiation has found its application in the synthesis of solid phase compounds and materials, which has become the basis for the development of many innovative approaches in materials science and chemistry. Such approaches exploit the unique ability of laser radiation to influence the reaction medium, allowing not only the formation of new phases of materials, but also the modification of the physical, chemical, and structural properties of existing

compounds. From the point of view of creating enzyme-free sensors for the detection of important analytes, laser-induced synthesis at the substrate-reaction medium interface can be highlighted among many laser approaches, since LIS allows the controlled production of a wide range of conducting nanostructured materials that can become the basis for high-performance sensor platforms. LIS allows the synthesis of new solid phases with unique properties, in contrast to approaches such as laser-induced forward transfer (LIFT) [52,53], laser ablation [54–56], pulsed laser deposition (PLD) [57,58], and the formation of laser-induced periodic surface structures (LIPSS) [59,60]. The above mentioned approaches are also characterized by the spatial localization of the process and the possibility to create localized structures, but they are largely limited in the possible chemical transformations since they are based on the transfer and redistribution of the target substance in space and require the availability of initial pre-synthesized materials for transfer and modification. In contrast to these methods, LIS is not limited to the redistribution of the target substance in space, but allows chemical transformations that lead to the formation of new phases, thus expanding the possibilities for creating and modifying materials.

Laser-induced synthesis allows to obtain a wide range of solid phase materials of different nature (metals, oxides, composites, etc.) on the substrate [9,61–64]. In this work, special attention is paid to the processes of laser-radiation interaction at the substrate-reaction interface leading to the formation of metallic nanostructured materials on the surface of flexible and rigid substrates. Such materials have high electrical conductivity and can exhibit electrocatalytic activity towards a wide range of target analytes, making them promising for the synthesis of electrodes for electrochemical sensors. At the same time, transition metals such as nickel and copper, in addition to high electrocatalytic activity, have economic efficiency compared to noble metals, which makes their use as the main electrode material a promising solution [65,66]. In addition, the creation of polymetallic electrodes with a combination of noble and transition metals allows us to obtain systems that take into account economic aspects and show increased stability and activity due to synergistic effects [67,68].

Despite the great potential of LIS for the preparation of materials with high electrochemical activity, it has not been widely published to date. Many studies describe methods for the synthesis of metal structures that could be used as working electrodes in electrochemical analysis, but the main focus of the works is directed to the development of methods and, to a large extent, to the discussion of physical problems of interaction of laser radiation with the reaction system. The current state of research in the field of LIS of metallic structures that can serve as electrode materials for electrochemical sensors is analyzed below.

Laser-induced processes of synthesis of metallic structures on the surface of substrates can be divided into two groups:

1. The first type: local laser activation of the substrate followed by chemical metallization in the area exposed to laser irradiation. In this case, the processes of metal ion reduction, crystallization and structure growth occur without laser irradiation. Laser irradiation determines the shape of the structure by changing the composition and morphology of the substrate, rather than as a direct result of the metal ions reduction reaction under the influence of radiation.

2. The second type: laser-induced metal reduction from the precursor under the action of laser radiation, resulting in the localized formation of conductive metal electrodes on the substrate. Since these processes take place in a strictly limited volume in the microreactor formed by the laser beam, it opens the possibility of implementing the so-called laser writing, where the geometric shape of the synthesized structure is determined by the trajectory of the laser beam. It should be noted that within the framework of this type of laser-induced processes, it is also possible to modify the substrate during the formation of the metal phase.

The first type includes the laser direct structuring (LDS) method [69–72], this approach is a two-step methods where the substrate activation and metallization stages are separated in time.

This method can be divided into three stages:

1. Substrate preparation, where a composite material is created from a polymer matrix and special additives that are further activated by laser irradiation;

2. Laser scanning of the substrate along the trajectory of the required geometry, which activates the additives, i.e. transfers them to a catalytically active state for further chemical metallization;

3. The stage of direct metallization, which takes place selectively in the areas activated by laser radiation.

Direct laser structuring uses a specially designed polymer composite doped with an additive whose activation occurs under the influence of laser radiation [37]. The additive absorbs the laser radiation, resulting in ablation of the polymer with release of gases and carbonization of the surface. As a result, there is a local change in the morphology of the substrate and the formation of catalytically active centers for the further stage of metallization [73]. The main direction of research in this area is the selection and optimization of additives. Among promising examples are $Cu_2(OH)PO_4$, mixed oxides $CuO\text{-}Cr_2O_3$, carbon nanotubes [74]. In the research of the group of Zhou et al. different variants of the direct laser structuring process have been developed for the metallization of a wide range of polymer surfaces. For example, antimony doped tin oxide (ATO) has been shown to be an effective additive for activating the polystyrene surface under the action of a pulsed IR laser [75]. In turn, copper oxalate CuC_2O_4 and copper acetylacetonate $Cu(O_2C_5H_7)_2$ can be used to fabricate copper structures on the surface of acrylonitrile butadiene styrene (ABS) [76]. For the metallization of polydimethylsiloxane (PDMS), [$Cu_2(OH)PO_4$] and ATO are effective [77]. One of the newest and most promising additives is compounds based on

molybdenum oxides, since their activation is possible under the action of laser radiation with different wavelengths from UV to IR [78].

One of the main disadvantages of this approach is the necessity to use special composite as a substrate, which significantly limits the variety of surfaces that can be metallized. This limitation is not present in the related method of laser-induced synthesis at the substrate-air interface, which is the focus of the current work. In the approach proposed here, the need for special composite substrates is eliminated. The catalytic properties of the surface with respect to copper reduction are imparted through the use of metal salts and complexes, which can be applied to the surface of any polymer [79]. For example, the use of organometallic compounds of palladium ($Pd(AcAc)_2$), which are applied to the dielectric surface before irradiation and decompose under the action of a laser, allows selective activation of the surface of polyphenyl-quinoxaline and polyethylene terephthalate [80,81]. The formation of palladium grains as a result of laser-induced decomposition of $Pd(AcAc)_2$ allows not only to create local metal structures on the surface of “soft” dielectrics, but also increases the adhesion of the deposited films [82]. The work of K. Ratautas et al. [83–85] made it possible to replace palladium compounds with cheaper silver salts at low concentrations (up to 10^{-4} M) and to significantly expand the range of hard and soft substrates whose surface can be modified by this approach. In the case of surface activation using silver salt solutions, it has been shown that exposure to laser radiation leads to the formation of surface aldehyde groups that have the ability to recover silver ions from the solution [85].

The second type of methods includes laser-induced synthesis at the interface “substrate-solid reaction medium” and laser-induced synthesis at the interface “substrate-liquid reaction medium”. The latter approach consists of laser-induced decomposition of the metal precursor in the microreactor at the focus of the laser beam and the reduction of the ion to the metallic state [25,86–89]. This approach emerged as a modification of the traditional electroless deposition of metals, while the use of laser heating allowed to accelerate and localize the process. The pioneering works of Kordas K. and Shafeev G.A. [90,91] laid the foundation for the concept of simultaneous activation of the surface and local formation of metallic nanostructured layers. Subsequent studies were aimed at sinvestigation of the deposition processes of various noble and transition metals, which allowed to deepen the understanding of the influence of the solution composition and synthesis conditions on the functional properties of the fabricated materials [92–95]. Laser-induced synthesis at the substrate-liquid reaction medium interface shows significant potential for the development of electrochemical enzyme-free sensors, including the high electrocatalytic activity of synthesized copper electrodes towards glucose, hydrogen peroxide, and L-alanine was demonstrated. The synthesized materials exhibit developed nanostructured surface with abundant active sites, which provides high sensitivity and selectivity of analysis [96–98].

In laser-induced synthesis at the substrate-solid reaction medium interface, in contrast to solution synthesis, systems based on metal oxide nanoparticles are used as precursors [16,99,100]. At the same

time, precursors based on copper (II) oxide nanoparticles are among the most studied with respect to the application of conductive copper structures in microelectronics [15]. Laser-induced thermochemical reduction of CuO nanoparticles and their sintering resulted in the formation of conductive structures. The sintering mechanism is shown in Figure 7.

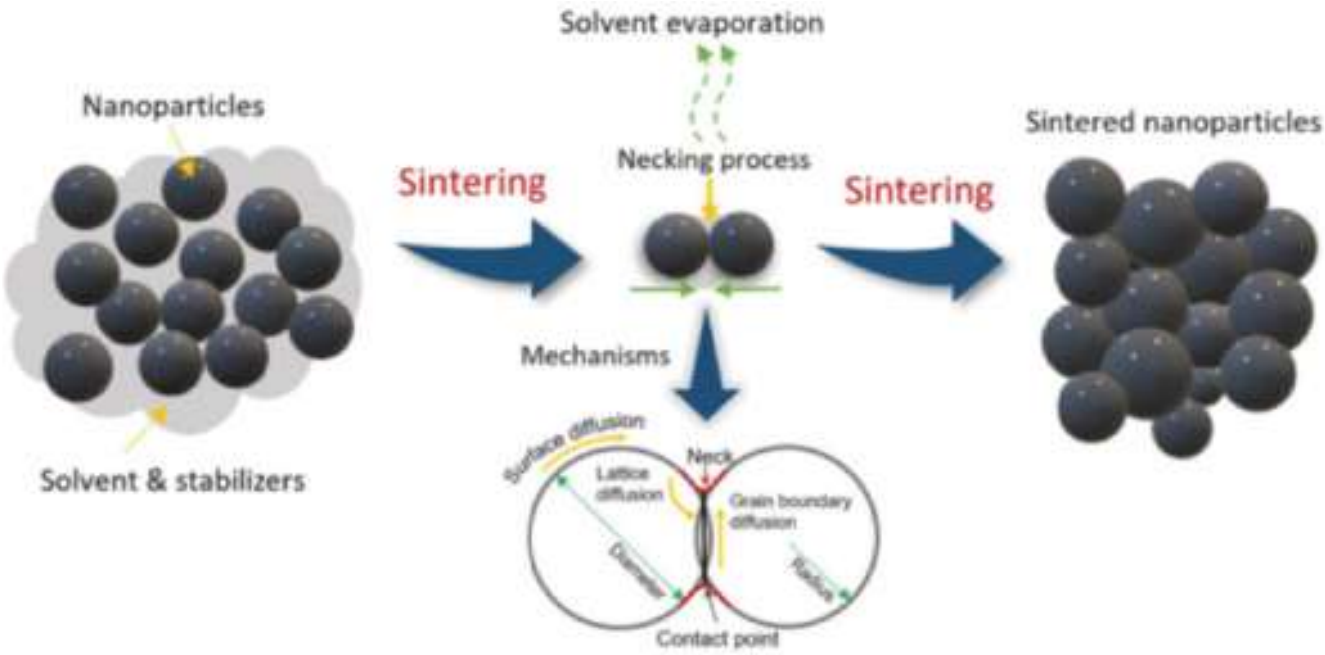

Figure 7 - Mechanism of the nanoparticle sintering [16]

The thermal effect created by the laser radiation leads to the heating of the reduced Cu NPs and to the migration of the surface atoms, resulting in the formation of a neck between the particles. As a result, a copper layer is formed that provides a continuous path for the flow of electrons. It has been shown that the conductivity of structures fubricated by laser-induced synthesis at the substrate-solid reaction medium interface can be controlled by varying the size of CuO particles included in the precursor. The addition of CuO nanoparticles (<100 nm) in the ink containing larger particles significantly reduces the resistance of the synthesized structures [18].

In addition to copper structures, laser-induced synthesis at the substrate-solid reaction medium-air interface using oxide NPs as precursors has been demonstrated for the creation of nickel, cobalt, and polymetallic structures. Based on the synthesized conductive materials, the possibility of fabricating a number of functional devices and elements has been demonstrated, including transparent electrodes [101,102], temperature sensors [103,104], planar Bragg gratings [105], and optoelectronic systems [106].

Thus, based on the above review of laser-induced metal reduction processes, we can conclude that laser-induced synthesis at the interface offers effective approaches for creating complex micro- and

nanostructures with a wide range of compositions and morphologies, in part due to the unique variability of synthesis conditions, both in terms of laser radiation (wavelength, pulse time, power, etc.) and precursor compositions. LIS is a rapidly developing field at the intersection of many disciplines, which explains the complexity of the challenges faced by researchers. Understanding the mechanisms of interaction of laser radiation with the reaction medium and optimizing processes to fabricate materials with specified properties requires taking into account a variety of factors that affect the system as a result of the use of laser radiation. Thus, the study of LIS processes at the substrate-reaction medium interface will allow the development of new synthesis methods and the establishment of composition-structure-property relationships for sensor materials. This will not only deepen fundamentals of LIS, but also significantly expand the field of application of these materials, including the creation of electrochemical sensors. The development of mono- and polymetallic electrode materials based on copper and nickel and their combination with noble metals will allow to obtain highly efficient systems for the non-enzymatic detection of various analytes due to their high electrocatalytic activity as well as the developed morphology of the materials obtained by LIS.

1.4 Non-enzymatic electrochemical sensors

Electrochemical sensors are devices designed for qualitative and quantitative analysis of liquid and gaseous media, where the analytical signal is provided by the electrochemical reaction in the near-electrode region. The main feature of sensors as a class of devices, which distinguishes them from classical analytical devices, is the possibility of field qualitative and quantitative analysis in real time and with minimal sample preparation. Due to the above advantages, electrochemical sensors are widely used in many fields of science and industry, including public health, medicine, ecology, forensics, etc. (Figure 8).

Traditionally, enzymes have been used in electrochemical sensors because of their ability to bind to the analyte with high specificity, thus ensuring selectivity of analysis (Figure 9). Enzymatic sensors include a biorecognition agent (enzyme) immobilized on the surface of the working electrode, such as glucose oxidase (GOx) or glucose dehydrogenase for glucose detection, or lactose oxidase for lactate detection [107]. However, enzymatic sensors have a number of significant drawbacks that are directly related to the use of enzyme molecules. Enzymes, like many biological molecules, are very sensitive to environmental conditions, they can lose their activity at pH below 2 and above 8, they are also sensitive to temperatures above 40^{o}C, surfactants, humidity and the presence of dissolved oxygen in the system [65]. A promising alternative to enzyme sensors are non-enzymatic ones, which lack biological functional units (Figure 9).

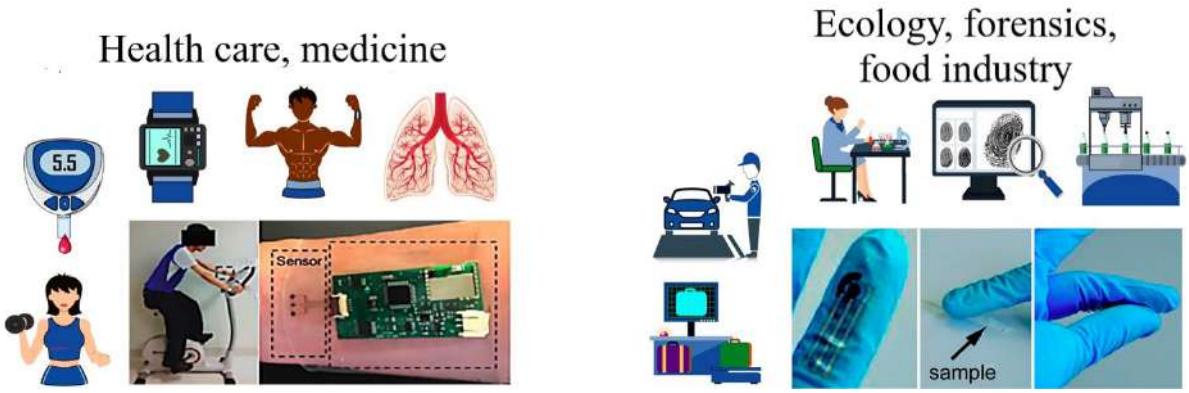

Figure 8 - Electrochemical sensor applications

Non-enzymatic sensors are characterized by structural simplicity, which allows higher reproducibility and quality control for mass production, and do not have the aforementioned disadvantages of enzyme sensors [108]. In addition, they have higher sensitivity due to the direct electron transfer from the molecule of the substance to the electrocatalytically active center of the electrode without the involvement of a mediator or enzyme. There is also the potential to create electrodes for reusability and long continuous operation, as the materials used can withstand recovery procedures and sterilization in aggressive environments after analysis.

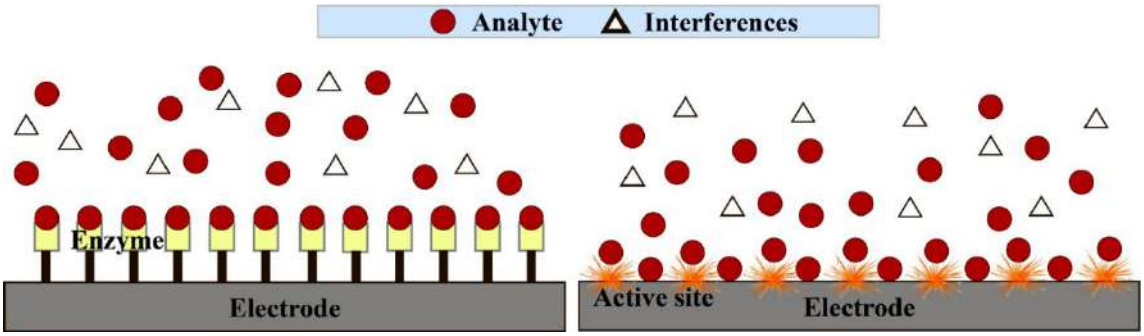

Figure 9 - Architecture of enzymatic (on the left) and non-enzymatic electrochemical sensors (on the right)

Thus, non-enzymatic sensors have unique characteristics compared to traditional enzyme systems. Non-enzymatic platforms have shown promise in the detection of a wide range of analytes [66,109–114] The electrochemical detection of glucose has received particular attention in the literature and in this work, as the control of glucose concentration in biological fluids is a key task in the diagnosis and monitoring of diabetes [109,112]. With the number of diabetic patients worldwide increasing every year, the development of reliable, accurate and affordable glucose detection methods is an important area of research [66].

In enzymeless sensors, the oxidation of the analyte occurs directly on the surface of the working electrode. To reveal the mechanism of direct electrooxidation of glucose on various metal surfaces and to choose the conditions of analysis, an important point is to determine its form of presence in solution depending on pH. In aqueous solutions, the linear molecule of γ-D-glucose as a result of rapid hydrolysis transforms into a five-membered (furanose) or six-membered ring (pyranose) due to the formation of a semi-acetal bond (Figure 10). Depending on the cis- or trans-position of the hydroxyl group at the first carbon atom, cyclic forms of glucose are divided into α and β anomers. At the same time, in equilibrium aqueous solutions at room conditions, the α-D-glucopyranose and β-D-glucopyranose forms of the five-membered cycle significantly predominate [115]. The ratio of α and β forms is largely determined by the pH of the medium [116]:

the equilibrium ratio of α and β isomers at pH = 1 is 56:44

the equilibrium ratio of α and β isomers at pH = 13 is 22:78

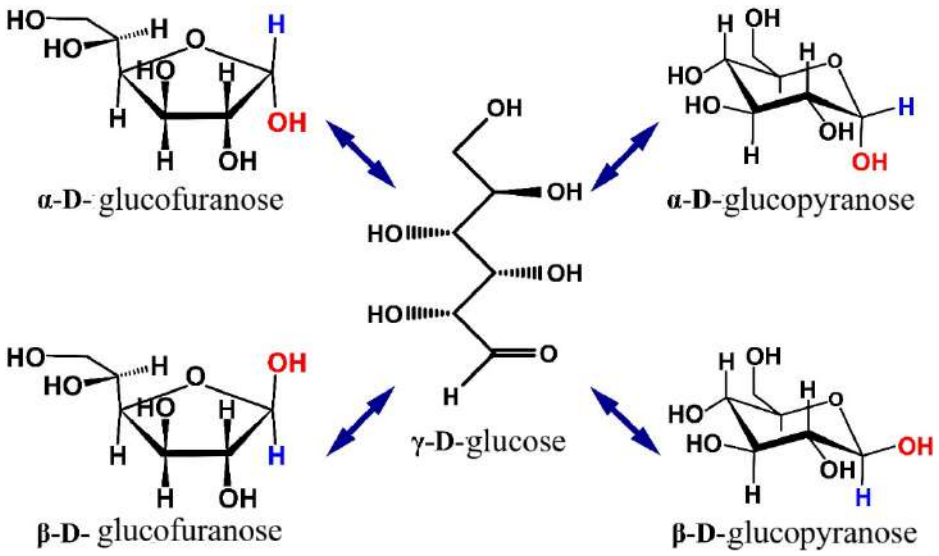

Figure 10 - Structural isomers of glucose [117]

In the glucose electrooxidation, abstraction of the hydrogen atom at C-1 is the rate-limiting step, with the β-anomer having a relatively more accessible axial H than the equatorial hydrogen of the α-form. The greater electroactivity of the β-anomer and its higher content in aqueous solutions at alkaline pH provides an opportunity to improve the analytical performance of the sensor by selecting an optimal background electrolyte in applications where solutions with a high pH value are acceptable [117].

The mechanism of direct electrooxidation of glucose at the active centers of the electrode depends on its material. For noble metals such as gold, platinum, etc., where there is no formation of oxide compounds on the electrode surface when the working potential of the sensor is applied, this process proceeds according to the mechanism shown in Figure 11. As the glucose molecule approaches the

electrode, its hydrogen atom on the first carbon interacts with the surface, resulting in dehydrogenation followed by oxidation to gluconolactone [86].

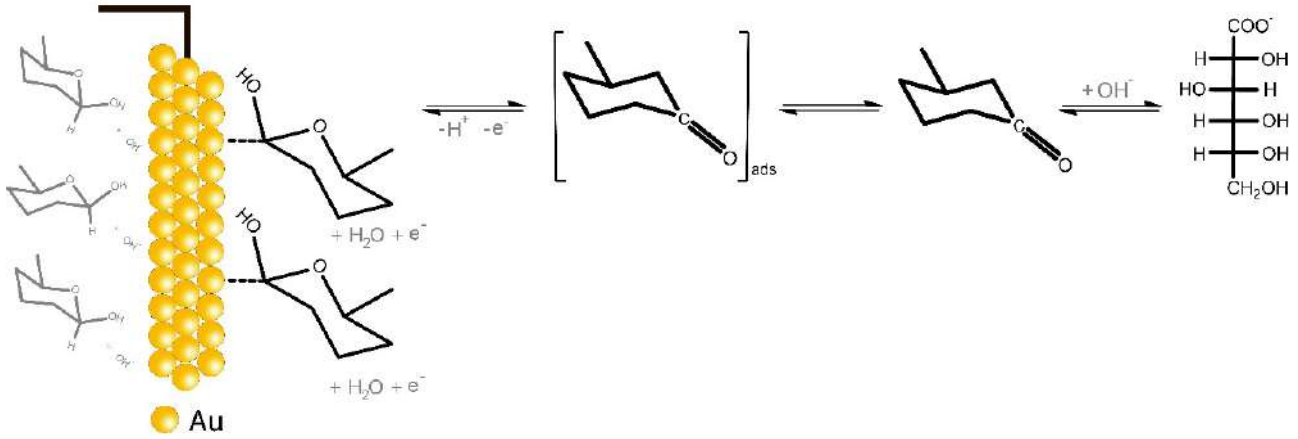

Figure 11 - Electrooxidation of glucose at the surface of a gold electrode [118]

In addition to the chemisorption-based mechanism described above, surface hydroxyl radicals (OH_{ads}) formed during electrocatalysis play an important role in the electrooxidation of glucose with noble metals, which can also oxidize glucose directly (incipient hydrous oxide/ adatom mediator (IHOAM) model) [119].

In the case of alkaline background solutions and electrode materials based on 3d transition metals such as copper, nickel, cobalt, their electrocatalytic activity is explained by the formation of Me^{3+} species on the surface (Figure 12):

$$Cu + 2OH^- \leftrightarrow Cu(OH)_2 + 2e^- \quad (1)$$

$$Cu(OH)_2 + OH^- \leftrightarrow CuOOH + H_2O + e^- \quad (2)$$

$$CuOOH + glucose \leftrightarrow Cu(OH)_2 + gluconolactone \quad (3)$$

The main oxidation product for both noble and transition metals is gluconolactone, which is rapidly hydrolyzed to gluconic acid.

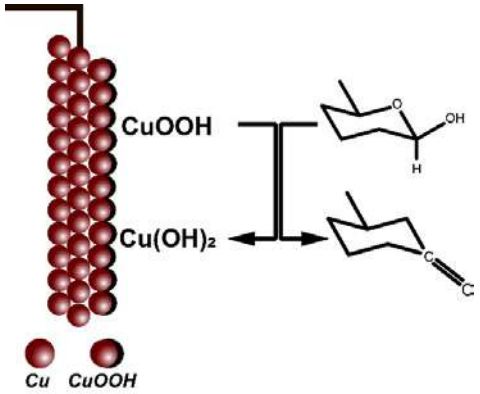

Figure 12 - Electrooxidation of glucose on the surface of a copper electrode [118]

Thus, LIS of materials based on transition (Cu, Ni) and noble (Au, Pt) metals exhibiting electrocatalytic activity towards glucose allows to obtain nanostructured electrodes for non-enzymatic sensor platforms. Favorable conditions for the electrooxidation of glucose on the surface of metals are the alkaline environment with respect to the predominance of β-D-glucopyranose at higher pH due to mutarotation, as well as the instability of electrode materials based on 3d metals and their oxides in acidic media.

1.5 Nanomaterials for non-enzymatic sensors

Nanostructured and nanoscale functional materials have been intensively studied in many fields of science in recent decades due to the their special surface chemistry, which entail the appearance of properties not characteristic of the same substance with larger particle sizes [120].

In the context of considering non-enzymatic sensors and electrocatalytic activity of metals towards oxidation or reduction of various analytes, the nanostructured electrode surface can have a significant impact in terms of the following aspects [117]:

1. Increase in the number of electrocatalytic active sites.

Crystal planes with high Miller indices and other structural features of nano-objects are more prone to the formation of hot spots that serve as active sites where the electrochemical reaction takes place.

2- Formation of confined space surrounded by electrically conductive surfaces.

Nanoscale cavities inside nanopores, under certain conditions, cause changes in the interaction of detectable molecules with the surface, creating an environment favorable for catalysis. The electric field applied to the nanoporous electrode creates a field gradient inside the nanopores on a scale comparable to the Debye length, which is the characteristic thickness of the electric double layer.

3. Increase in surface area

Nanomaterials increase the specific surface area of the electrode, resulting in an increase in the electrochemically active surface area that can participate in oxidation/reduction reactions.

In addition, the nanostructured electrode surface contributes to the selectivity of glucose analysis, which is critical for non-enzymatic sensors due to the absence of a biorecognition element. The oxidation kinetics of some common interferents in real samples, such as 4-acetamidophenol (paracetamol) and ascorbic acid, are much faster than that of glucose. Park et al. showed that the Faraday current generated by interfering molecules with fast electrokinetics is proportional to the geometric area of the electrode rather than the electrochemically active surface area, since all reactants are oxidized once they reach the outer surface of the nanoporous electrode [121–123]. On the other hand, unreacted glucose can diffuse into deeper pore regions, thereby introducing active centers into the reaction that are inaccessible to

interfering agents (Figure 13). Thus, the use of nanostructured electrodes with a high ratio of electrochemically active area to geometric area contributes to a significant increase in the selectivity of glucose detection.

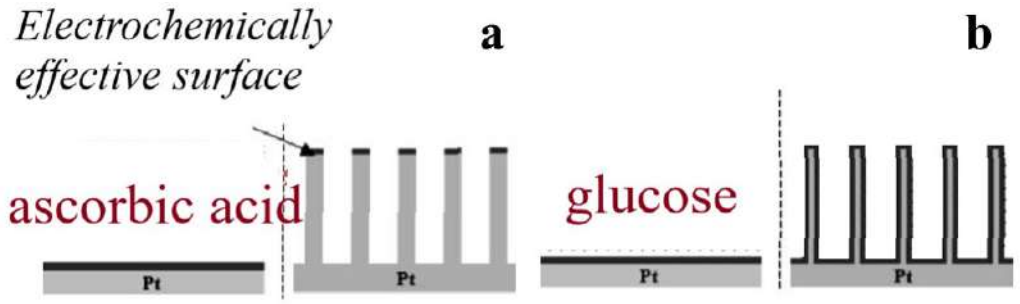

Figure 13 - Electrooxidation of (a) ascorbic acid and (b) glucose on platinum surface [122]

Thus, synthesis of electrode materials with nanostructured surface morphology can significantly increase the efficiency of analysis.

1.6 Flexible electrodes for electrochemical sensors

Particular attention is currently being paid to the development of flexible electrochemical sensors with high sensitivity and selectivity [67,124]. This is due to their wide range of potential applications, including biomedical diagnostics, environmental monitoring, and various fields of industry and engineering [125–127]. Flexible electrochemical sensors offer significant advantages over their rigid counterparts, including better integration with wearable electronics and the ability to be used on arbitrary surfaces and in dynamic environments without loss of functionality [128].

One of the key challenges in the synthesis of flexible electrochemical sensors is to ensure stable and reliable electrical contact between the sensor's active layer and the flexible substrate. This requires the development of methods for the synthesis and/or deposition of active materials that ensure not only high analytical performance of the sensors, but also their stable adhesion to the substrate. Typically, polymers are used as flexible substrates, but the range of approaches is limited due to the low thermal stability of polymeric materials.

Currently, the search for the most ergonomic form factor of sensor platforms for various applications is underway [129], and the possibility of creating flexible wearable devices in the form of temporary tattoos [130,131], mouth guards [132], contact lenses [133], wristbands [134–136], patches [137,138], and gloves [139] has been demonstrated. The materials and approaches used to fabricate these devices are also very diverse and depend on the intended application. The most commonly used polymeric materials as substrates are polyethylene naphthalate (PEN), polyethylene terephthalate (PET),

polyvinyl membranes (PVA), acrylic tape, polyimide (PI), polyester (PE) [140]. Among them, PI is widely used in the manufacture of flexible sensor devices because of its relatively high chemical and thermal resistance (up to 300^{o}C) [141], but its natural yellow color limits the application of this polymer where substrate transparency is required. PET and PEN substrates can provide transparency; their transmittance in the visible range is about 85%.

In the field of analysis and monitoring of biological analytes, including glucose, blood plasma has traditionally been used as the initial sample, but this approach is associated with high patient discomfort, motivating the development of alternative methods. Along with saliva [142–144], tears [145,146], and tissue fluids [147,148], sweat is considered as one of the alternatives because it contains many metabolites and other compounds that reflect the physiological state of the human body [149–153]. For sweat analysis, constant contact with the human skin is necessary, providing an interface for information acquisition. This approach allows the detection of a wide range of significant analytes, including ions (Na^+, Cl^-, K^+, NH_4^+), molecules (cortisol, urea, lactate, glucose, ethanol), and even some small proteins and peptides (cytokines and neuropeptides), among others. Analytes such as glucose and cortisol, which are the focus of research due to the practical need of their monitoring in relevant clinical conditions, should be highlighted [154–156]. It is important to note that there is a high degree of correlation between the content of analyzed substances in sweat and in blood, which indicates that the information obtained is sufficiently reliable and applicable to disease diagnosis, monitoring of sports performance and stress conditions [157].

The vast majority of research in the field of wearable sensor platforms is aimed at detecting biologically relevant analytes and monitoring human health, but the potential of such devices is much broader, in particular, they can find applications in environmental safety, food industry and forensic science. For example, portable sensor platforms are promising for the detection of state-regulated drugs, explosives and other toxic and dangerous compounds for transportation security and rapid crime scene analysis [158] Thus, the possibility of quantitative determination of caffeine in sweat was demonstrated [159], and the temporal dependence of caffeine content on the time of its oral ingestion was revealed. This work demonstrates the possibility of not only detecting caffeine, but also determining the time intervals of its consumption through the content of metabolites in sweat. Wearable sensor platforms can also be a powerful tool for detecting chemical threats to vulnerable individuals (people in the area of man-made and natural disasters, etc.). For example, the possibility of detecting nerve agents and explosives through such devices has been demonstrated [160].

Due to the high practical importance of electrochemical sensors, considerable attention is paid to the development of new techniques for the synthesis of sensor platforms with excellent analytical performance. The most common methods for the synthesis of electrode materials, which require a separate step to create a templates, are screen printing [161], roll-to-roll (R2R) printing [162], stamp

transfer electrodes (STE), and lithographic methods including soft lithography, photolithography, and electron beam evaporation. Additive approaches include inkjet printing [163] and laser direct writing [164,165].

Screen printing is one of the most widely used methods for creating wearable sensor devices because it is a mature industrial technology that ensures low cost. Roll-to-roll printing produces thinner films than screen printing, but often the resulting materials are not conductive enough, requiring additional layers to be applied beforehand to create a stable electrical contact. An alternative to the methods described above is electrode stamp printing, this method allows the fabrication of electrochemical sensors on non-planar surfaces of simple shape with a small radius of curvature. The performance of the electrode system obtained by this method is shown on the example of model systems containing dopamine and ascorbic acid [161]. Lithographic methods are characterized by high equipment requirements (high vacuum, clean rooms) and multistage, while allowing to achieve record resolution in the deposition of different structures, but this parameter is determinant only in the creation of wearable sensor platforms in the form of lenses, which makes this family of methods optimal for this application. The main disadvantages of the above methods are the complexity of obtaining alloys and composites of controlled composition, which requires careful selection of ink composition and synthesis conditions [166]. In addition, the surface morphology is the determining factor for the functional properties of non-enzymatic sensors. More developed surface provides a larger number of active centers per unit geometric area, in many cases it is very difficult to obtain structures with such characteristics using the above methods. Also in comparison with additive technologies, screen and roll printing methods are inferior in the ease of changing the shape of the applied electrodes, which is set in CAD systems, and in the minimum necessary consumption of materials, which is especially important when using noble metals.

In the light of the above, the development and improvement of the method of laser-induced synthesis is one of the promising directions in the field of creating efficient and reliable electrochemical sensor platforms. In laser-induced synthesis, in addition to the formation of nanostructured electrode surface, it is possible to obtain electrochemically active materials with unique functional properties due to the peculiarities of the processes occurring at high temperatures in a limited volume of the reaction system. The relevance of the development of new laser methods is also due to the need to ensure the stability and durability of sensors during their operation in dynamic and often aggressive environmental conditions. High adhesion of sensor materials to the substrate ensures the preservation of sensor functionality under mechanical deformation, which expands the possibilities of their use as portable devices. The combination of laser-induced synthesis with wet-chemical methods for additional modification of the working electrodes opens the way to a significant expansion of the application of sensor systems. This approach allows not only to increase the electrochemically active area in relation

to the geometric area, but also to create conditions for more effective interaction with analytes, which together can significantly increase the sensitivity and accuracy of sensors.

Thus, the development and improvement of laser-induced synthesis methods is not only an urgent, but also a challenging task that requires a deep understanding of the physicochemical processes that occur during the interaction of laser radiation with the material. This research direction has a significant potential in the field of electrochemical sensing technologies, providing new opportunities for the creation of highly active sensing devices.

CHAPTER 2. EXPERIMENTAL PART

This section is dedicated to the description of the main experimental techniques of laser-induced synthesis at the substrate-reaction medium interface, as well as techniques for modification of materials obtained by LIS. In addition, the instrumental methods used for the comprehensive characterization of the composition and morphology of the synthesized materials, as well as for the study of their electrochemical properties, are described. All chemical reagents used in this work were of analytical grade purity and are commercially available. Some experimental details that are relevant for the discussion of the results, including the optimization of the synthesis conditions, are presented in the relevant sections of the thesis. The thesis focuses on the synthesis of copper and nickel electrode materials and their modification with noble metals. The proposed sensor materials, including both noble and transition metals, allow to obtain electrodes that combine economic efficiency with increased activity and stability due to the synergistic effect that can be realized in a multicomponent system.

2.1 Laser-induced synthesis

Laser-induced synthesis at the substrate-air interface

The laser-induced synthesis at the substrate-air interface followed by selective metallization consists of several steps (Figure 14).

(I) Laser-induced modification of the substrate in air;

(II) Chemical activation of the modified surface using silver nitrate solution;

(III) Chemical copper plating of the activated area;

(I) The last step was the modification of the copper structures to impart the required functional properties, in particular to increase the electrocatalytic activity towards the target analytes.

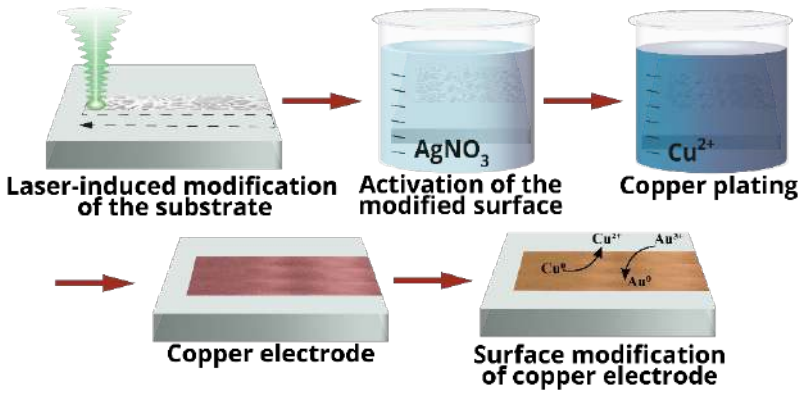

Figure 14 - Laser-induced synthesis at the substrate-air interface followed by selective metallization

As substrates were used: polyethylene terephthalate (PET), polyethylene naphthalate (PEN), polyimide (PI), glass slide: SiO_2 (72.2%) - Na_2O (14.3%) - CaO (6.4%) - MgO (4. 3%) - Al_2O_3 (1.2%) and glass-ceramic Sitall ST-50-1 (hereinafter - glass-ceramic): SiO_2 (60.5%), Al_2O_3 (13.5%), CaO (8.5%), TiO_2 (10.0%) and MgO (7.5%).

Laser-induced modification of the substrate in air was performed using focused (25 μm focal spot diameter) pulsed laser radiation with a wavelength of 532 nm, pulse duration of 10 ps, pulse repetition rate of 5 kHz - 200 kHz, and average power of up to 15 W. A pulse selector was used to vary the pulse repetition rate, and a lens with a focal length of 160 mm was used to focus the laser beam on the substrate. Ehe laser beam was moved relative to the substrate using a galvanometer scanner (Scanlab AG).

Chemical activation of the surface was performed by incubating the irradiated substrate in a silver nitrate solution with a concentration of $5*10^{-4}$ M for 8 minutes at room temperature, followed by thorough washing with copious amounts of distilled water to remove silver ions from the non-irradiated areas.

For selective electroless copper deposition on the activated surface, the substrate was placed in an aqueous plating solution for 30 minutes at 30°C, the composition of which is shown in Table 1. The reduction of copper ions by formaldehyde proceeds according to the reaction shown in Figure 15 [167]. The process is autocatalytic, after the formation of the first copper crystals due to the activation of the surface in the previous stages of synthesis, further growth of the deposit occurs, catalyzed by the formed metallic copper [12].

Table 1 - Composition of copper plating solution

Substance	**Copper sulfate**	**Formaldehyde**	**Sodium hydroxide**	**Sodium potassium tartrate**
Function	copper ion source	reducing agent	pH regulator	ligand
Concentration, M	0.12	0.3	1.2	0.35

Figure 15 - Copper reduction reaction with formaldehyde in alkaline medium

Electrode surface modification

In order to improve the analytical properties of the synthesized materials and to extend the list of analytes available for detection, copper electrodes were modified. To demonstrate the capabilities of the

proposed methods, the flexible polymer PEN and the rigid glass-ceramic substrates were chosen as representative substrates.

In the course of the work, two methods of surface modification of copper electrodes were investigated.

1. Synthesis of gold nanostructures on the electrode surface

The synthesis of gold nanoparticles on the electrode surface (Figure 16) was carried out based on a modified technique proposed by Muench et al. [168]. To localize the reduction of gold from $HAuCl_4$, synthesized metallic copper was used as a reducing agent. An aqueous solution of hydrogen tetrachloroaurate ($HAuCl_4$) 0.007 M and 4-dimethylaminopyridine 0.1 M (DMAP) was heated to a temperature of 60 °C (the optimal synthesis parameters selected experimentally are described below), then the copper structure synthesized on the substrate was immersed in this solution for 5 min. The last step of synthesis was washing the sample with copious amounts of distilled water and air drying.

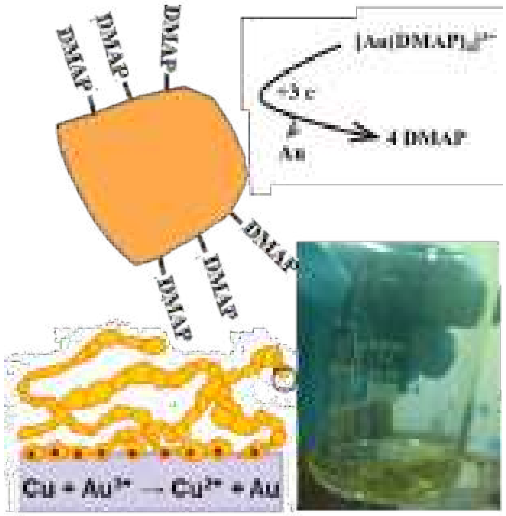

Figure 16 - Scheme of synthesis of gold nanostructures on the surface of copper electrode [168]

2. Synthesis of CuO nano-needles on copper surface

The formation of oxide-hydroxide nanostructures on the surface of the synthesized copper structures was carried out by electrochemical oxidation. The synthesis was carried out in a standard three-electrode undivided cell, where the working and auxiliary electrodes were the obtained copper structures and platinum wire, respectively, and the Ag/AgCl electrode was used as a reference electrode (Figure 17). The synthesis was carried out for 600 s at a potential of -200 mV (vs. Ag/AgCl) in a background electrolyte of 1 M NaOH; under these conditions, various oxidation processes of the copper electrode are possible, leading to the formation of products such as copper (I) oxide, copper (II) oxide, and copper (II) hydroxide [169]. The electrode was then annealed at 95 °C for 20 min to form CuO nano-needles on the electrode surface.

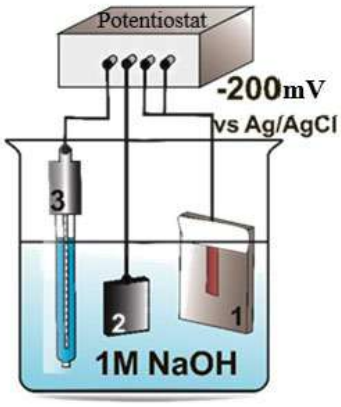

Figure 17 - Scheme of the electrochemical cell for synthesis of oxide and hydroxide structures on the surface of copper electrodes

Laser-induced synthesis at the interface between substrate and liquid reaction medium

Laser-induced synthesis at the interface between a substrate and a liquid reaction medium is a one-step process consisting in the localized interaction of laser radiation with a liquid precursor, which leads to the reduction of metal ions from the solution with the subsequent formation of a new phase of the material on the substrate. In the presented case, the target metal was nickel, and an aqueous solution containing nickel chloride (2 mM), potassium sodium tartrate (7 mM), and sodium hydroxide (10 mM) was used as the precursor. Irradiation of the substrate-solution interface with a continuous laser source at a wavelength of 532 nm leads to the formation of conductive nickel structures on the glass substrate. The scheme of the setup for laser-induced synthesis at the interface between substrate and liquid reaction medium is shown in Figure 18 [170].

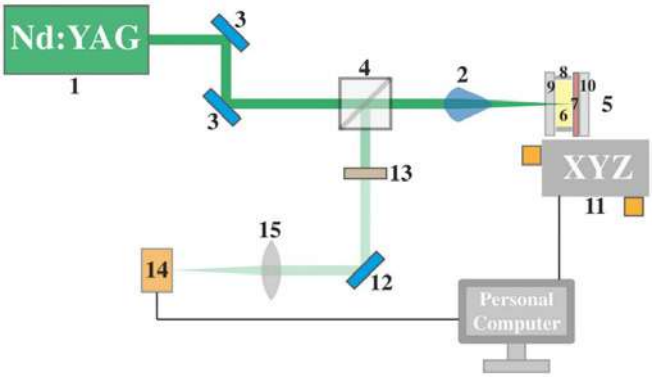

Figure 18 - The setup for laser synthesis (1 - solid-state laser, 2 - lens, 3 - collimating mirror system, 4 - beam-splitting cube, 5 - cuvette with solution, 6 - precursor solution, 7 - substrate, 8 - cuvette, 9, 10 - quartz glass, 11 - sliding, 12 - rotating mirror, 13 - filter, 14 - web camera) [170]

The beam of a continuous solid-state laser (532 nm) passes through a system of collimating mirrors and a beam-splitting cube, then the radiation hits the substrate, passing through the cuvette wall and the liquid reaction medium. A portion of the light reflected from the substrate travels in the opposite direction to the web camera, which is used to monitor the reaction online. The cuvette is moved relative to the beam by means of a motorized translation stage.

Glass slode was used as a substrate, since LIS at the interface between substrate and liquid reaction medium implies heating of the solution to high temperatures, at which polymer substrates are degraded.

An aqueous solution of nickel chloride, potassium sodium tartrate and sodium hydroxide was used as precursor for laser-induced synthesis of nickel structures at the substrate-liquid reaction medium interface (Table 2). Metal tartrate complexes have shown promise for LIS in previous studies using copper structures as an example [92]. It was shown that when using this type of systems there is no need to introduce a separate component into the solution, acting as a reducing agent, thus the composition presented in Table 2 can serve as a precursor.

Electrode surface modification

In the case of laser-induced synthesis at the interface between substrate and liquid reaction medium, LIS was used as a modification method, i.e. sequential synthesis with precursor replacement was carried out (Figure 19). After the formation of nickel structures, the substrate was washed with copious amounts of distilled water and dried in air. After that, the substrate with nickel structure was placed again in a cuvette (element 5, Figure 18), which was filled with solution for synthesis of gold or platinum nanostructures based on commercially available complexes of these metals (chlorotriphenylphosphine of gold and dichlorodicyclopentadienyl of platinum) (Table 2). Using the web camera (element 14, Figure 18), precise positioning of the laser beam was performed to rescan over the surface of the presynthesized nickel layer.

Figure 19 - Laser-induced synthesis at the interface between substrate and liquid reaction medium

Table 2 - Composition of solutions used for laser-induced synthesis at the interface between substrate and liquid reaction medium

Metal	Precursor	Concentration, mM	Solvent
Ni	Nickel chloride ($NiCl_2 \times 6H_2O$)	2	H_2O
	Sodium potassium tartrate ($KNaC_4H_4O_6 \times 4H_2O$)	7	
	Sodium hydroxide (NaOH)	10	
Au	Gold Chlorotriphenylphosphine ($(Ph_3P)AuCl$)	1	DMF
Pt	Platinum dichlorodicyclopentadienyl ($C_{10}H_{12}Cl_2Pt$)	1	DMF

Laser-induced synthesis at the interface between substrate and solid reaction medium

This approach is based on the local interaction between laser radiation and the film of oxide nanoparticles, which leads to their complete or partial reduction and the formation of structures with the desired geometry on the substrate. The target materials were Ni, Cu based composites and therefore the corresponding commercially available oxide nanoparticles of the aforementioned metals were used as the ink base. The ink was prepared by mixing 3 components: polyvinylpyrrolidone (PVP, average molecular weight 10kD), ethylene glycol (EG) and metal oxide nanoparticles (average size 50 nm). First, PVP was mixed with EG, then CuO NPs were added to the resulting solution, the ratios of components are shown in Table 3. The ink was applied to the surface of the substrates by spincoating for 5 seconds at 500 rpm and then 30 seconds at 7000 rpm [171]. The synthesis scheme is presented in Figure 20.

Table 3 - Composition of solutions used for laser-induced synthesis at the interface between substrate and solid reaction medium

Substance	**CuO**	**NiO**	**PVP**	**EG**
Function	source of copper	source of nickel	stabilizer	reducing agent
Mass, g	3	1.5	0.65	0.65

A femtosecond laser (Toptica, FemtoFiber proNIR, pulse duration 120 fs, wavelength 780 nm, repetition rate 80 MHz) was used as a source of laser radiation for laser-induced synthesis at the interface between substrate and solid reaction medium.

The surface of all substrates used (glass-ceramic, polyethylene naphthalate - PEN, polyethylene terephthalate - PET, polyimide - PI) underwent two-stage cleaning: (1) sequential ultrasonic treatment in acetone, ethanol and water for 10 min in each solvent, (2) irradiation with an excimer lamp for 90 seconds (FLAT EXCIMER EX-mini, Hamamatsu Photonics).

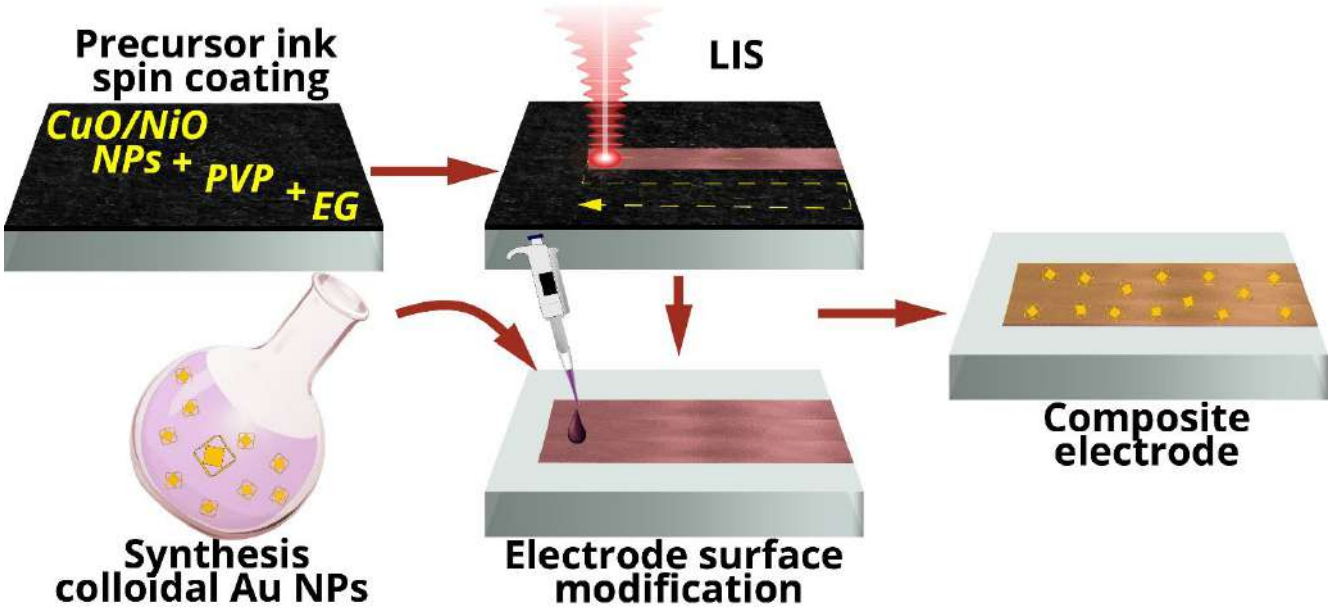

Figure 20 – The laser-induced synthesis at the interface substrate - solid reaction medium with subsequent modification of electrode surface

Electrode surface modification

Separately synthesized gold nanoparticles of complex shape were used to modify the electrodes fabricated at the interface between substrate and solid reaction medium. These nanoparticles as core-cage nanoparticles, as they have a nucleus in the center of the perforated shell, with the nucleus associated with one of the cell walls. The proposed core-cage terminology reflects the unique structural features of these particles, which have holes in the shell and an accessible space around the core, allowing the analyte to approach the core and the inner surface of the shell, resulting in a significant increase in the available electrode area. The synthesis was carried out using the seed-mediated growth, the following methodology was developed to obtain particles with a core-cage structure with a high specific surface area [172]:

(I) formation of Au seeds,

(II) growth of octahedral Au nanoparticles,

(III) growth of Ag shell to form Ag nanocubes with octahedral Au core,

(IV) galvanic replacement of the outer layer of Ag cubes with Au, resulting in a perforated Au outer cage structure

(V) complete dissolution of the remaining Ag from the inner part of the structure.

A schematic of the core-cage nanoparticle synthesis is shown in Figure 21, and the details of each stage are described below.

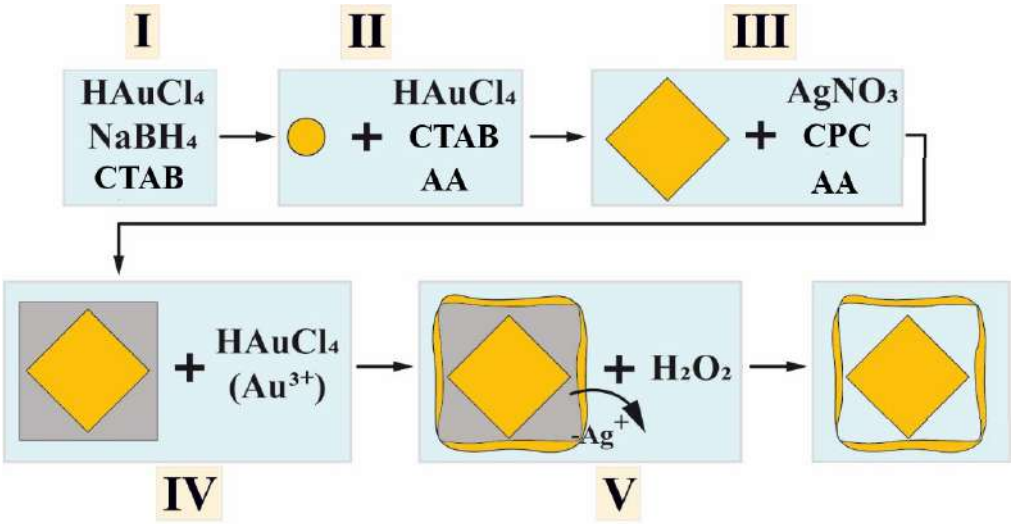

Figure 21 - Scheme of synthesis of core-cage nanoparticles

- Synthesis of Au octahedral NPs.

To synthesize 3 nm Au seeds (step I), freshly prepared $NaBH_4$ (10 mM, 0.6 mL) was added to a solution of $HAuCl_4$ (15 mM, 0.167 mL) and CTAB (cetyltrimethylammonium bromide) (0.1 M, 10.0 mL) under stirring. After stirring for 2 min, the solution was kept for 2 h at room temperature without stirring. The obtained Au NPs solution was diluted with water to 50 mL.

For synthesis of octahedral Au NPs (step II), 100 mL of 0.2M CTAB, 2.66 mL of 15mM $HAuCl_4$ and 50 mL of 0.12M ascorbic acid were mixed, the resulting colorless solution was diluted to a total volume of 1L, then 6 mL of previously prepared Au NPs (step I) were added to the system and left at room temperature for 12h. After synthesis, the NPs were concentrated to 5 mL by centrifugation (15 min, 16000 g) and washed twice with water.

- Synthesis of Au@Ag nanocubes (NCs).

To synthesize Au@Ag nanocubes (step III), 2.5 mL of concentrated octahedral Au NPs (step III), 5 mL of 0.3 M aqueous solution of CPC (cetylpyridinium chloride), 1 mL of 10 mM $AgNO_3$, and 4 mL of 1 mM ascorbic acid were mixed under stirring. The resulting solution was incubated at 60°C for 1 h with stirring. The reaction was quenched by rapid cooling of the solution. The resulting colloidal Au@Ag NCs solution was centrifuged at 1000 rpm for 10 min to remove the AgCl precipitate, then washed twice at 10000 rpm for 15 min and redispersed in 62.5 mL of water.

- Synthesis of Au core-cage NPs.

To synthesize Au core-cage NPs, 0.1 mL of 1 mM $HAuCl_4$ was added dropwise (addition rate of 2 mL/min) to 1 mL of diluted Au@Ag nanocubes under stirring (step IV). After 10 min, 50 µL of 30% H_2O_2 was added (step V). The Au core-cage NPs were washed by centrifugation first at 16000 g for 15

min and then at 1000 for 20 min to remove AgCl powder. Then 10 μl of colloidal solution were applied by dropcasting onto the surface of the working electrode and air dried.

Thus, summarizing the above techniques, this work develops three cases of laser-induced synthesis, leading to the formation of working electrodes for non-enzymatic sensors. Several possible methods for electrode surface modification have also been investigated, including colloidal NPs synthesis, LIS, galvanic replacement and electrochemical oxidation on the electrode surface. Table 4 systematizes the above LIS techniques and the approaches used for electrode surface modification.

Table 4 - Methods used for synthesis and modification of electrodes

	Synthesis at the interface between substrate and air	**Synthesis at the interface between substrate and liquid reaction medium**	**Synthesis at the interface between substrate and solid reaction medium**
Modification method	Galvanic replacement Electrochemical oxidation	LIS	Synthesis of colloidal with subsequent dropcasting
NPsFeatures	Use of electrode material as sacrificial layer for synthesis localization	LIS for both the electrode and its modification to maintain the spatial selectivity of the process	Ability to synthesize various complex shaped nanoparticles

2.2 Characterization of the composition and morphology of the materials

The synthesized materials were comprehensively characterized using advanced instrumental methods of analysis. The studies were carried out using the equipment of SPBU Research Park, including “Nanotechnology”, “X-ray Diffraction Studies”, “Optical and Laser Materials Research”, and “Physical Methods of Surface Investigation” facilities.

Optical microscopy

The samples were studied by optical microscopy using Olympus BX-51 microscope for initial express assessment of morphology. Based on the obtained data, optimization of laser surface modification ragimes and selection of optimal parameters of synthesis conditions were carried out.

Scanning electron microscopy (SEM), Energy-dispersive X-ray spectroscopy (EDX)

Electron microscopic characterization of the materials was carried out on a Zeiss Supra 40VP SEM with a Field Emission cathode, a GEMINI electron optics column and a fully oil-free vacuum system with a low vacuum (VP) mode of operation at an accelerating voltage of 20 keV.

Transmission electron microscopy (TEM)

The synthesized samples were studied using a Hitachi S5200 microscope at an accelerating voltage of 10-30 keV.

X-Ray Diffraction (XRD).

The synthesized samples were studied on a Bruker D2 Phaser diffractometer equipped with a LynxEye detector using CuKα radiation in the 2θ-band 10°-100°.

Raman spectroscopy.

The synthesized samples were studied using a SENTERRA Raman spectrometer (Bruker) equipped with a visualization system of the object of study. An excitation laser with a wavelength of 488 nm and a power of 20 mW was used for measurements.

X-ray XPS spectroscopy (XPS).

The synthesized samples were studied using a Thermo Fisher Scientific Escalab 250Xi integrated spectrometer equipped with a hemispherical analyzer with two detectors and a surface imaging system with a resolution of less than 20 μm.

2.3 Characterization of electrocatalytic properties of the materials

All the electrochemical studies of the non-enzymatic sensors were carried out in a three-electrode undivided cell, where the synthesized strucures served as the working electrode, the reference electrode was Ag/AgCl electrode and the auxiliary electrode was platinum wire (Figure 22). All potentials were measured relative to the Ag/AgCl reference electrode (3.5M KCl).

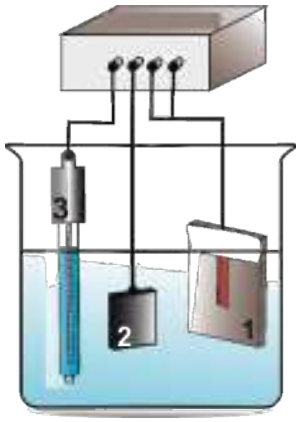

Figure 22 - Three-electrode electrochemical cell, 1 - synthesized electrode, 2 - platinum auxiliary electrode, 3 - Ag/AgCl reference electrode

Cyclic voltammetry (CV)

CV was used to determine the optimal potential for further studies by chronoamperometry. For all samples, CVs were obtained in background electrolyte and then with the addition of a known concentration of the target analyte. The investigation was performed using Corrtest CS300 and Elins

P30I potentiostats. The conditions of the CV experiments for the different analytes are summarized in Table 5.

Table 5 - CV acquisition conditions for different analytes

Analyte	Potential range, V	Scan rate, mV/s	Electrolyte
Glucose	-0.2 – 0.8	50	0.1 M NaOH
Hydrogen peroxide	-0.8 – 0.2	50	0.1 M phosphate buffer (pH 7.0)
Dopamine	-0.2 – 0.8	50	0.1 M phosphate buffer (pH 7.0)

Impedance spectroscopy

Impedance spectra were obtained using the original custom made device developed at SPbAU RAS [173]. The studies were carried out in a two-electrode electrochemical cell with synthesized structures as working electrodes and a platinum auxiliary electrode in 0.9% NaCl solution. Ehe frequency range was 100 Hz to 40 kHz with a resolution of 2 Hz. The impedance spectra were approximated with the NELM software package for MATLAB using the complex nonlinear least squares (CNLS) method [173].

Chronoamperometry

Measurements were carried out in a three-electrode electrochemical cell using a Corrtest CS300 and Elins P30I potentiostats. Chronoamperograms were recorded by stepwise addition of known amounts of the target analyte under constant stirring. Comparison of the current obtained by adding the analyte and its concentration allows to plot calibration curves and determine the linear response range and sensitivity of the sensors.

CHAPTER 3. DISCUSSION OF RESULTS

3.1 Laser-induced synthesis at the substrate-air interface followed by copper plating

3.1.1 Laser-induced surface modification followed by copper plating

This work is devoted to the study of the processes that occur during the laser-induced synthesis of nanostructured electrocatalytically active materials based on transition metals. Much attention is paid to the analysis of the laser-induced processes at the substrate-reaction medium interface, which is a key feature of this study. The special interest in the substrate-reaction medium interface allowed to perform a comprehensive characterization of the studied system, both from the point of view of the laser-induced chemical reductions and from the point of view of the influence of the laser action on the substrate. In the course of the work, three different cases of LIS have been studied, each differing in the state of the reaction medium.

The first of the LIS considered consisted of direct laser modification of the substrate in air followed by copper plating. A detailed study of the influence of the laser irradiation parameters on the morphology of different types of substrates, both flexible and rigid, allowed to identify the main principles contributing to the formation of nanostructured electrocatalytically active materials with high adhesion. The study of the influence of the laser irradiation parameters on the structural, morphological and electrochemical properties of the synthesized materials allowed to establish the composition-structure-property relationships for the fabricated materials.

The laser-induced synthesis at the substrate-air interface followed by copper plating on the substrate consists of several steps:

(I) Laser-induced modification of the substrate in air;

(II) Activation of the modified surface with silver nitrate solution;

(III) Selective chemical copper plating of the activated area;

This work focused on the first stage of the process, the interaction of the laser radiation with the substrate in air, since this is the stage that determines the adhesion properties of the copper electrodes. Chemical copper plating was carried out using a widely studied technique that is the basis of many industrial processes and therefore of less scientific interest. At the same time, it allows to obtain conductive copper layers with low resistance under sufficiently mild synthesis conditions, suitable for flexible polymeric materials with commertialy available chemicals [12].

The main parameters of the laser radiation that influence the processes occurring during the irradiation of the substrate-air interface are

(1) Laser power density (P)

(2) Pulse repetition rate (f)

(3) Scanning speed of the laser beam (v)

(4) Distance between scanning lines (h)

The ranges of variation of the above parameters in the experimental studies are presented in Table 6. The boundary conditions were chosen based on previous experiments using the proposed approach, taking into account the thermal resistance and ablation threshold of the substrate material [36,83,85]. The laser power density (P) and pulse repetition rate (f) were kept constant for each type of surface. Optimization of laser exposure was performed by varying the scanning speed (v) and the distance between scanning lines (h) (Figure 23), since the use of fixed and sufficiently high power densities of LR (P) it is possible to select conditions that ensure maximum speed and productivity of the process, i.e. high scanning speed v with maximum h. Changing the scanning speed (v) at a fixed laser power density is an effective means to control the thermal field in the sample, as it allows to regulate the amount of energy received by the irradiated material and its distribution over the surface, as well as to control the processes of heat accumulation and dissipation. Usually, at lower scanning speeds, an increase in temperature in the irradiation zone and intense heat accumulation both on the surface and in the depth of the sample are observed, whereas higher scanning speeds result in less heat accumulation due to energy dissipation caused by the motion of the laser spot [174].

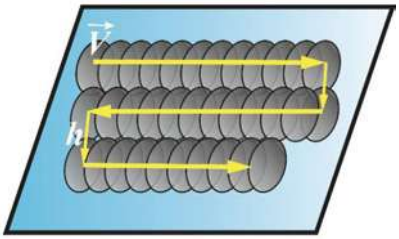

Figure 23 - Schematic representation of laser beam scanning parameters of the substrate

Table 6 - Parameters of laser-induced synthesis at the substrate-air interface

Substrate	Scanning speed (v), m/s	distance between lines (h), мкм
Glass-ceramic	0.1 - 0.2	10 - 15
Glass	0.2 - 0.8	10 - 20
Polyimide (PI)	2.0 - 6.0	10 - 20
Polyethylene naphthalate (PEN)	2.0 - 6.0	10 - 20
Polyethylene terephthalate (PET)	2.0 - 6.0	10 - 20

Figures 24-28 show SEM images of the surface of the investigated substrates after laser exposure under different conditions and optical micrographs of copper structures obtained after the chemical copper plating stage of the activated region under appropriate conditions.

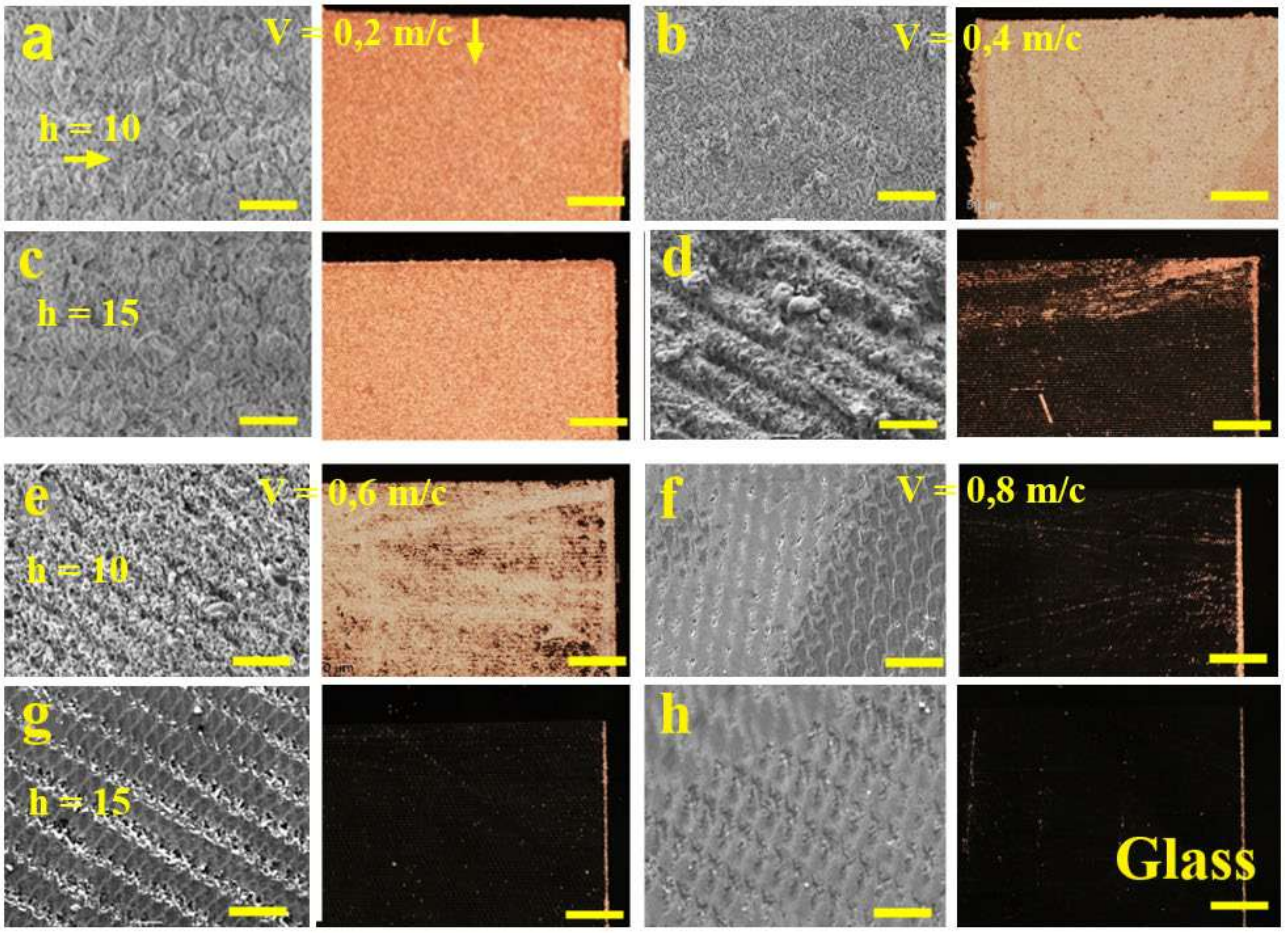

Figure 24 - SEM images and optical micrographs of copper structures on glass after laser modification performed at different scanning speeds (m/s) and line spacings (μm). (a) v=0.2, h=10, (b) v=0.4, h=10, (c) v=0.2, h=15, (d) v=0.4, h=15, (e) v=0.6, h=10, (f) v=0.8, h=10, (g) v=0.8, h=15, (h) v=0.4, h=15. The size scale corresponds to 35 μm for SEM images and 400 μm for optical micrographs

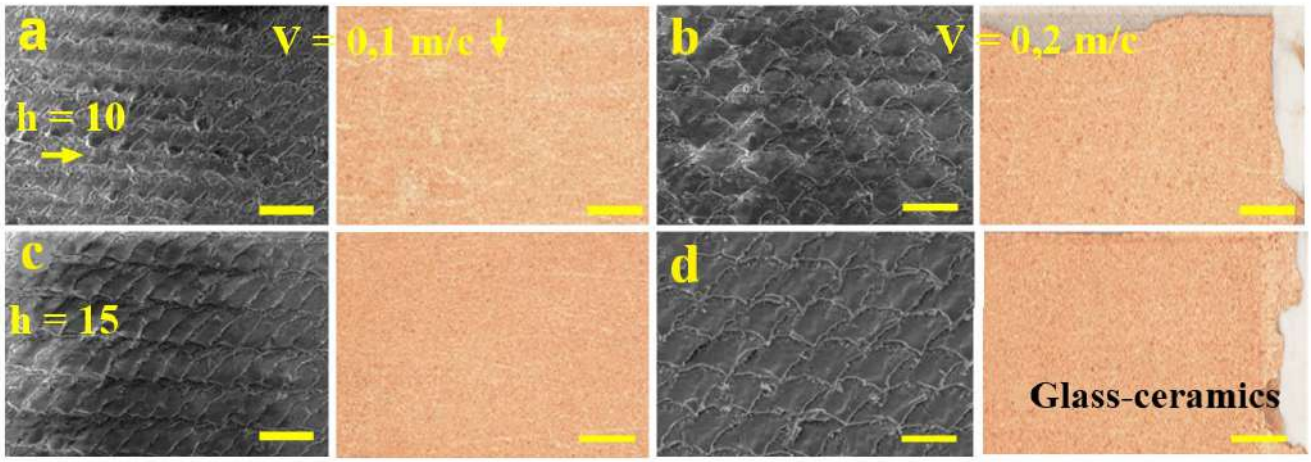

Figure 25 - SEM images and optical micrographs of copper structures on glass-ceramic after laser modification performed at different scanning speeds (m/s) and line spacings (μm). (a) v=0.1, h=10, (b) v=0.2 , h=10, (c) v=0.1, h=15, (d) v=0.2, h=15. The size scale corresponds to 35 μm for SEM images and 400 μm for optical micrographs

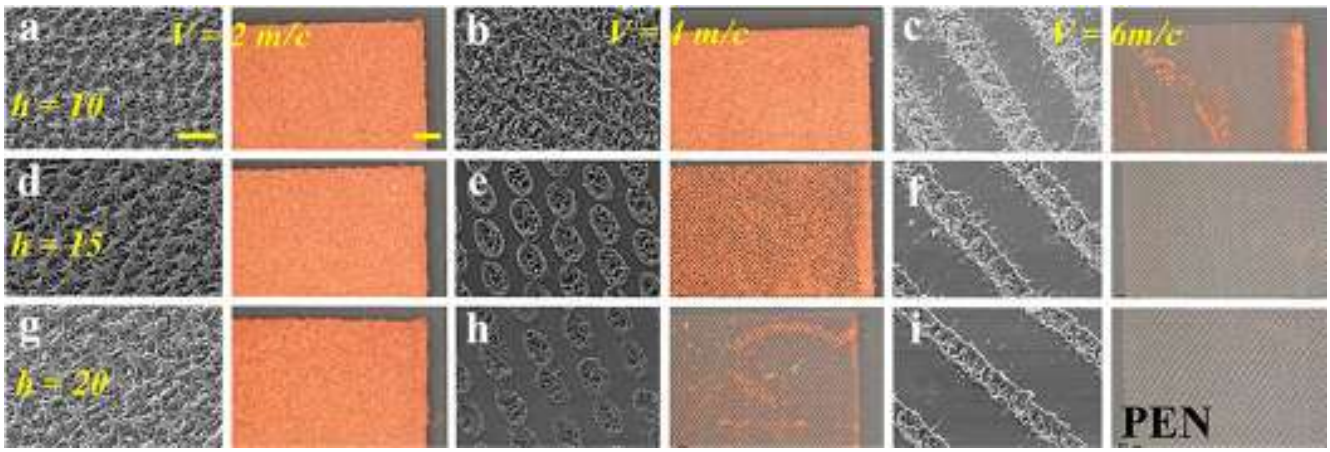

Figure 26 - SEM images and optical micrographs of copper structures on PEN after laser modification performed at different scanning speeds (m/s) and line spacings (μm). (a) v=2, h=10, (b) v=4, h=10, (c) v=6, h=10, (d) v=2, h=15, (e) v=4, h=15, (f) v=6, h=15, (g) v=2, h=20, (h) v=4, h=20, (i) v=6, h=20. The size scale corresponds to 35 μm for SEM images and 400 μm for optical micrographs

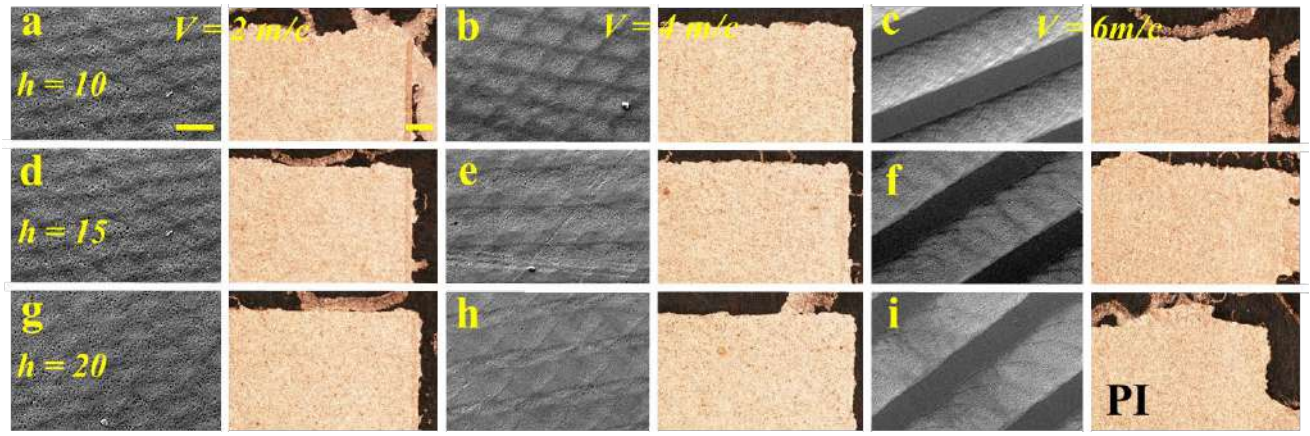

Figure 27 - Optical micrographs and SEM images of copper structures on PI after laser modification performed at different scanning speeds (m/s) and line spacings (μm). (a) v=2, h=10, (b) v=4, h=10, (c) v=6, h=10, (d) v=2, h=15, (e) v=4, h=15, (f) v=6, h=15, (g) v=2, h=20, (h) v=4, h=20, (i) v=6, h=20. The size scale corresponds to 35 μm for SEM images and 400 μm for optical micrographs.

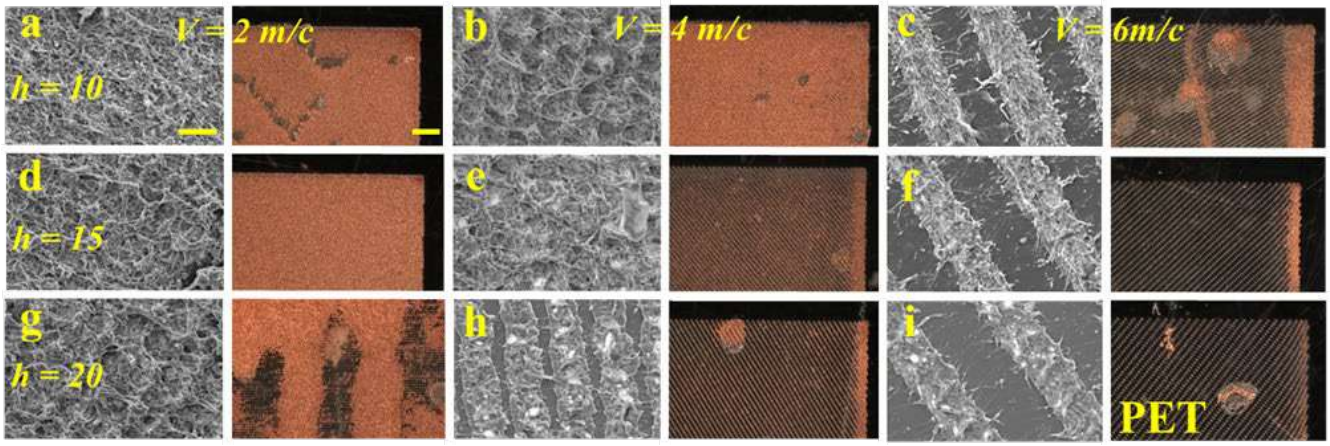

Figure 28 - Optical micrographs and SEM images of copper structures on PET after laser modification performed at different scanning speeds (m/s) and line spacings (μm). (a) v=2, h=10, (b) v=4, h=10, (c) v=6, h=10, (d) v=2, h=15, (e) v=4, h=15, (f) v=6, h=15, (g) v=2 , h=20, (h) v=4, h=20, (i) v=6, h=20. The size scale corresponds to 35 μm for SEM images and 400 μm for optical micrographs

It can be observed that decreasing the distance between the lines (h) and the scanning speed (v) leads to the formation of a continuous metal film. The absence of structural defects ensures the electrical conductivity of the structure, which is a necessary condition for the further use of synthesized materials as working electrodes and the investigation of their electrochemical properties. When h and v increase, the thermal effect per unit surface area decreases, which in extreme cases leads to the formation of a periodic morphology, where modified areas alternate with areas that retain the original morphology of the substrate.

The optimal conditions of laser modification were chosen based on the resistance, adhesion, as well as qualitative morphology assessment of the structures. The optimal synthesis conditions for all the substrates are listed in Table 7, photos of the structures fabricated in these regimes are presented in Figure 29.

The melting temperatures of polymeric materials are much lower than those of glass-ceramics and glass (T_{melt} (PET) = 263ºC, T_{melt} (PEN) = 269ºC, T_{melt} (PI) ~ 360ºC, T_{melt} (glass-ceramic) ~ 1200ºC [175], T_{melt} (glass) ~ 1600ºC [176]). The average bond energies in polymers are also lower (e.g. CH_3CO-OCH_3 bond energy 406= kJ/mol [178]) than in glasses (Si-O bond energy = 798 kJ/mol [177]), which is one of the reasons for a significant difference in the thresholds of surface modification of these classes of materials, which can also explain the difference in the optimal parameters of laser exposure necessary for surface modification. However, it should be noted that among the studied substrates, glass-ceramic is a polyphase material with crystalline and amorphous components. It has been shown that laser irradiation of such materials has significant features, since the presence of phase boundaries allows laser radiation to form a large number of defects that serve as active centers for metal reduction, making it possible to modify glass-ceramic substrates at lower powers densities [95].

Table 7 - Optimized conditions of laser modification of substrates using radiation with a wavelength of 532 nm and pulse duration of 10 ps (focal spot diameter 25 μm)

Substrate	W, W	P, kW/cm^2	f, kHz	v, m/s	h, μm
Glass	6.23	1270	100	0.2	15.0
Glass-ceramic	0.61	124	10	0.1	15.0
PEN	0.98	200	100	2.0	10.0
PET	4.63	944	100	2.0	20.0
PI	3.00	612	100	4.0	15.0

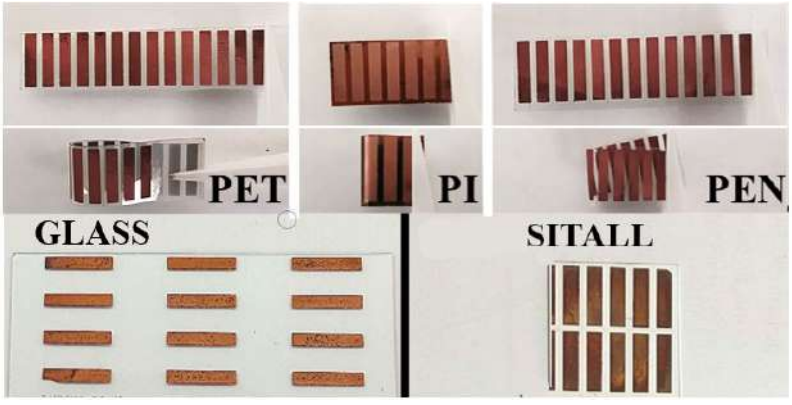

Figure 29 - Photographs of copper structures on different substrates fabricated under optimal synthesis conditions

The electrode materials were examined by XRD (Figure 30) and SEM (Figure 31) to characterize the morphology and composition. All samples were found to be pure metallic Cu, with reflection angles from the (111), (200) and (220) planes consistent with Cu [178]. Substrate reflections are observed on the surface of the glass-ceramics due to the presence of the crystalline phase in it. According to the SEM images, all structures have no breaks, which should provide a stable electrical contact during electrochemical studies. It can also be noted that the structures inherit the morphology of the substrate exposed to the laser, there are characteristic grooves formed at the stage of interaction of the laser radiation with the surface. The results of EDX, presented in the insets of Fig. 31 in the corresponding tables, confirm the XRD data. The presence of such elements as oxygen, carbon, magnesium, calcium in the signal spectra can be explained by the elemental composition of the substrates.

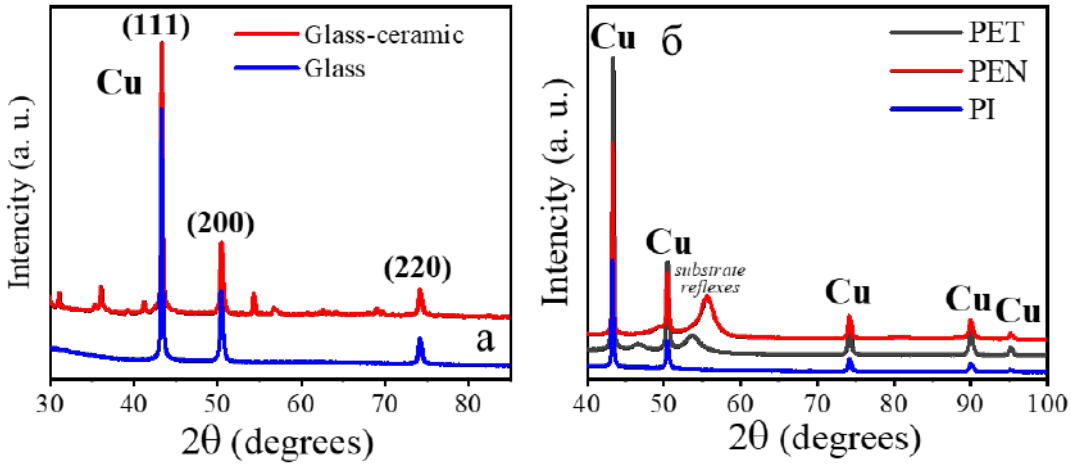

Figure 30 - XRD patterns of copper structures on the surface of (a) rigid, (b) flexible substrates

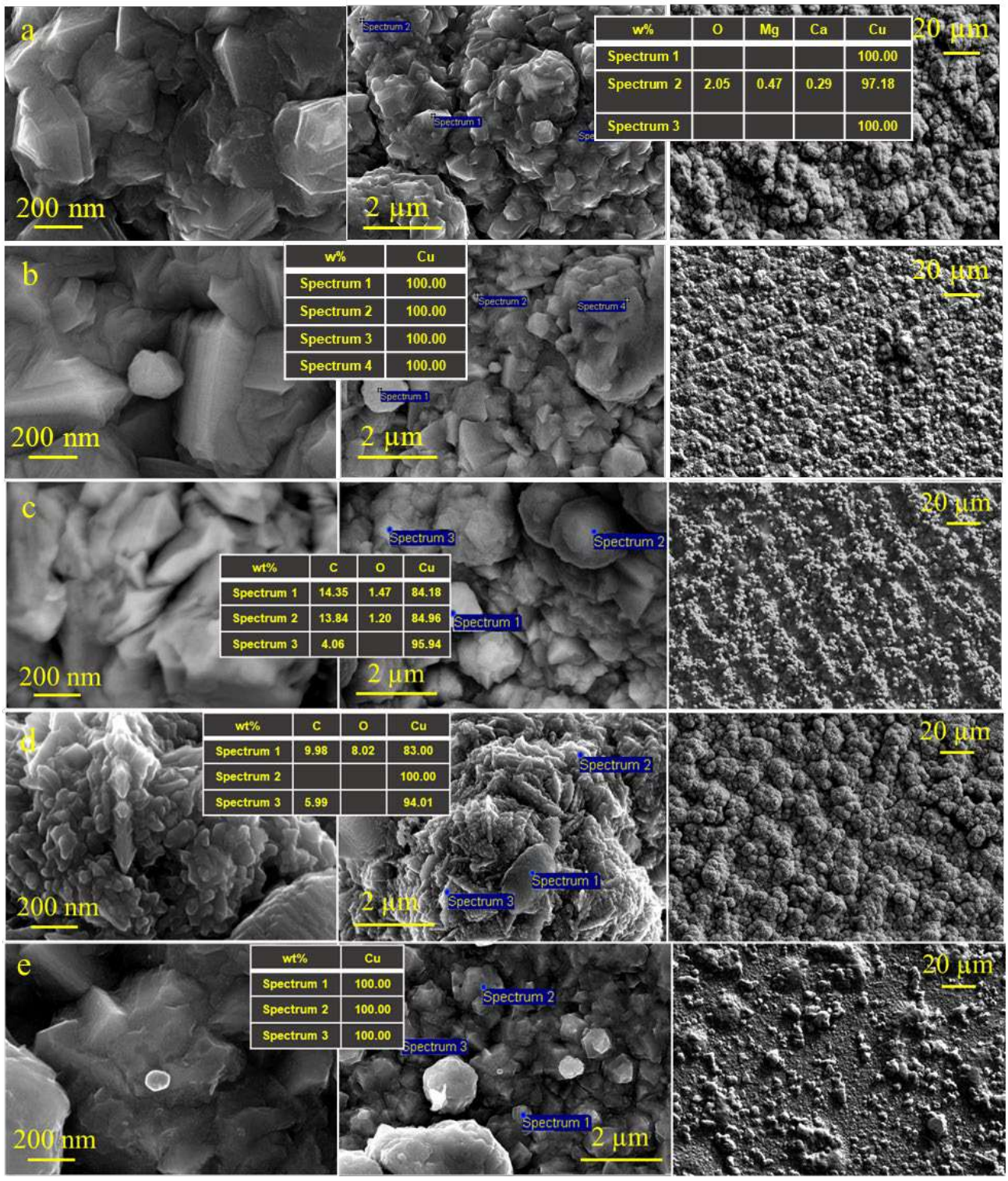

Figure 31 - SEM images and EDX analysis of copper structures (a) glass, (b) glass-ceramic, (c) PEN, (d) PET, (e) PI

Bending tests were performed to investigate the adhesion and mechanical stability of copper electrodes on the surface of flexible substrates. Polymer substrates with synthesized copper structures were subjected to repeated bending using a test bench, while on-line resistance monitoring was performed. It was shown that, there was a gradual increase in the resistance of the electrode during the

test, with the resistance value moving to a saturation state at the end of the cycle. The total increase in resistance after 1000 cycles was 13.2%, 13.8% and 20% of the initial value for PI, PET and PEN, respectively (Figure 32). It should be noted that the mechanical properties of the substrate polymers also differ and may contribute to the final result. The Young's modulus is 1.3 GPa, 2.8 GPa, and 5.5 GPa for PI, PET, and PET, respectively. The greater the ability of the substrate material to resist elastic deformation, the greater the relative increase in resistance observed for the copper layers.

The increase in resistance is probably due to the formation of defects in the structure that break the electrical contact between the copper crystals. At the same time, no visible changes in morphology (cracks, etc.) were detected according to the scanning electron microscopy study (Figure 33). It can be assumed that in case of formation of microcracks visible in SEM, the increase in resistance could be more significant. Nevertheless, the synthesized electrodes on flexible substrates showed high resistance to bending deformation, preserving the visual structure integrity and morphology at the micro level, as well as low values of electrical resistance, which makes them promising for further application as flexible working electrodes for non-enzymatic electrochemical sensors.

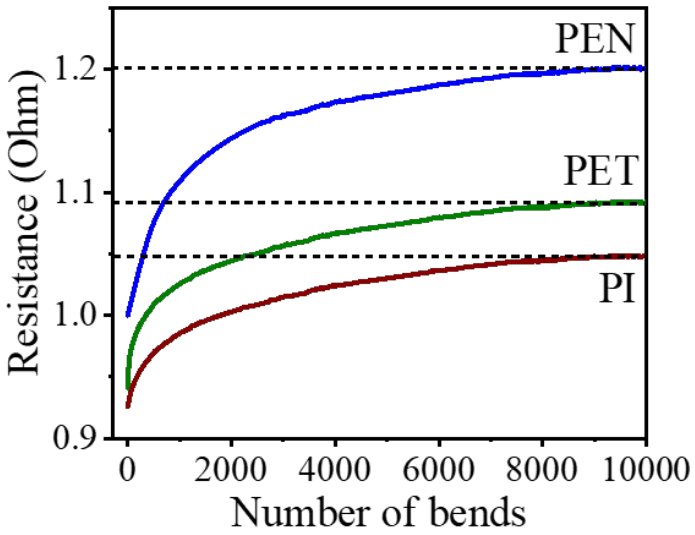

Figure 32 - Change in resistance of samples during bending tests

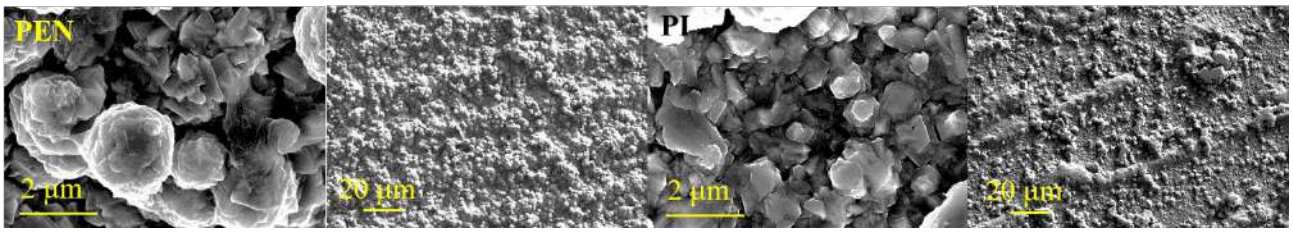

Figure 33 - SEM images of Cu-PEN and Cu-PI electrodes after bending tests

3.1.2 Modification of the electrodes

In order to improve the analytical characteristics of the synthesized materials, as well as to expand the list of analytes available for detection, modification of copper electrodes was performed.

Modification of the electrode surface in particular with nanomaterials can significantly change the electrocatalytic activity of the system, as it is determined not only by its nature, but also by the surface morphology, with the highest sensitivity shown by nanostructured, highly porous electrodes due to the higher electrochemically active surface area (EASA). Also, modification and decoration of electrodes with nanoparticles (NPs) of different shapes allows to obtain materials that can exhibit a synergistic effect of significant enhancement of catalytic properties compared to individual components [179]. There are many studies on the synergistic effect of different types of materials in a single multi-component system [180], as it has very positive effects on electrode properties, including it can lead to facilitation of electron transfer or other processes that increase electrochemical efficiency. Copper and gold (Cu-Au) based bimetallic materials show outstanding sensing performance compared to pure gold and copper based materials [181–183].

The combination of precious (Au) and transition (Cu) metals can lead to increased Cu stability and oxidation resistance, which can improve sensor lifetime and reproducibility of analysis. Gold was chosen as the noble metal because of its high stability compared to silver-based nanomaterials and its relatively low price compared to Pd, Pt, etc.

The choice of modification methods was based on the possibility of preserving the electrode geometry given by the laser-induced surface modification in air. These requirements can be met by transformations in which the copper structures obtained act as a sacrificial layer or as a precursor in the synthesis, thus ensuring the reaction on the electrode surface.

The following approaches have been investigated:

I. Synthesis of gold nanostructures directly on the electrode surface using elemental copper as a reducing agent.

II. Electrochemical oxidation of the copper electrode surface to form a surface layer of copper oxide.

Copper structures on the surface of PEN and glass-ceramics as prime examples of flexible and rigid substrates were chosen as model systems.

3.1.2.1 Synthesis of gold nanostructures on the electrode surface

The optimal conditions for synthesis of Cu-Au-based bimetallic electrode materials have been determined. The use of a special component acting as a reducing agent leads to the formation of gold

nanoparticles in the entire volume of the solution. In turn, carrying out the reaction under conditions where the reduction of gold occurs due to the partial dissolution of the pre-synthesized copper layer, allows the process to be localized on the surface of the electrode(Figure 34). In the latter case, the oxidation of copper $Cu^0 \rightarrow Cu^{2+}$ and the transition of copper ions into solution occurs, which is accompanied by the reduction of gold $Au^{3+} \rightarrow Au^0$ and its deposition on the electrode surface. An aqueous solution of 0.007 M chloroauric acid ($HAuCl_4$) and 0.1 M 4-dimethylaminopyridine (DMAP) was used as precursor. Before immersing the copper electrode in this solution, it was thermostated under selected conditions (80°C, 60°C, 40°C or at room temperature).

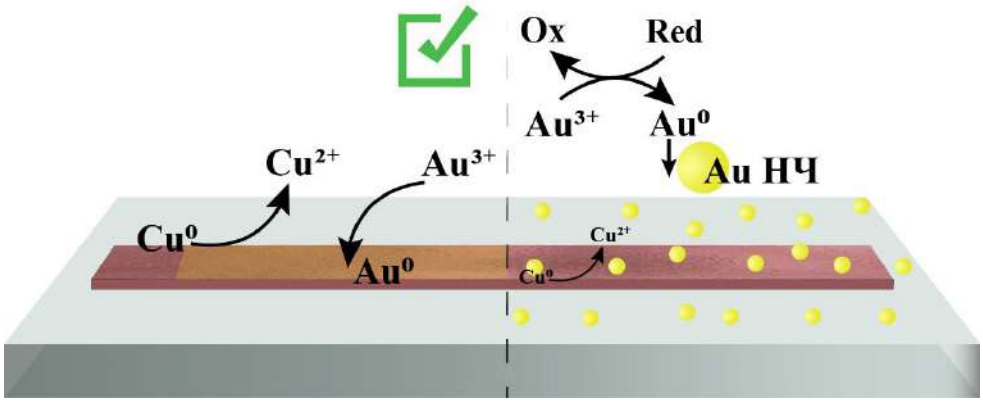

Figure 34 - Schematic representation of possible ways to modify the synthesized electrodes by partial dissolution of the pre-synthesized copper layer (left) and using a special component as a reducing agent (right)

The morphology and composition of the structures on the glass-ceramic surface under different synthesis conditions were investigated by scanning electron microscopy and EDX analysis (Figures 35-36). The effect of solution synthesis time ranging from 5 to 40 minutes and temperature from room temperature to 80 °C was studied.

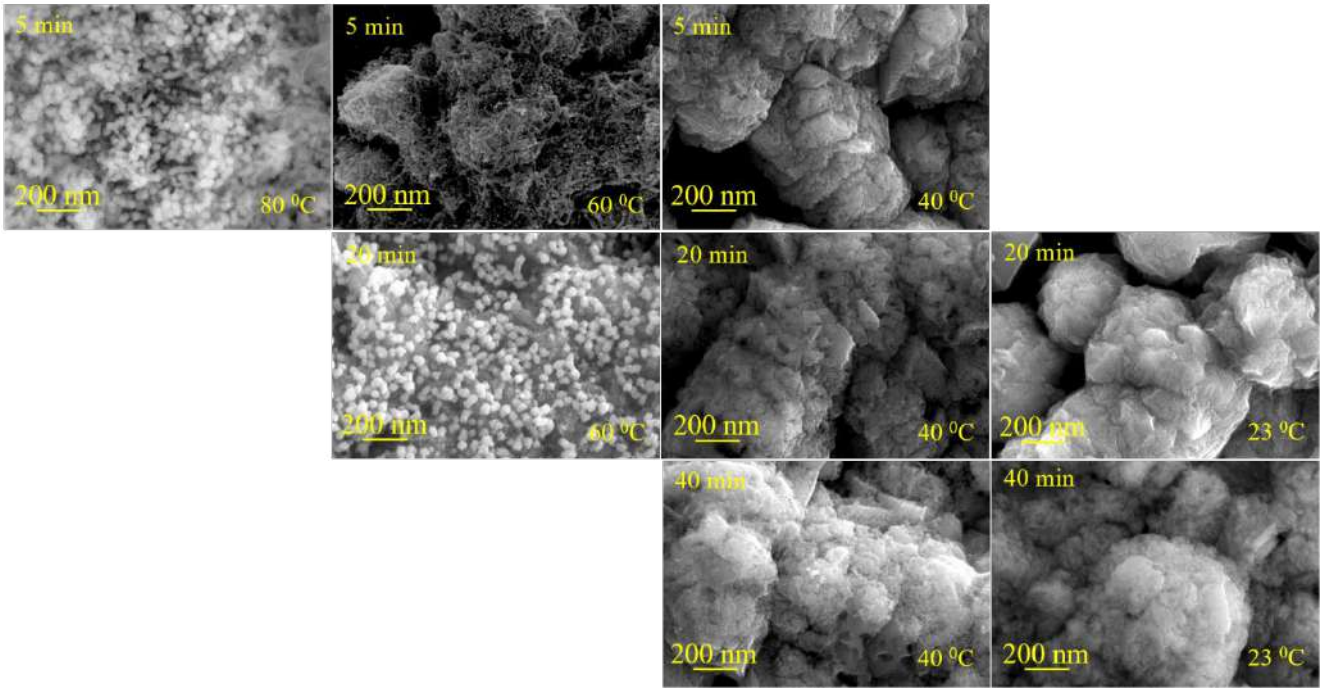

Figure 35 - SEM images of bimetallic Cu-Au nanostructures at different synthesis time and temperature on glass-ceramic surface

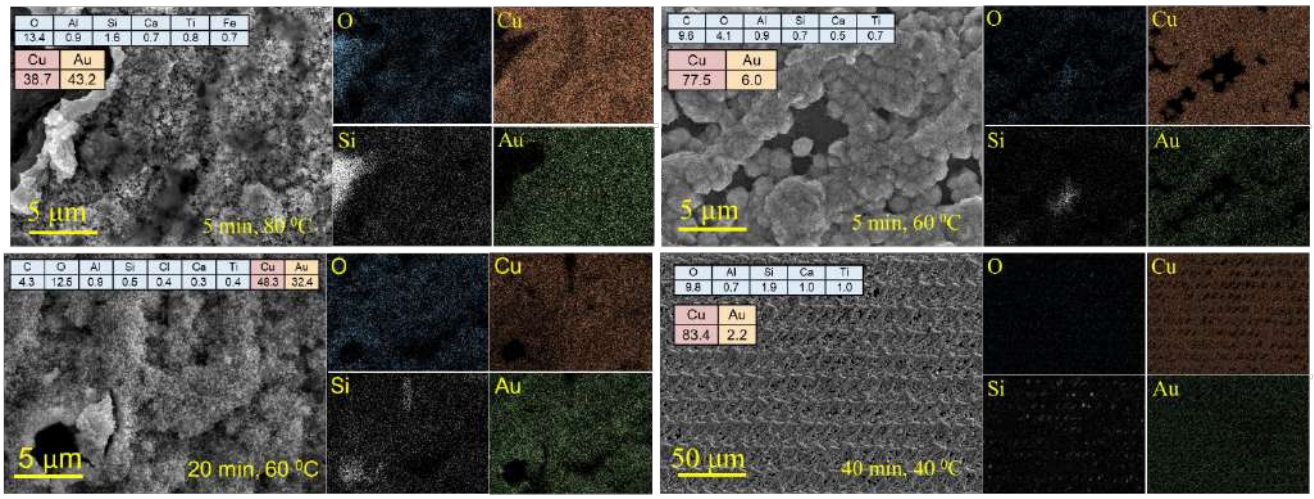

Figure 36 - SEM images and EDX mapping of bimetallic Cu-Au structures synthesized under different conditions on the glass-ceramic surface (a) 5 min, 80ºC, (b) 5 min, 60ºC, (c) 20 min, 60ºC, (d) 40 min, 40ºC

Similarly, copper electrodes on the surface of flexible polymer PEN were modified. The morphology and composition of the structures on the surface of PEN depending on the synthesis conditions were investigated by scanning electron microscopy and EDX analysis, the results are shown in Figures 37-38.

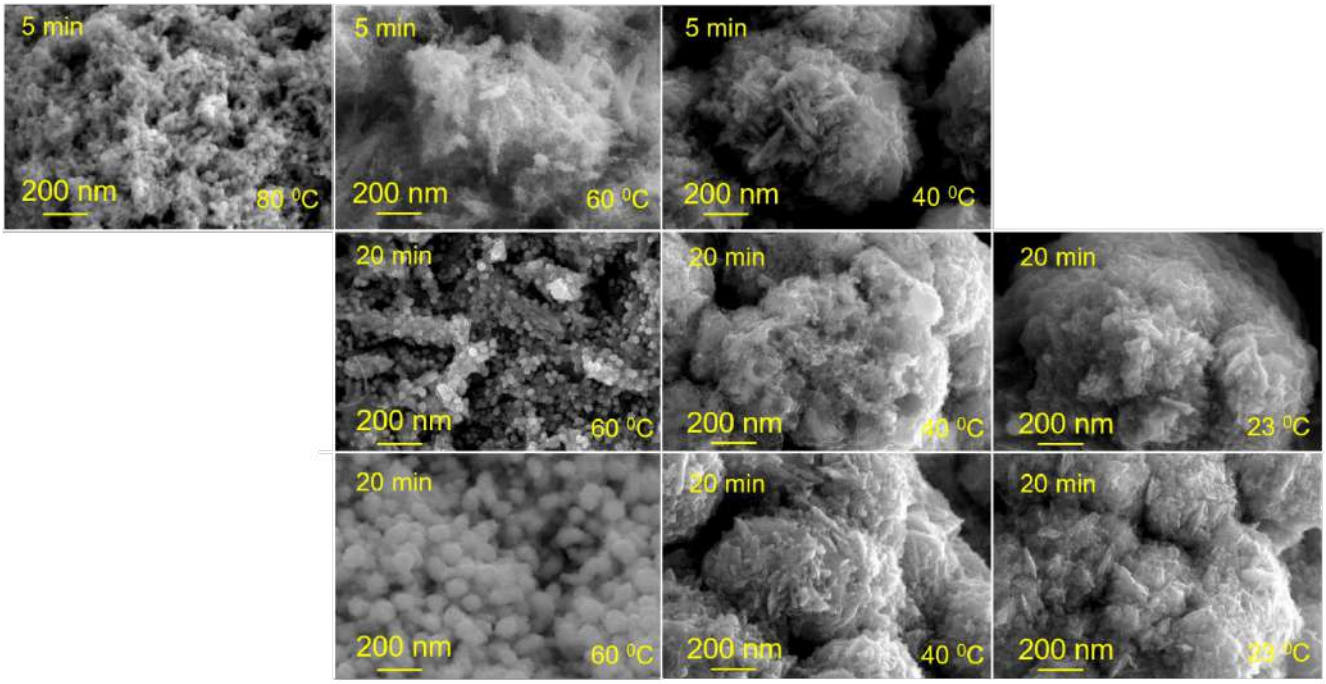

Figure 37 - SEM images of bimetallic Cu-Au nanostructures on PEN surface at different synthesis time and temperature

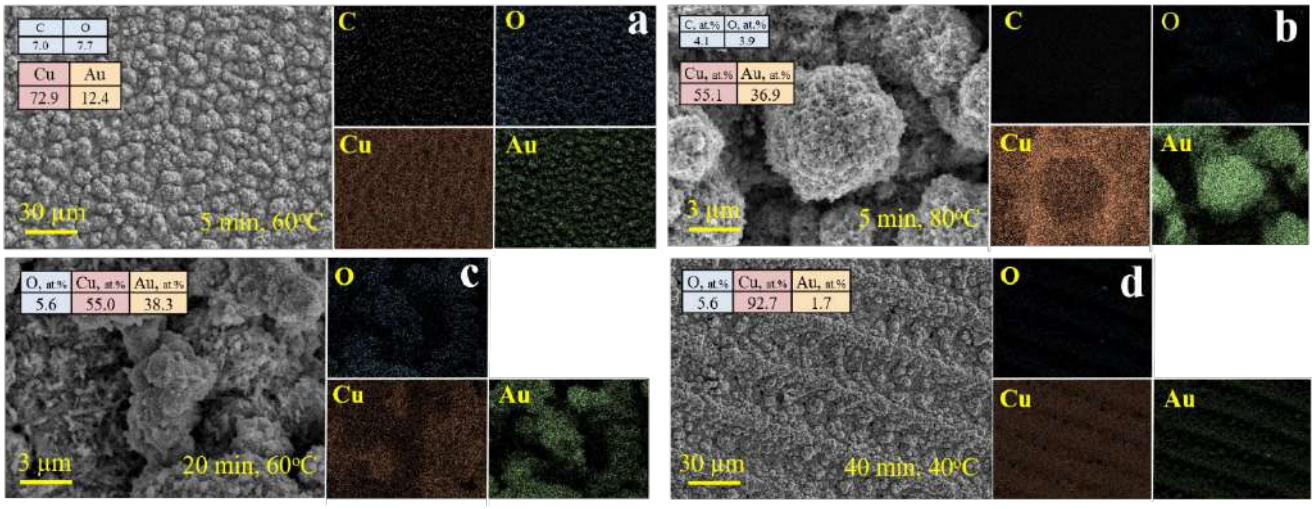

Figure 38 - SEM images and EDX mapping of Cu-Au bimetallic structures on PEN surface synthesized under different conditions (a) 5 min, 60ºC, (b) 5 min, 80ºC, (c) 20 min, 60ºC, (d) 40 min, 40ºC

Depending on the synthesis time and temperature, the morphology of the structures varies over a fairly wide range. Deposition of an insignificant amount of gold particles is observed at low times and low temperatures (about 2% by weight according to EDX data). The morphology of the structures also changes insignificantly, and there is no significant increase in surface area. As the reaction speed increases due to the rise in temperature, there is an active reduction of gold that leads to the formation of a large number of spherical particles (about 30-40% by weight according to EDX data) on the surface

of the copper structure. Excessive modification and the formation of a dense layer of gold particles can prevent the appearance of the synergetic effect between the two metals. In all cases, a fairly uniform distribution of gold on the surface of the sample is observed. Thus, the optimal conditions for the formation of gold nanostructures is to carry out the synthesis for 5 minutes at 60ºC (Figure 39), which allows to obtain gold nano-needles with developed morphology on the surface of copper electrodes.

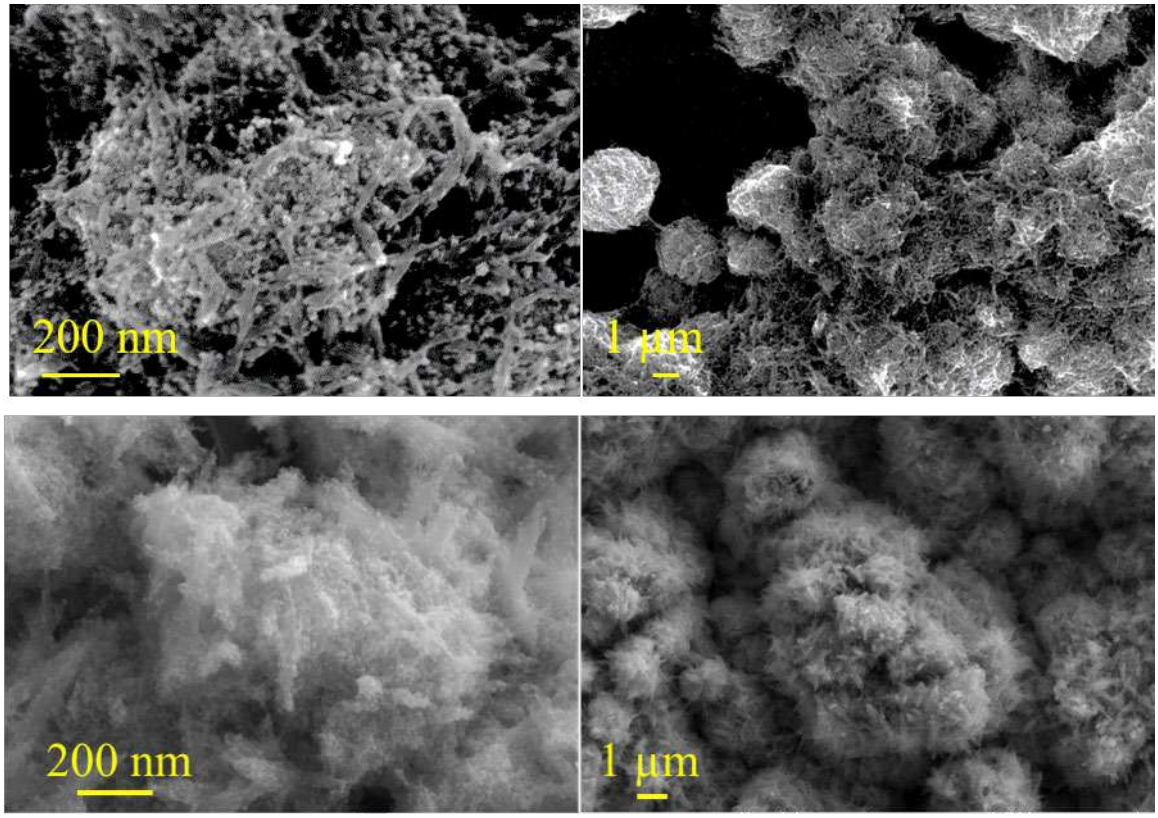

Figure 39 - Figure. SEM images of bimetallic Cu-Au structures under optimal synthesis conditions on the surface of (a) glass ceramics, (b) PEN

$HAuCl_4$ reduction and Au^0 formation are confirmed by XPS spectroscopy data (Figure 40) [184,185]. The lack of pronounced satellite lines in the XPS spectra of Cu indicates the absence of significant surface oxidation during synthesis and storage [186–188].

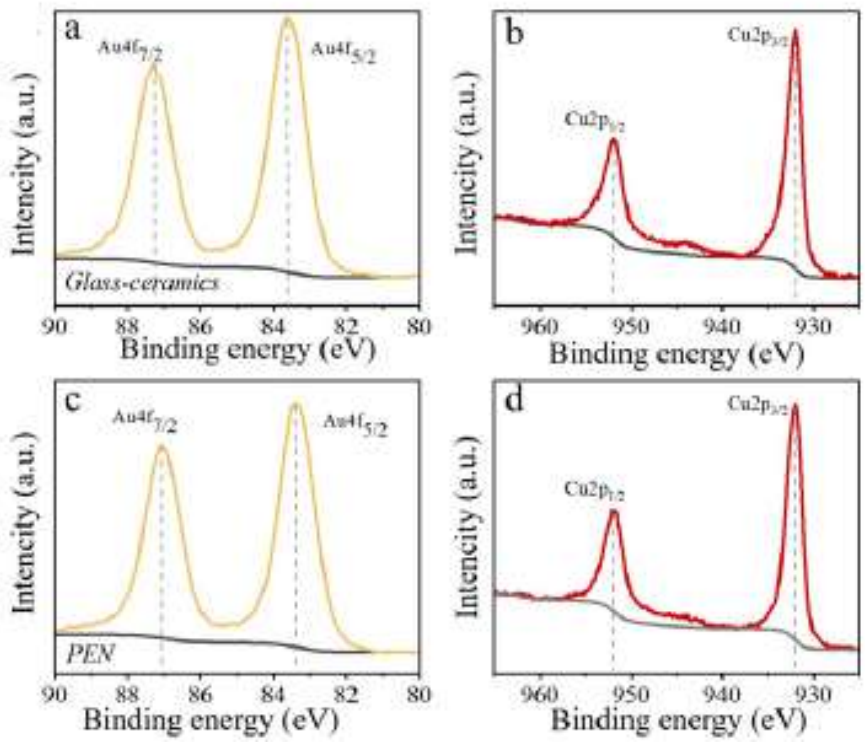

Figure 40 - XPS spectra of bimetallic Cu-Au structures on the surface of (a,b) glass-ceramics, (c,d) PEN

Thus, the optimal conditions for the synthesis of Cu-Au based bimetallic electrode materials were determined by studying the changes in the morphology of the structures as a function of the synthesis time and temperature. Optimal synthesis conditions, providing the best combination of morphological characteristics and composition, were obtained when the reaction was carried out for 5 min at 60°C. Under these conditions, the formation of gold nanostructures with developed morphology on the surface of copper electrodes was observed, which could contribute to the improvement of the electrocatalytic properties of the material due to the increase of the active surface and the synergistic interaction between the metals.

3.1.2.2 Electrochemical oxidation of electrode surface

The electrode materials considered so far, based on copper and gold, have metallic conductivity, which maximally facilitates the transfer of the analytical signal from the electrocatalytically active electrode surface to the measuring circuit of the analytical device. However, many other materials also show high electrocatalytic activity in various reactions and great prospects for use as non-enzymatic sensors [66]. For example, oxygenated copper(II) compounds show high activity in a number of practically important processes, among which the electrochemical oxidation of methanol, water splitting, oxidation of ascorbic acid and glucose [189]. In addition, the formation of oxide nanostructures on the

surface of copper electrodes can help to increase the stability of the system, since in the phosphate buffer medium, when the potential is applied, copper ions on the electrode surface can interact with phosphate ions from the solution to form insoluble salts. Such processes can lead to a decrease in the sensing performance of the working electrode, as contaminating species reduce the number of available active centers at which the reaction involving the target analyte takes place.

Electrochemical oxidation in alkaline medium was used to synthesize oxygen-containing copper compounds on the electrode surface. According to literature data [169,190–192], at a potential of -200 mV (vs. Ag/AgCl) in a highly alkaline medium (1 M NaOH), various oxidation processes of the copper electrode are possible, leading to the formation of products such as copper (I) oxide, copper (II) oxide and copper (II) hydroxide in accordance with the following reactions:

$$\mathbf{2Cu} + 2OH^- = Cu_2O + H_2O + 2e^-$$

$$\mathbf{Cu} + 2OH^- = Cu(OH)_2 + 2e^-$$

$$\mathbf{Cu} + 2OH^- = CuO + H_2O + 2e^-$$

$$Cu_2O + 2OH^- + H_2O = 2Cu(OH)_2 + 2e^-$$

$$Cu(OH)_2 = CuO + H_2O$$

The influence of the potentiostatic synthesis time on the morphology and composition of the formed layers was investigated (Figure 41). According to the SEM data, the synthesis results in the formation of nanoneedles on the surface, the length of which increases with increasing synthesis time from 15 to 600 seconds. The formation of hydrophilic oxide-hydroxide structures with a high aspect ratio provides access of the electrolyte with dissolved analyte to the active centers of the electrode, which results in an increase not only of the real surface area, but also of the electrochemically active surface area.

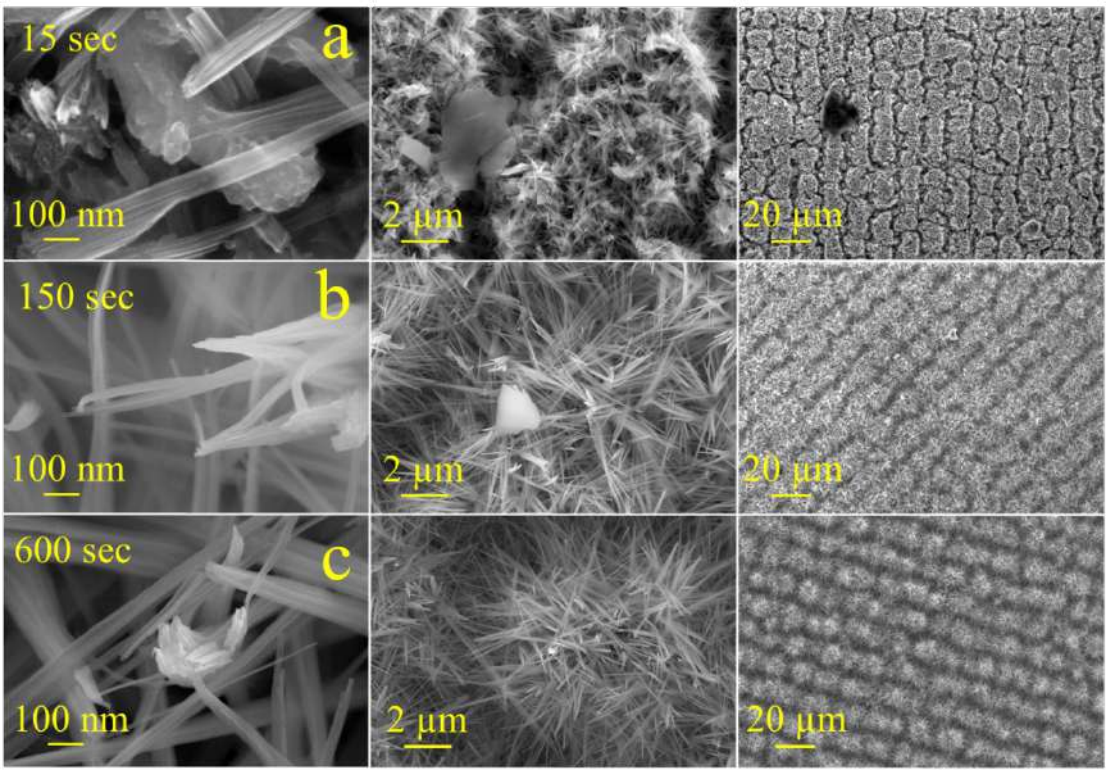

Figure 41 - SEM images of Cu_xO_y-$Cu(OH)_2$ nano-needles on the surface of copper electrode after (a) 15, (b) 150, (c) 600 seconds of electrochemical oxidation

EDX mapping of the samples, in addition to a fairly uniform distribution of elements on the electrode surface, showed an increase in the oxygen content with increasing synthesis time, as well as a gradual decrease in the carbon content, the signal of which refers to the PEN substrate material (Figure 42). This fact confirms the increase in the layer thickness of the formed oxides with increasing synthesis time. In addition, based on the atomic composition and Cu : O ratio, we can assume the prevalence of compounds containing copper (II) over compounds containing copper (I), i.e. copper (II) oxide and copper (II) hydroxide over copper (I) oxide (Figure 42).

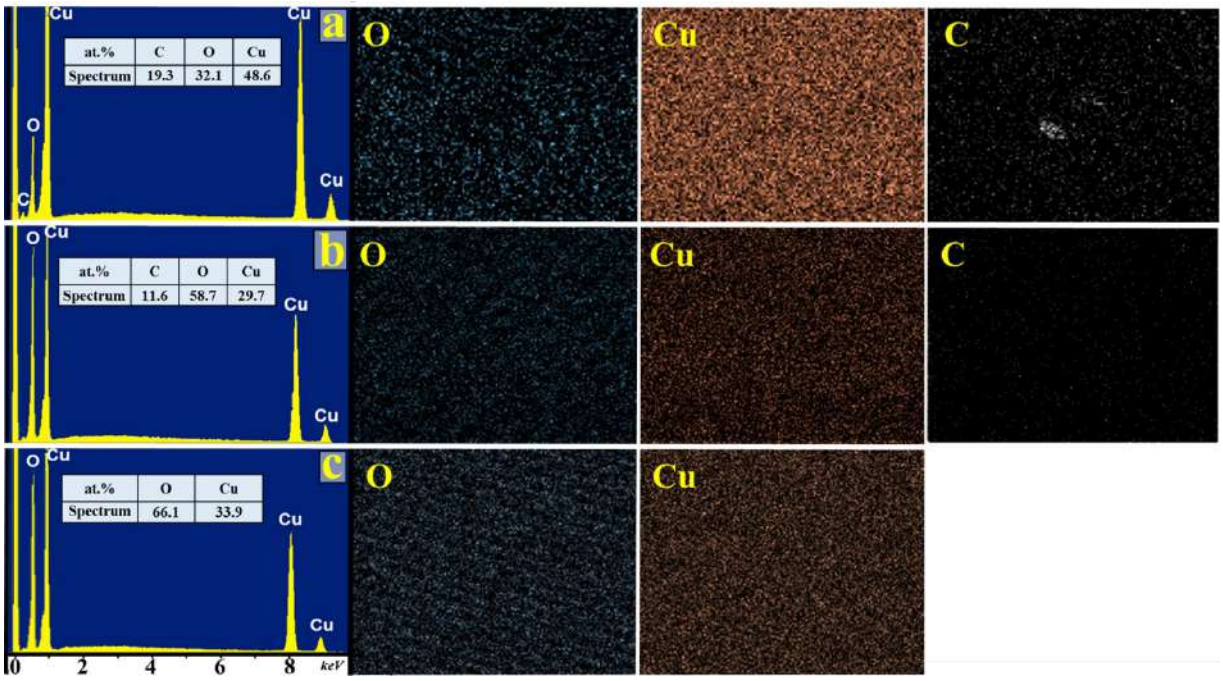

Figure 42 - EDX mapping of the electrode surface after (a) 15, (b) 150, (c) 600 seconds of electrochemical oxidation

The amperometric curve for potentiostatic oxidation of copper structures on the surface of PEN is shown in Figure 43 a. The curve has a pronounced maximum. The initial increase in current density may indicate an active reaction with an increase in surface area due to the onset of oxide layer growth. The further decrease of the current density is probably due to the elongation of the nano-needles, which leads to an increase of the resistance in the system, as the charge has to pass through the growing layer of material with high resistance compared to metallic copper[169]. After reaching the plateau, the surface morphology does not change as much, thickening and elongation of the nanowires are observed, which is consistent with the SEM data (Figure 41).

In addition, the samples were analyzed by X-ray powder diffraction and Raman spectroscopy to determine the qualitative composition. The sensitivity of the first method was insufficient to detect the presence of new phases (Figure 43 b) [193]. Since the modification leads to the formation of a thin surface layer of oxygenated copper compounds, the mass fraction is insufficient for detection by XRD. The XRD pattern shows only peaks of initial metallic copper for samples with short synthesis time, weak reflections of copper hydroxide $Cu(OH)^2$ appear only after long oxidation (Figure 43 b). Raman spectroscopy allows a more complete characterization of the sample, with bands of Cu_2O, CuO and also $Cu(OH)_2$ present in the spectrum (Figure 43 c) [194–197]. Taken together, the qualitative compositional data do not contradict the hypothesized mechanism of copper electrooxidation in highly alkaline solutions described at the beginning of this section [169,190–192].

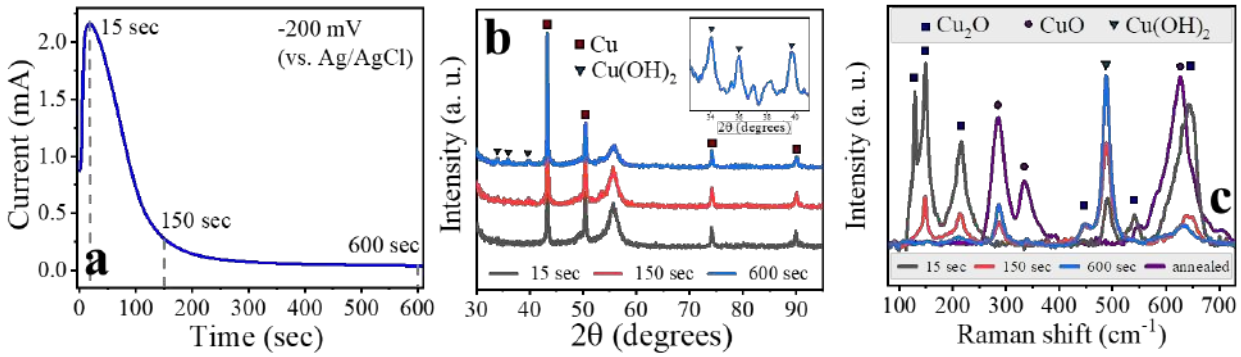

Figure 43 - (a) Amperometric curve for oxidation of copper structures on PEN surface, (b) XRD patterns, (c) Raman spectra of nano-needles on copper electrode surface

After temperature treatment of the samples for 1 hour at 130°C, the Raman spectrum contains bands mainly related to CuO (Figure 43 c), also a color change of the samples (Figure X) from blue characteristic of $Cu(OH)_2$ to black CuO is observed, while the morphology of the nano-needles remains unchanged (Figure 44).

Thus, techniques for electrochemical oxidation of copper electrodes obtained using LIS were developed. SEM, EDX mapping, XRD and Raman spectroscopy confirmed the formation of oxygen-containing copper compounds on the electrode surface and revealed the dynamics of changes in their composition and structure depending on the synthesis conditions. It was also shown that temperature treatment leads to a change in the composition of nano-needles and the formation of predominantly copper (II) oxide while preserving the morphology.

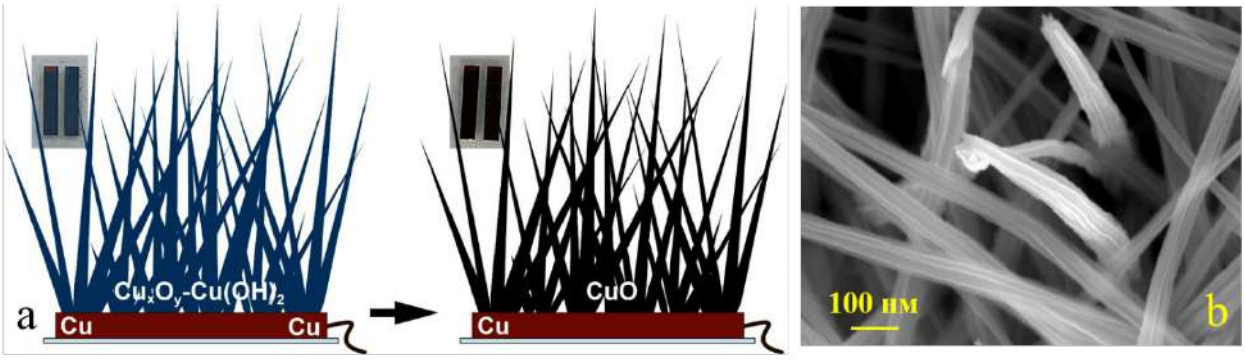

Figure 44 - (a) Schematic illustration of the process and photographs of samples before and after heat treatment, (b) SEM images of CuO nano-needles on the surface of copper electrode after heat treatment

During the research, the methods of modification of copper electrodes to improve their analytical properties were considered. Two main modification approaches were applied in the study: synthesis of gold nanostructures directly on the electrode surface using elemental copper as a reducing agent, and electrochemical oxidation of the copper electrode surface to create a surface layer of copper oxides and

hydroxides. The results obtained confirm that the selected modification methods can be effectively used to improve the functional properties of copper electrodes, since both approaches allowed obtaining promising systems while maintaining the spatial selectivity of the process and the original geometry of the electrodes.

3.1.3 Electrocatalytic activity of synthesized materials

Electrocatalytic activity toward target analytes, including D-glucose, hydrogen peroxide, and dopamine, was investigated by cyclic voltammetry and chronoamperometry.

CVs were obtained for all the studied electrodes in background electrolyte and in solution with the addition of the target analyte to determine the working potential for further potentiostatic studies by chronoamperometry. The study of the amperometric response of the synthesized electrode materials at successive increases of the analyte concentration in the background solutions allowed to plot calibration curves in the coordinates current - concentration of the analate.

In the description of the experiment, the following abbriviation of analytes and interferent agents were used Gl - glucose, H_2O_2 - hydrogen peroxide, AP – acetaminophen (paracetamol), UA - uric acid, AA - ascorbic acid, DA - dopamine.

3.1.3.1 Study of electrocatalytic activity of Cu-Au electrodes

The CV of copper electrodes in alkaline background electrolyte (0.1 M NaOH) has characteristic anodic and cathodic peaks. The CV shape is practically independent of the substrate material. All of the following potentials were measured relative to a Ag/AgCl reference electrode. Peak 1 (-0.39 V, Figure 45a) corresponds to the oxidation process in which copper Cu(0) is converted to copper (I) oxide (Cu_2O). Peak 2 (-0.15 V, Figure 45a) is associated with the formation of divalent surface oxygen-containing compounds such as CuO and $Cu(OH)_2$, where both the oxidation of Cu_2O to CuO and the direct transition of Cu(0) to Cu(II) are possible [198,199]. The sharp increase in current when the potential reaches 0.6 V is due to the onset of the water electrolysis reaction. The Cu(II)/Cu(III) transition and the formation of catalytically active species for glucose oxidation occur around the potential of 0.45 V. This peak is not pronounced, which may be due to the fact that Cu(III) species can be detected only at high concentration of hydroxide ions. The strong increase of the anodic current at 0.45 V (peak 3, Figure 45a) upon glucose addition is attributed to the electrooxidation of the analyte by the forming Cu(III) [65]. Therefore, a potential of 0.5 V relative to Ag/AgCl was chosen as the working potential for the amperometric detection of glucose. The processes described above can be illustrated as follows (reactions (1)-(6)):

Peak 1

$2Cu + 2OH^- = Cu_2O + H_2O + 2\bar{e}$ (1)

Peak 2

$Cu_2O + H_2O + OH^- = Cu(OH)_2 + e^-$ (2)

$Cu + 2OH^- = Cu(OH)_2 + 2e^-$ (3)

$Cu(OH)_2 = CuO + H_2O$ (4)

Peak 3

$Cu(OH)_2 + OH^- = CuOOH + H_2O + \bar{e}$ (5)

$CuOOH + glucose = Cu(OH)_2 + gluconolactone$ (6)

The cathodic peaks correspond to copper reduction processes (peaks 4 and 5, Figure 45a), corresponding to the Cu(III)/Cu(II) transition. In the case of glucose presence in the electrolyte, a decrease in peak 4 is observed, confirming the participation of Cu(III) in the electrocatalytic process [200,201].

The response of all the sensors to successive increases in the concentration of glucose in the background solution was studied at a constant potential by CA. Based on the collected data, calibration curves were plotted (Figure 45 c, 45 g, 46 c, 46 g, 46 g, 47 c, 47 g). In addition, the selectivity of the non-enzymatic sensors was investigated. For this purpose, the response of the electrodes in the presence of interfering substances that may be present in the real samples, including 4-acetamidophenol (AP), ascorbic acid (AA) and uric acid (UA), was investigated (Figure 45 g, 45 h, 45 h, 46 g, 46 h, 46 h, 47 g, 47 h). Selectivity studies for all electrodes were performed by sequentially adding 100 μM analyte, 20 μM of each interfering substances, and then another aliquot of analyte to a final concentration of 200 μM. All the synthesized copper electrodes were found to be highly selective and showed a much higher response at the working potential for D-glucose than for interfering substances.

Cu-Au based bimetallic systems were investigated in a similar manner (Figure 48 and Figure 49). The CVs for Cu-Au electrodes have a shape close to that of pure copper, probably due to the relatively low gold content, but nevertheless the modification of the copper electrodes allowed to significantly increase the slope of the calibration curve and consequently the sensitivity of the analysis.

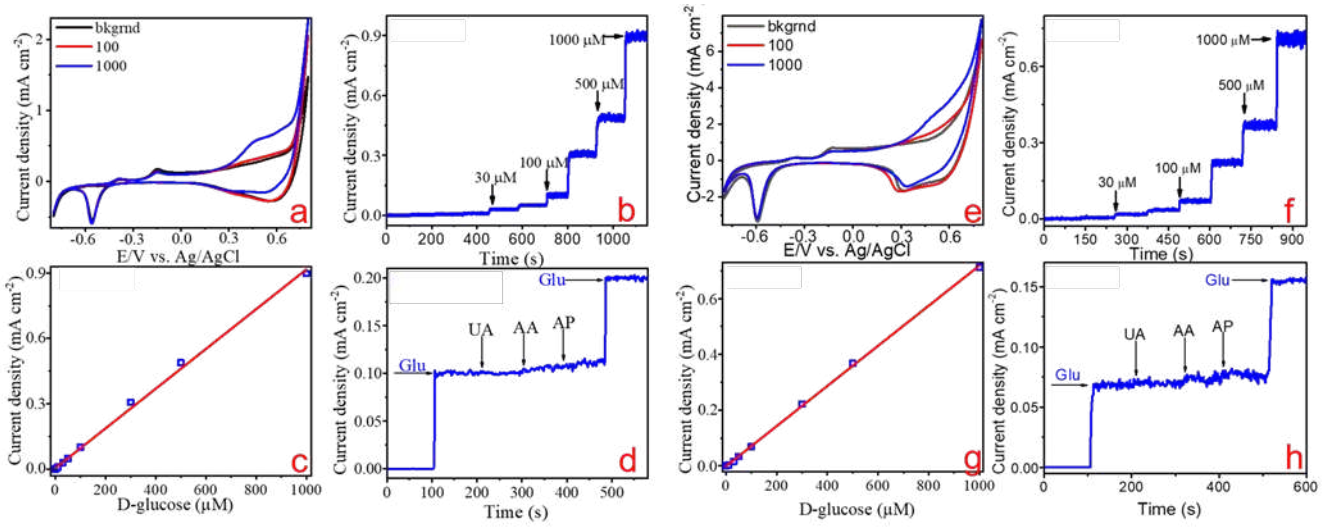

Figure 45 - CV of Cu electrode on the surface of (a) glass-ceramic, (e) glass in background electrolyte at glucose addition; amperometric response of Cu electrode on the surface of (b) glass-ceramic, (f) glass at different glucose concentrations; linear dependence of the measured current on glucose concentration for Cu electrode on the surface of (c) glass-ceramic, (g) glass; amperometric response of Cu electrode on the surface of (d) glass-ceramic, (h) glass in the study of selectivity of glucose detection

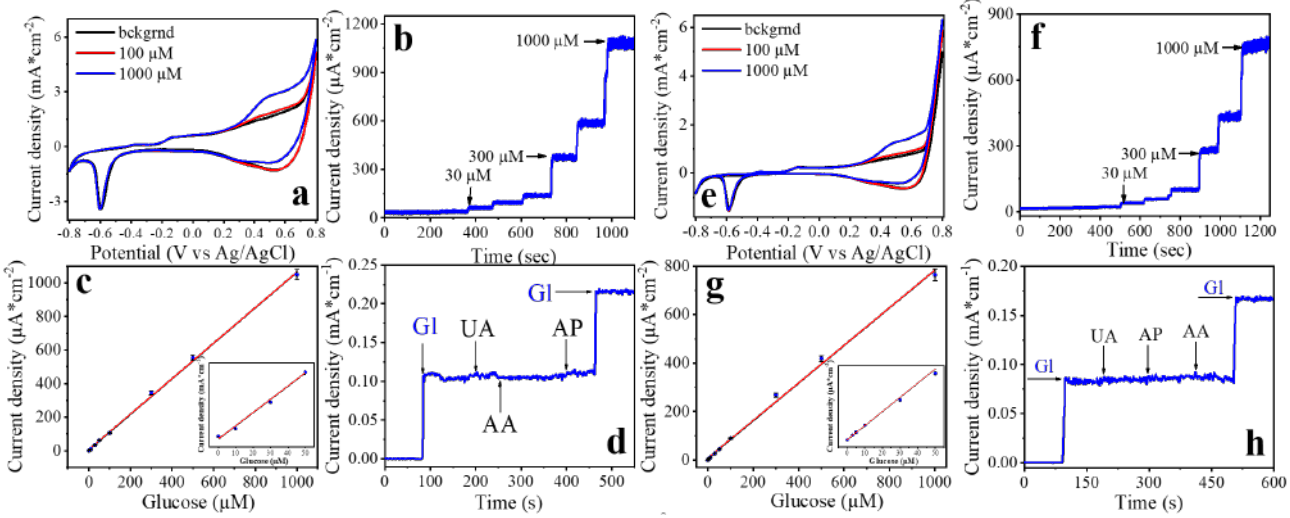

Figure 46 - CV of Cu electrode on the surface of (a) PET, (e) PI in background electrolyte at glucose addition; amperometric response of Cu electrode on the surface of (b) PET, (f) PI at different glucose concentrations; linear dependence of the measured current on glucose concentration for Cu electrode on the surface of (c) PET, (g) PI; amperometric response of Cu electrode on the surface of (d) PET, (h) PI in the study of glucose detection selectivity.

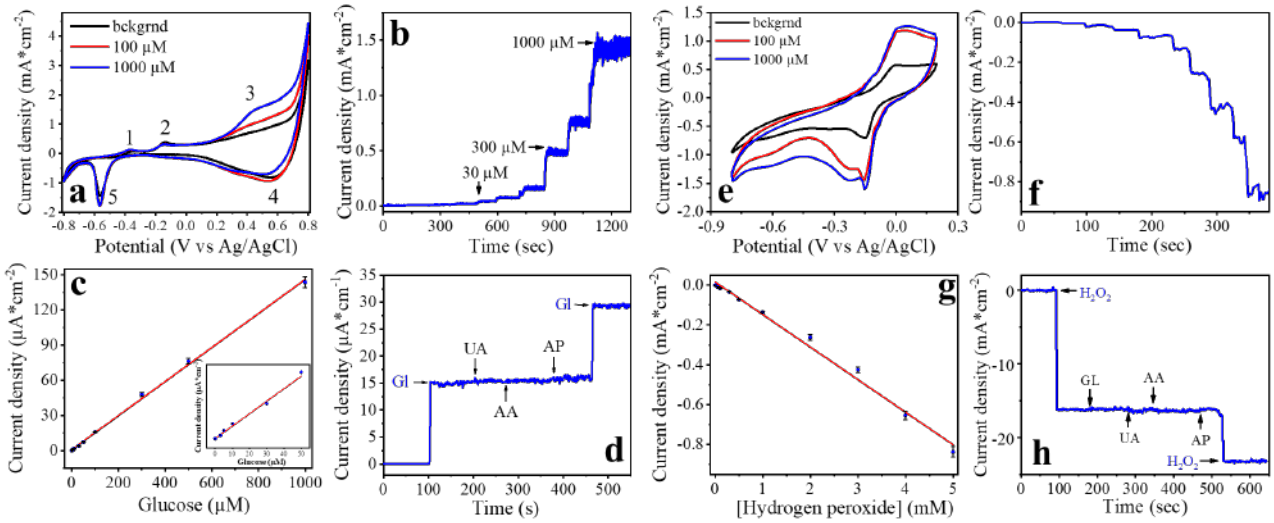

Figure 47 - CV of Cu electrode on PEN surface in background electrolyte at addition of (a) glucose, (e) hydrogen peroxide; amperometric response of Cu electrode on PEN surface at different concentrations of (b) glucose, (f) hydrogen peroxide; linear dependence of the measured current on the concentration of (c) glucose, (g) hydrogen peroxide; amperometric response of Cu electrode on the surface of PEN during the study of selectivity of detection of (d) glucose, (h) hydrogen peroxide

In addition, the electrocatalytic activity of bimetallic Cu-Au-PEN and Cu-PEN electrodes towards hydrogen peroxide was investigated (Figure 48 and Figure 49). H_2O_2 is related to reactive oxygen species (ROS) and is often used as a marker to analyze oxidative stress, which is a common cause of many life-threatening diseases [202,203]. The concentration of H_2O_2 in urine can be used as an indicator of whole body oxidative stress to regulate renal function and diagnose a number of diseases.

When conducting CV in 0.1M phosphate buffer with pH=7.0 measurements, the potential range from -0.8 V to 0.2 V was chosen, since the reduction of hydrogen peroxide according to literature data occurs in the negative potential range according to the reaction $2Cu + H_2O_2 \rightarrow Cu_2O + H_2O$ [203–206]. The study of the sensor by chronoamperometry showed an increase in current with successive increases in the concentration of analyte in the background solution in a wide range of concentrations.

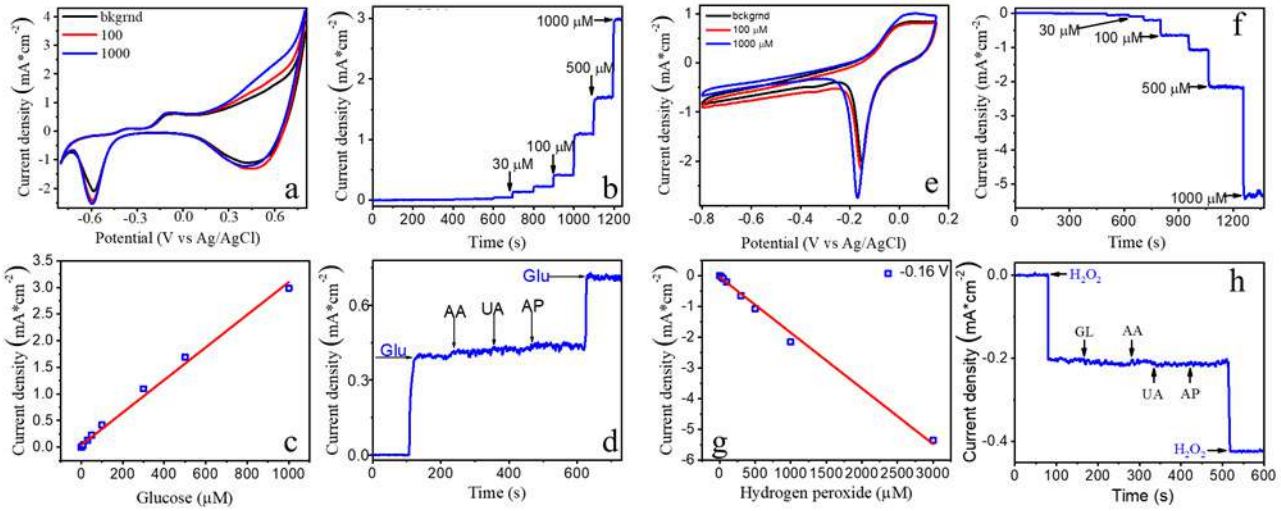

Figure 48 - CV of Cu-Au electrode on glass-ceramic surface in background electrolyte at addition of (a) glucose, (e) hydrogen peroxide; amperometric response of Cu-Au electrode on glass-ceramic surface at different concentrations of (b) glucose, (f) hydrogen peroxide; linear dependence of the measured current on the concentration of (c) glucose, (g) hydrogen peroxide; amperometric response of Cu-Au electrode on the glass-ceramic surface in the study of selectivity of detection of (d) glucose, (h) hydrogen peroxide

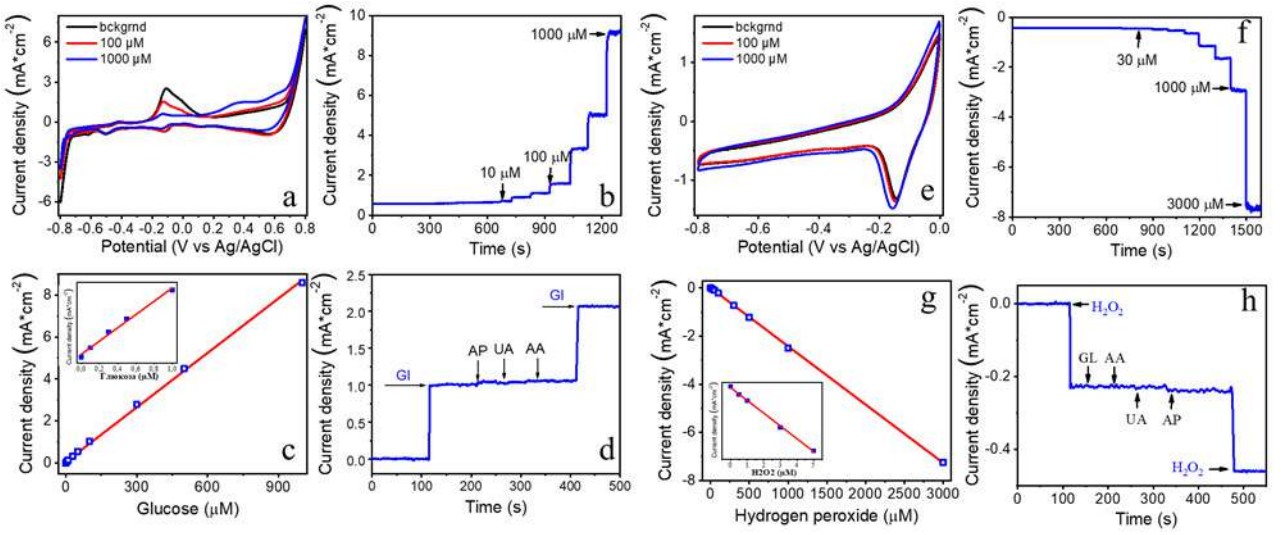

Figure 49 - CV of Cu-Au electrode on PEN surface in background electrolyte at addition of (a) glucose, (e) hydrogen peroxide; amperometric response of Cu-Au electrode on PEN surface at different concentrations of (b) glucose, (f) hydrogen peroxide; linear dependence of the measured current on the concentration of (c) glucose, (g) hydrogen peroxide; amperometric response of Cu-Au electrode on the surface of PEN during the study of selectivity of detection of (d) glucose, (h) hydrogen peroxide

The electrocatalytic activity of the synthesized materials, specifically copper and bimetallic Cu-Au electrodes, was investigated with respect to D-glucose and hydrogen peroxide. The electrodes exhibited distinct anodic and cathodic peaks in cyclic voltammetry (CV), corresponding to copper redox

processes, as well as glucose electrooxidation and hydrogen peroxide electroreduction. Bimetallic Cu-Au electrodes exhibited superior electrocatalytic activity and sensitivity towards D-glucose and hydrogen peroxide compared to their monometallic copper counterparts. This suggests that the proposed electrode modification approach is promising.

3.1.3.2 Study of electrocatalytic activity of CuO-Cu electrodes

Insoluble copper phosphates may be formed when analytes are electrooxidized on the surface of copper electrodes in neutral media with 0.1 M PBS as the background electrolyte. The salt crystals can block the active centers and reduce the reproducibility and repeatability of the analysis. The formation of oxide nanostructures on the electrode surface can prevent the presipitation of copper salts, allowing analysis in a neutral environment in a biocompatible buffer solution.

Dopamine (DA), which is one of the key neurotransmitters and plays a critical role in the functioning of a number of biological systems, including the central nervous system, was chosen as the analyte. An abnormal level of this biogenic amine is an indicator of pathological conditions of the organism, including its deficiency is associated with Alzheimer's and Parkinson's diseases, while a high level of dopamine leads to Huntington's disease [207].

The methodology of the study is similar to that described above for Cu-Au based bimetallic systems. First, CVs (Figure 50 a) were collected, followed by chronoamperometry studies (Figure 50 b, c), and then dopamine detection selectivity was evaluated (Figure 50 d). CV in background electrolyte and in the presence of analyte showed that the synthesized electrode has a pronounced response to the presence of dopamine. Amperometric measurements showed a wide linear range of current dependence on analyte concentration and no sensor response to interfering substances such as paracetamol, glucose and uric acid.

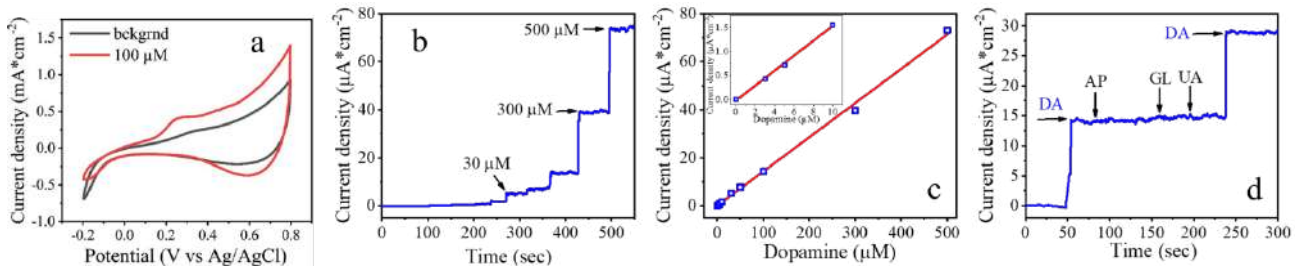

Figure 50 - CV of CuO-Cu electrode on PEN surface in background electrolyte wirh dopamine addition (a); amperometric response of CuO-Cu electrode at different concentrations of dopamine at potential 0.25 V (b); linear dependence of measured current on dopamine concentration (c); amperometric response of CuO-Cu electrode during selectivity study (d)

In addition, the stability of the analytical signal over time was investigated for the detection of glucose, hydrogen peroxide, and dopamine. Modified Cu-Au-PEN and CuO-Cu-PEN were used as working electrodes. A set of five samples of each type was used for the experiments, and a background solution with 100 μM analyte addition was used as a test system. The results showed high stability of the sensor response throughout the 21-day study period (Figure 51). Relative current density was used as a measure of signal stability, i.e., the ratio of the current density upon detection of 100 μM analyte on a given day to the initial current density. The decrease in relative current density was ~10% for all electrodes, which is satisfactory for the up-to date non-enzymatic sensors. According to the experimental protocol, each specific electrode out of five was used for analysis 11 times (every 2 days for 21 days). After the measurement, the sample was washed with sufficient water, dried by air flow and stored under room conditions. Thus, the results obtained not only show the high stability of the electrodes, but also demonstrate the possibility of their repeated use.

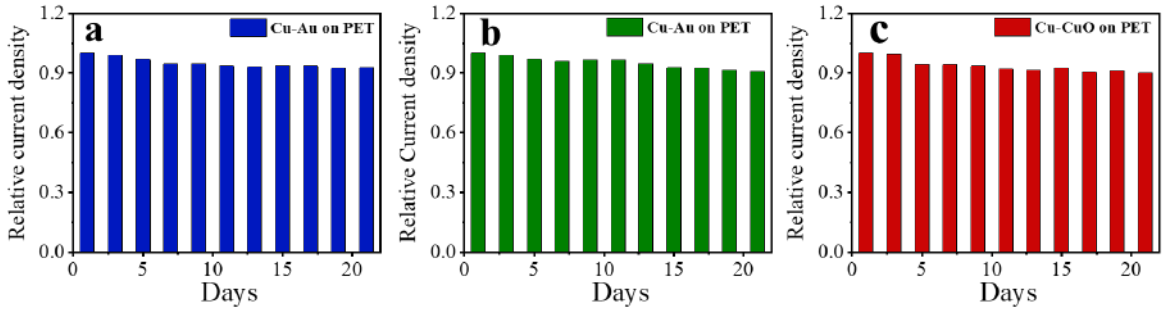

Figure 51 - Stability of the analytical signal of Cu-Au-PEN and CuO-Cu-PEN electrodes during non-enzymatic determination of (a) glucose, (b) hydrogen peroxide and (c) dopamine tested over 21 days

Repeatability and reproducibility were also evaluated using Cu-Au-PEN and CuO-Cu-PEN modified electrodes. The repeatability of the detection of glucose, hydrogen peroxide and dopamine with Cu-Au and CuO-Cu modified electrodes was checked by performing 5 consecutive measurements in the corresponding background solution containing 100 μM of analyte. The calculated relative standard deviations (RSDs) were 2.80%, 3.51% and 3.95% for glucose, H_2O_2 and dopamine, respectively, showing the high repeatability of the fabricated sensors. The reproducibility of detection of glucose, hydrogen peroxide and dopamine was studied using sets of 5 electrodes in the corresponding background solution containing 100 μM of analyte. The calculated RSDы were 1.95%, 2.03% and 2.58% for glucose, H_2O_2 and dopamine, respectively, showing the high reproducibility of the fabricated sensors.

In this work, it has been demonstrated that the developed non-enzymatic sensors exhibit excellent characteristics for their effective practical application.

Table 8 summarizes the analytical characteristics of the sensors discussed in this chapter, including data on sensitivity, detection limit, and linear concentration range. In addition, Figure 52 shows the

calibration curves of the sensors for the glucose and hydrogen peroxide detection. The data presented clearly show the increased sensitivity of the analysis when the electrodes are modified with gold nanostructures.

Table 8 - Analytical characteristics of the sensors studied in Section 3.1

Material	Analyte	Linear range, μM	Limit of detection*, μM	Sensitivity, μA $mM^{-1}cm^{-2}$
Cu-Au PEN	Glucose	0.1-1000.0	0.05	8640.0
	H_2O_2	0.5-3000.0	0.20	2420.0
Cu-Au glass-ceramic	Glucose	0.3-1000.0	0.10	3060.0
	H_2O_2	1.0-3000.0	0.30	1810.0
Cu PET	Glucose	10.0-1000.0	2.40	1050.0
Cu PEN	Glucose	3.0-1000.0	1.10	1401.0
	H_2O_2	50.0-5000.0	20.10	139.0
Cu PI	Glucose	3.0-1000.0	0.90	775.0
Cu glass-ceramic	Glucose	3.0-1000.0	0.80	911.0
Cu Glass	Glucose	10.0-1000.0	2.70	719.0
CuO-Cu-PEN	Dopamine	3.0–500.0	0.57	142.5

*Detection limit = 3σ/m, where σ is the standard deviation from linearity and m is the slope of the calibration curve.

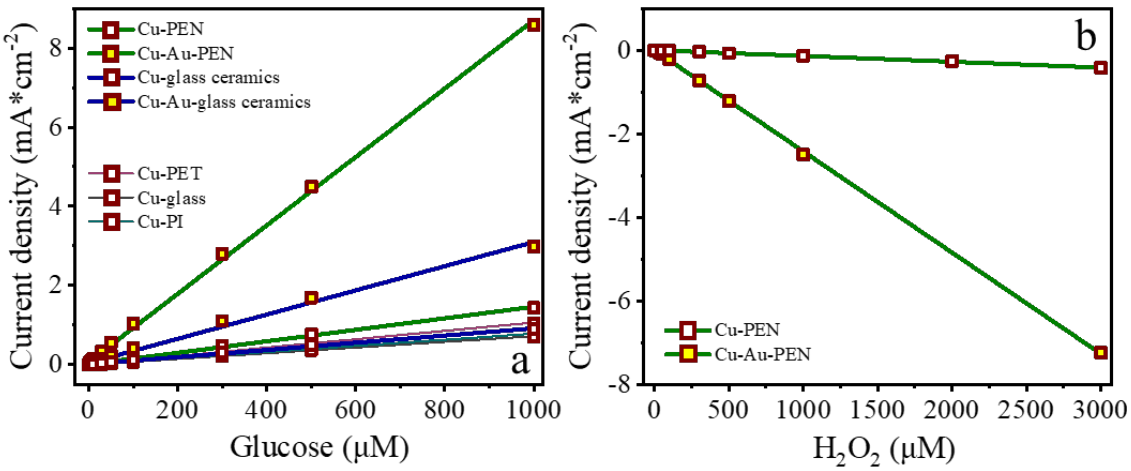

Figure 52 - Calibration curves at different concentrations of (a) glucose, (b) hydrogen peroxide

Thus, Cu-Au-PEN bimetallic electrodes show more than 8-fold increase in sensitivity compared to Cu-PEN (Figure 52). In addition, the linear range is extended to submicromolar concentrations. Similarly, the modification of copper electrodes on the surface of a rigid glass-ceramic substrate leads to a significant increase in sensitivity and an expansion of the range of detectable concentrations. In turn,

CuO-Cu-PEN composite electrodes allow the expansion of the list of analytes available for analysis, opening the possibility of dopamine detection in neutral media.

The fabricated samples have comparable electroanalytical performance to the similar sensors with respect to D-glucose, hydrogen peroxide and dopamine, which is confirmed by the literature data presented in Table 9, Table 10 and Table 11.

Table 9 - Analytical characteristics of copper-based D-glucose sensors described in the literature [117]

Material	Sensitivity, $\mu A\ mM^{-1}cm^{-2}$	Linear range, μM	Limit of detection*, μM
Cu coating	2149.1	1–4600	0.03
Cu microparticle	2432	0–4711	0.19
Cu NP	412	0–700	2.76
Cu thin coating	3643	0–811	0.59
Au NP film	749.2	55.6–13890	9.0
Pt-Cu nanochain	135	10–17000	2.5
Pt-nanoporousAu	145.7	500–10000	0.6
CuO porous film	2900	1–2500	0.14

Table 10 - Analytical performance of copper-based H_2O_2 sensors described in the literature

Material	Sensitivity, $\mu A\ mM^{-1}cm^{-2}$	Linear range, μM	Limit of detection*, μM	Reference
Cu-Au PEN	2420	0.0005–3	0.2	This work
AuCu/SPCE	133.74	0.05–10	10.93	[181]
AuCu nanowires/GCE	2710	0.000005–0.00036	0.002	[182]
CuCP-AuNPs	6800	1–2110	0.22	[208]
CG:Cu	–	0.32–0.803	0.64	[209]
Cu-MoO_2-C	144	0.25–6.25	0.16	[210]
$Cu_2O@Cu_9S_5$ yolk-shell	299.7	0.001–3.5	0.02883	[211]
Ag-Au/Cu_2O	4.16	up to 1.4	1.3	[212]

Table 11 - Analytical performance of copper-based dopamine sensors described in the literature

Material	Sensitivity, μA $mM^{-1}cm^{-2}$	Linear range, μM	Limit of detection*, μM	Technique	Reference
Cu-CuO PEN	142,5	3-500	0,57	CA*	Эта работа
CuO-MgO	69	10–100	6,4	CA	[213]
g-C_3N_4/ CuO/GCE	316	0,02–71,1	0,0001	CA	[214]
CuO-PDI-GPE	4000	5–100	0,006	CA	[215]
CuO/CN-5	331	16–78,7	0,06	DPV**	[216]
CuO nanowire/GCE	63	0,1–105	0,1	DPV	[217]

*CA - chronoamperometry, **DPV - differential pulse voltammetry

In this section of the thesis, the processes of laser-induced surface modification at the substrate-air interface followed by copper plating were investigated. It was demonstrated that laser radiation allows spatially selective modification of the substrate, thus significantly affecting the morphology and adhesion of synthesized copper structures in the area of modification. The application of LIS at the substrate-air interface allowed the spatially selective modification of a broad range of both flexible and rigid substrates. This highlights the versatility and adaptability of the proposed method. The optimal laser irradiation parameters, including power density, pulse repetition rate, scanning speed, and scanning line spacing, were determined for all investigated materials. Under optimized conditions, laser-induced surface modification led to the formation of metal structures characterized by high adhesion and low resistance. These are essential functional properties for the working electrodes of non-enzymatic sensors. The materials produced exhibit high electrocatalytic activity and selectivity under the chosen analytical conditions towards biologically relevant analytes, such as glucose, hydrogen peroxide, and dopamine.

An important result of this work is the development of techniques for the synthesis of gold and CuO nanostructures on the surface of copper electrodes. Bimetallic Cu-Au sensors exhibit high electrocatalityc activity and sensitivity to glucose and hydrogen peroxide, presumably due to the synergistic effect between these metals. The synthesized CuO-Cu sensors also showed high efficiency and stability for dopamine detection in neutral medium.

In the course of the research conducted, the following techniques were developed:

- Techniques of laser-induced synthesis at the substrate-air interface and selective copper plating of glass, glass-ceramics and flexible polymeric materials (PEN, PET, PI) have been developed. It was found that the optimal scanning speed and power density of the laser radiation of the substrate is determined by its composition. A significant difference in scanning speed between polymeric and inorganic substrates was observed, being 2 m/s for glass and 0.2 m/s for PEN, respectively.

- Methods for modifying copper electrodes through approaches such as galvanic replacement and electrochemical oxidation have been developed. These methods allowed the fabrication of Cu-Au and Cu-CuO composites. The critical parameters for the spatially selective synthesis of nanostructures on the surfaces of copper electrodes were identified as synthesis time and temperature. The ability to create sensor materials highly active towards glucose, hydrogen peroxide and dopamine based on the synthesized electrodes was demonstrated.

- The electrocatalytic properties of the fabricated materials were investigated with respect to biologically relevant analytes. It was shown that the modification of the electrodes with gold-based nanostructures significantly improves the analytical properties of the sensors. This includes a more than eightfold increase in the sensitivity of glucose analysis and a reduction of the minimum detectable concentration from 3 μM to 0.1 μM. The formation of a CuO layer on the surface of a copper electrode, in turn, allows the expansion of the list of detectable analytes, facilitating the detection of dopamine under neutral pH conditions. Therefore, it is possible to create sensor platforms with sensing activity for a wide range of analytes based on a single initial system, taking into account the modification of the electrodes.

This chapter is based on data and graphics presented in the following two publications, where the PhD candidate is the primary author [118,218]:

Khairullina, Evgeniia M; Panov, Maxim S; Andriianov, Vladimir S; Ratautas, Karolis; Tumkin, Ilya I; Račiukaitis, Gediminas;
High rate fabrication of copper and copper–gold electrodes by laser-induced selective electroless plating for non-enzymatic glucose sensing,
RSC advances, 11, 32, 19521-19530, 2021, DOI: 10.1039/D1RA01565F

Khairullina, Evgeniia M; Ratautas, Karolis; Panov, Maxim S; Andriianov, Vladimir S; Mickus, Sarunas; Manshina, Alina A; Račiukaitis, Gediminas; Tumkin, Ilya I;
Laser-assisted surface activation for fabrication of flexible non-enzymatic Cu-based sensors,
Microchimica Acta, 189, 7, 259, 2022, DOI 10.1007/s00604-022-05347-w

3.2 Laser-induced synthesis at the interface between substrate and liquid reaction medium

3.2.1 Laser-induced synthesis and modification of electrodes

As part of the further study of the interaction between laser radiation and reaction medium, the next case of LIS was laser-induced synthesis at the interface between substrate and liquid reaction medium. In contrast to the substrate-air interface discussed in Chapter 3.1, where the interaction of laser radiation and substrate material leads to its local modification, in this case the laser radiation not only modifies the substrate, but also participates in the metal ion reduction processes from the precursor solution. The localized region of the interface between the substrate and the liquid reaction medium is heated, resulting in the reduction of metal ions from the solution. This results in the direct formation of a solid metallic phase from the liquid precursor on the substrate. Such a process, facilitated by the unique conditions created by laser radiation, opens new perspectives for the creation of nanostructured materials with special properties.

Laser-induced synthesis at the interface between the substrate and the liquid reaction medium was carried out in aqueous solutions containing nickel tartrate complex as a precursor. As a result of laser irradiation of the interface between the substrate and the liquid reaction medium, the reduction of nickel ions and the formation of metallic structures occurred as the substrate moved relative to the laser beam. Due to the high thermal impact on the system required for laser-induced reduction reaction, the glass was as the substrate. Exposure to laser radiation with the power required to laser-induced reduction results in thermal destruction of polymer substrates.

The modification of electrodes in the case of laser-induced synthesis at the interface between substrate and liquid reaction medium was also performed using this approach. The versatility of LIS allows synthesizing a wide range of materials with different composition and morphology. In addition, laser-induced synthesis at the interface between substrate and liquid reaction medium allows spatially selective modification of electrode materials. Similar to the LIS described in Section 3.1, polymetallic working electrodes as part of sensors, compared to monometallic systems, can exhibit significantly higher activity in the electrocatalytic glucose oxidation process due to synergistic effects between their constituent metals. For example, bimetallic systems containing metals such as gold and platinum in combination with transition metals can significantly enhance the catalytic properties and provide higher stability of sensor activity. It should also be noted that despite the high activity of gold and platinum electrodes used for non-enzymatic detection of glucose, they have some significant disadvantages, mainly related to their high cost and their tendency to be poisoned by oxidation products and matrix components. Thus, transition metal-based electrodes modified with noble metals (including Au and Pt) can overcome the limitations mentioned above.

To obtain bimetallic electrodes, a two-step LIS technique was developed, which is based on the replacement of the precursor solution and rescanning of the presynthesized metal layer. The experimental data suggest that this approach can be extended in the future to obtain three or more component systems. Surface modification with noble metals, including gold and platinum was carried out using commercially available complexes of these metals. Since the surface morphology is one of the factors determining the electrocatalytic activity, special attention has been paid to its detailed characterization, including the development of a methodology to study the structures obtained by laser-induced synthesis using impedance spectroscopy.

The first stage of the study of LIS at the substrate-liquid reaction medium interface was to determine the optimal conditions of laser exposure for the fabrication of conductive structures based on nickel. It was shown that using an aqueous solution of nickel tartrate as a precursor allows the synthesis of continuous nickel structures. The choice of precursor was based on previous studies of LIS at the substrate-liquid reaction medium interface, where it was shown that the use of copper tartrate complexes allows the deposition of conductive nanostructured copper layers [93]. In addition, the use of tartrate complexes as precursors allowed the synthesis of conductive copper structures without the need to add extra components to the solution, including those that act as reducing agents. This approach ensures high stability of the proposed system during storage and minimizes side processes of metal ion reduction in the solution volume. Consequently, the process is localized at the interface between the substrate and the liquid reaction medium. When optimizing the synthesis conditions for obtaining continuous nickel structures with low resistance, which can be further used as working electrodes for non-enzymatic sensors, the main variable parameters were laser power density (P) in the range of 120-300 kW/cm² and scanning speed (v) in the range of 2.5-15 μm/sec. As a result of the research it was shown that the optimal synthesis conditions are laser radiation power density equal to 250 kW/cm² and scanning speed equal to 5 μm/sec. Modification of nickel electrodes with gold and platinum nanostructures was performed under the same laser irradiation conditions. According to the SEM data presented in Figure 53, the nickel electrode obtained with LIS has a nanostructured developed surface of complex morphology.

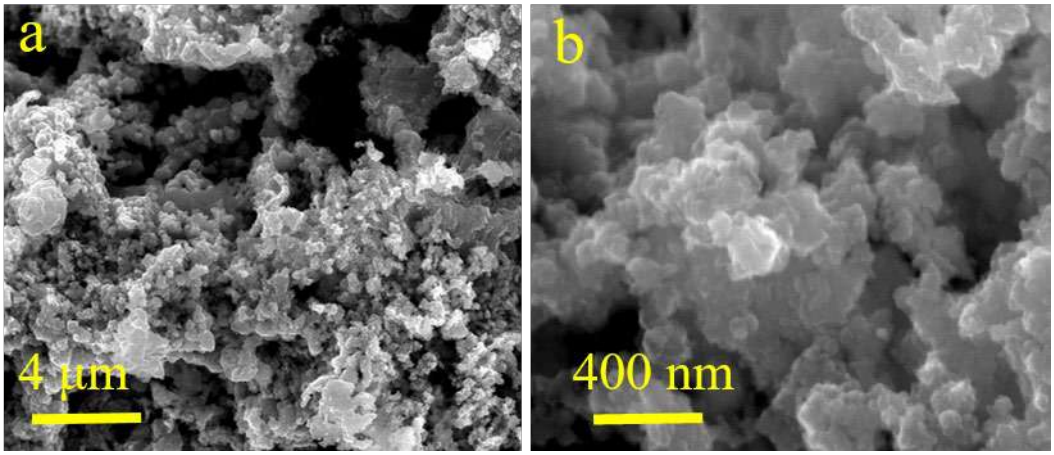

Figure 53 - SEM images of Ni structures at different magnifications

It was shown that modification of nickel electrodes with platinum- and gold-based nanostructures has a significant effect on the morphology of bimetallic electrodes (Figure 54 a-d). The porosity of Ni-Pt and Ni-Au structures was evaluated using ImageJ software package [219]. The analysis revealed that the surface of Ni-Pt electrode have a hierarchical structure and contains pores of different sizes, while the surface of Ni-Au electrode has no obvious separation between pore sizes. The average pore size of Ni-Pt electrode is smaller than that of Ni-Au, while the number of pores in Ni-Pt structure is much larger (Figure 55). Therefore, it can be concluded that Ni-Pt electrode has a more developed morphology compared to Ni-Au.

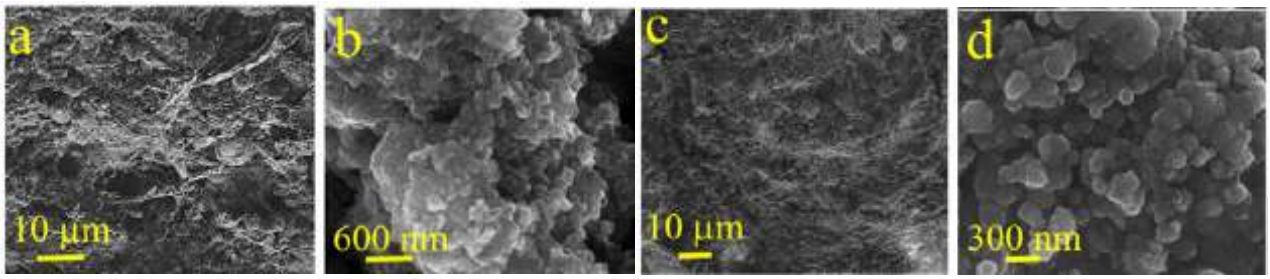

Figure 54 - SEM images of Ni-Au (a,b) and Ni-Pt (c,d)

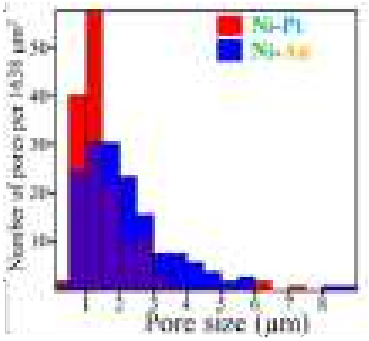

Figure 55 - Pore size distribution for Ni-Au and Ni-Pt structures

EDX (Figure 56 a, c, e) and XRD analysis (Figure 56 b, d, f) confirm the formation of Ni-Au and Ni-Pt bimetallic structures. The modification of the initial nickel structures results in its partial oxidation, which leads to the formation of a small amount of nickel oxide (NiO) while maintaining the metallic conductivity of the system. All electrodes showed conductivity higher than that for bulk metallic nickel, the electrical resistivity was ~10 Ohm, ~17 Ohm and ~19 Ohm for Ni, Ni-Au and Ni-Pt structures, respectively (length 10 mm, width 150 μm). The increase in resistance compared to bulk metallic nickel can be explained by the highly developed electrode structure. In the case of material with highly developed morphology, there is an increase in the current path due to the presence of pores, which also causes a decrease in the effective cross-sectional area of the conductor. It is also worth noting the possible contribution of contact resistance between the particles forming the structure, due to the smaller contact area and the possible presence of an oxide film on the surface of the particles. However, it is important to emphasize that the obtained values meet the requirements for working electrodes of non-enzymatic sensors and are promising for further studies of electrocatalytic activity. The increase in resistance in the Ni, Ni-Au, and Ni-Pt series can be explained by the formation of an oxide phase during repeated laser irradiation while modifying the original nickel electrode.

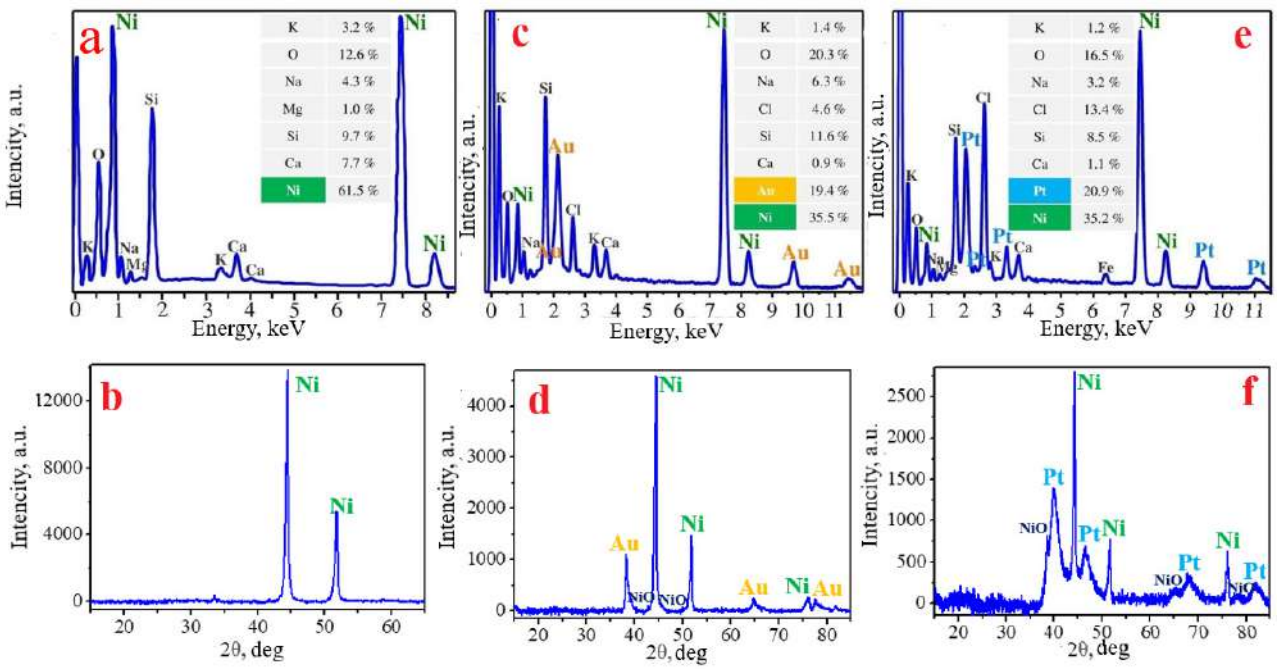

Figure 56 - EDX analysis for Ni (a), Ni-Au (c) and Ni-Pt (e) structures. XRD apatterns for Ni (b), Ni-Au (c) and Ni-Pt (f)

Within the framework of this work, it can be assumed that the mechanism of metal ion reduction from metal complexes is similar to the processes during laser pyrolysis of metal-organic frameworks,

where the destruction of organic ligands occurs with the formation of active reducing agents, including gaseous hydrogen and CO. These active compounds reduce metal ions to the atomic state, which in turn aggregate to form particles [220–222].

In addition, as mentioned above, the formation of centers capable of reducing metals from solutions of their complexes and salts can also occur on the substrate surface under the influence of laser radiation. The activity of the surface after laser irradiation can be attributed to the modification of the band structure of the dielectric, e.g. due to residual mechanical stresses resulting from the laser-induced destruction of the surface layer of the substrate [22–24].

After the reduction of ions and their aggregation with the formation of seeds on the substrate, according to the mechanisms described above, there is a change in the absorption coefficient in the laser beam impact zone due to the formation of a new metallic phase [223]. This leads to an increase in the efficiency of absorption of laser radiation by the substrate with formed metal seeds, which, in turn, contributes to a more intensive recovery of metal ions and the formation of a continuous metal layer on the substrate in the area of laser exposure. It is important to note that during surface modification, when synthesis takes place on the surface of a pre-deposited structure, it is critical to control the power density of the laser radiation to avoid destruction of the metal layer as a result of overheating.

Thus, laser-induced synthesis (LIS) of metallic structures on the substrate is a complex and multi-step process that involves a number of successive stages, starting from thermal decomposition of precursors, reduction of metal ions, nucleation, and ending with the growth of metallic structures. Each of these stages has its own characteristics and depends on a variety of parameters, including the chemical composition of the initial precursors, the type of substrate, and the laser exposure conditions such as radiation power, wavelength, pulse duration, and others. In the context of thermal LIS at the substrate-liquid reaction medium interface, general fundamental considerations applicable to a wide range of systems have been presented. However, a thorough understanding and determination of the exact reaction mechanisms requires additional studies that take into account the specificity of the selected system. The results of this work emphasize the importance of a comprehensive approach to the study of laser-induced synthesis of metallic structures and the need for further research in this area. Future experimental work may be aimed at a detailed study of the influence of laser exposure parameters and the chemical nature of the system on the mechanisms of formation and growth of metallic structures.

In addition to scanning electron microscopy, the morphology of the electrodes was also studied by impedance spectroscopy, the results of which are summarized in Figure 57 and Table 12. All the admittance spectra of the fubricated structures are approximated by the equivalent electrical circuit shown in Figure 57 d, the numerical values for the elements of the electrical circuit are presented in Table 12.

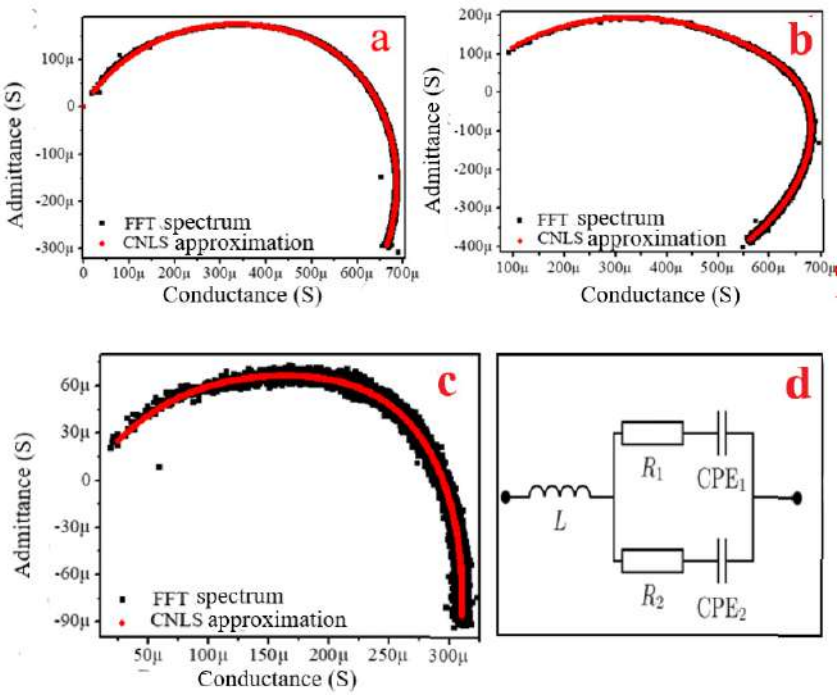

Figure 57 - Admittance spectra of (a) Ni, (b) Ni-Au and (c) Ni-Pt electrodes. (d) Equivalent electric circuit (L ~ fH - parasitic inductance caused by the time response of the ammeter).

Table 12 - Approximation results for Ni, Ni-Au and Ni-Pt electrodes, where CI is 99.9% confidence interval

		R_1, Ω	R_2, Ω	W_1 (S $s^{\alpha 1}$)	W_2 (S $s^{\alpha 2}$)	α_1	α_2
Ni	Value	2370	1840	1.31×10^{-6}	6.1×10^{-7}	0.652	0.556
	CI	60	30	5.0×10^{-8}	4.0×10^{-8}	0.005	0.08
Ni-Au	Value	1600	9000	6.3×10^{-6}	1.0×10^{-7}	0.685	0.68
	CI	30	1000	2.0×10^{-7}	4.0×10^{-8}	0.005	0.04
Ni-Pt	Value	3760	6800	9.3×10^{-7}	1.7×10^{-6}	0.5	0.588
	CI	60	300	4.0×10^{-8}	1.0×10^{-7}	exact	0.009

The impedance spectra of the synthesized electrodes can be described using capacitance dispersion because all non-ideality parameters α are significantly different from unity (Table 12). In impedance spectroscopy, the non-ideality parameter α describes deviation of electrochemical system from ideal behavior. Often the data obtained by impedance spectroscopy deviate from ideal half circles, which can be caused by electrode morphology and porosity, among other things. Unlike an ideal capacitor, whose impedance depends only on frequency and capacitance value, the impedance of constant phase element (CPE) depends on frequency, which makes it possible to describe with CPE also the porosity of the

electrode. The presence of two CPE in the equivalent circuit of an electrochemical system indicates its more complex structure than can be described by a single CPE. In the considered case this can also be related to the porosity of the electrodes. Thus one CPE can be associated with a description of the macro-level behavior of the system (e.g., total electrode porosity), while another can reflect micro-level processes (e.g., pores within pores) [224,225]. When approximating the data for Ni-Pt, α_1 was fixed at 0.5 as this value was stable for all experiments. The collected data are in agreement with the SEM results, Ni-Pt electrode has lower α values than Ni-Au based electrode. The presence of two R-CPE branches on the equivalent electrical circuit with different values of the non-ideality parameter α in the spectra of the Ni-Pt electrode can be explained by the presence of pores of different sizes on the electrode surface. The similar values of α for the Ni-Au electrode may indicate that there is no hierarchical surface structure for this electrode in contrast to Ni-Pt, whose non-ideality parameters have different values. In addition, the close values of α may indicate that the two-branch model (Figure 57 d) may be redundant for the Ni-Au electrode. The condition for this is that the ratio $R_1/R_2 = W_2/W_1$ is fulfilled when the scheme in Figure 57 g is simplified. However, the approximation data (Table 12) show that this condition is not fulfilled. In this case, the presence of two R-CPE branches for the Ni-Au electrode can be associated not only with the complex morphology of the electrode surface, but also with different resistive and capacitive properties of the electrode structural elements, which can be dictated, for example, by their elemental composition.

Biocompatibility of sensor materials becomes essential when they are used in biological systems, including invasive contact. The presence of noble metals in bimetallic sensors, including gold and platinum, significantly increases biocompatibility compared to monometallic systems [117]. In this regard, the influence of morphology and composition of nickel structures modified with gold and platinum on cytotoxicity was studied using HeLa cell lines as an example. The cells were obtained from the Cell Culture Bank of the Institute of Cytology of the Russian Academy of Sciences. Cells were seeded on the surface of synthesized electrodes and incubated for 24 hours at 37°C and 5% CO_2 concentration in Dulbecco's Modified Eagle Medium (DMEM, Dulbecco's Modified Eagle Medium) supplemented with 10% fetal bovine serum and 40 μg/ml gentamicin. Before microscopic examination, HeLa cells were treated with fluorescent dye (dibenzoazacyclooctin, DIBAC), then the cell medium was replaced with phosphate-salt buffer with the addition of propidium iodide as a dye to visualize dead cell nuclei. In a living cell, the membrane maintains its integrity and functions as a barrier to large molecules, including propidium iodide. When membrane integrity is compromised, propidium iodide binds to DNA, greatly increasing its red fluorescence. Images of the cells were acquired on a Leica DMB-4000 microscope and are presented in pseudo-color (Figure 58). Pseudocolored images were obtained as a superposition of three photographs: 1) taken in visible light in transmitted light mode (gray scale,

membrane imaging); 2) DiBAC fluorescence (green channel); and 3) propidium iodide fluorescence (red channel).

As can be seen from the presented data (Figure 58), the synthesized Ni-Au and Ni-Pt electrodes are non-toxic, since live cells were preserved on their surface as a result of testing. The live cells show green coloration, while the dead cells show yellow coloration due to the appearance of a red color channel from propidium iodide fluorescence. However, the Ni-Au-based electrode has much higher biocompatibility than the Ni-Pt electrode, which is probably due to the more complex morphology of the Ni-Pt surface, as well as the material composition, since Pt NPs are more prone to exhibit cytotoxic effects compared to Au NPs [226].

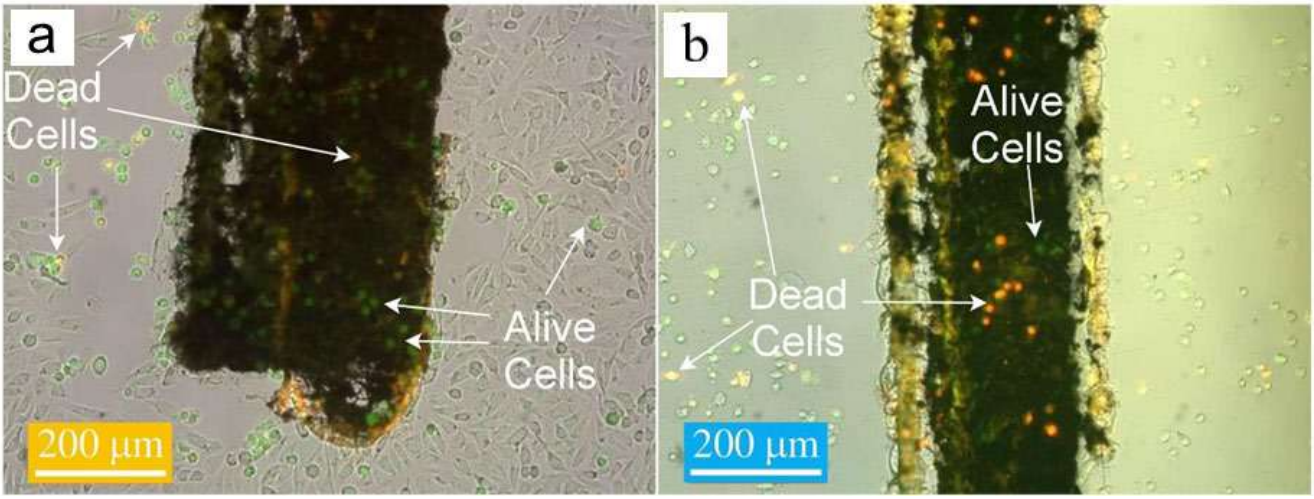

Figure 58 - Microscopic photographs of Ni-Au (a) and Ni-Pt (b) electrodes taken during biocompatibility study

3.2.2 Study of electrocatalytic activity of synthesized materials

Electrocatalytic activity toward D-glucose was investigated by cyclic voltammetry and chronoamperometry. All potentials shown below were measured relative to a Ag/AgCl reference electrode.

The CV of the nickel electrode (Figure 59 a) in 0.1 M NaOH background electrolyte has characteristic anodic and cathodic peaks. The electrochemical behavior of the nickel electrode in highly alkaline medium is similar in many respects to the copper electrode described earlier. The catalytically active species, as in the case of copper, are Ni^{3+}. The redox processes are reflected in the peaks 1 and 2 on the CV (Figure 59 a) [227,228]. Modification of the nickel surface with platinum and gold leads to an increase in the area under the CV curve, which is an indirect indicator of a highly developed surface in view of the increase in the capacitive component of the current. Figure 59 b shows the CV for Ni-Pt

electrode obtained in the background electrolyte containing 100 μM and 1000 μM D-glucose. It is possible to note a gradual increase in the oxidation current with increasing glucose concentration in the solution, which indicates the presence of electrocatalytic activity of the electrode in relation to glucose. Further electrocatalytic activity studies were performed using chronoamperometry (Figure 59 c). The Ni and Ni-Pt based electrodes show two linear regions of the calibration curve (Figure 59 d) unlike the Ni-Au electrode which has only one region of linearity. In the first linear region, the amperometric current increases rapidly with increasing glucose concentration, whereas in the second linear region, the growth of the analytical response slows down. This behavior correlates with the assumption of the presence of different types of pores on the hierarchical surface of Ni and Ni-Pt electrodes. The decrease in sensitivity at higher glucose concentrations may be due to stronger adsorption of intermediates and partial blocking of the electrode active centers [229]. It should be noted that the Ni-Pt electrode with the most developed surface shows the highest sensitivity among all synthesized materials within the range of glucose concentration up to 300 μM (Figure 59 d). Also, all investigated nickel-based electrodes demonstrated a much higher amperometric response to glucose than to potential interfering substances, indicating sufficient selectivity of the analysis. In addition, the stability of the response of the synthesized electrodes over time during storage under room conditions for 1 month was investigated (Figure 59 e). The relative current density I_x/I_0 was used as an evaluation parameter, where I_x and I_0 are the current densities exhibited by the synthesized electrodes upon addition of 100 μM D-glucose, recorded on day x and the day of the beginning of the experiment, respectively. It was found that modification of the Ni electrode surface with precious metals significantly improved its stability, such that the relative current density of the Ni-Pt electrode was maintained above 85% of its initial value for 1 month.

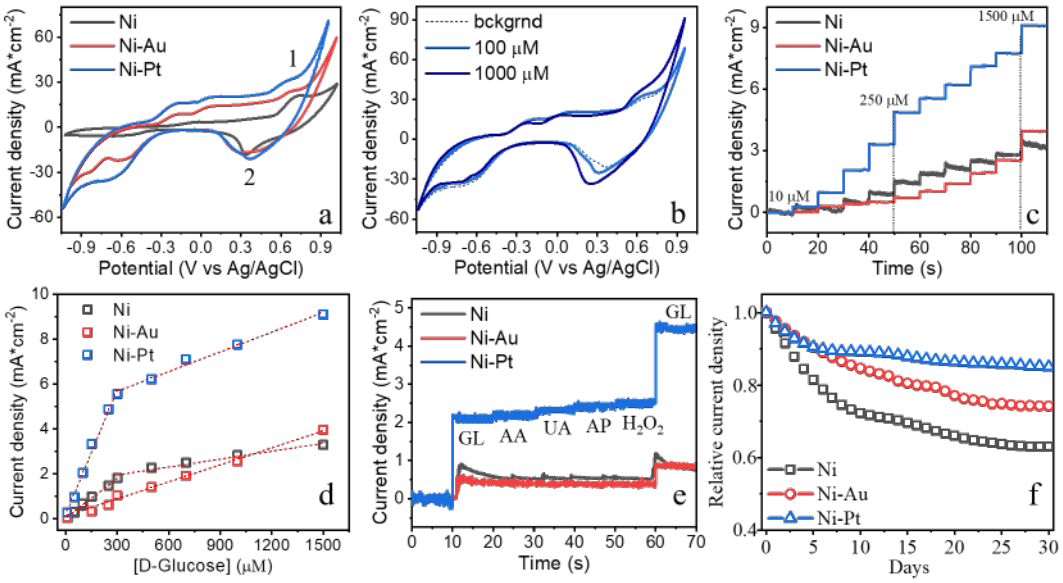

Figure 59 - (a) CV of synthesized electrode materials taken in 0.1 M NaOH. (b) CV of Ni-Pt electrode taken in background solution with D-glucose additives; (c) Amperometric response of the synthesized electrodes in the presence of different concentrations of D-glucose at potentials of 0.60 V (for Ni), 0.64 V (for Ni-Au) and 0. 62 V (for Ni-Pt), respectively; (d) Calibration relationships for non-enzymatic detection of D-glucose on Ni, Ni-Au and Ni-Pt electrodes; (e) Selectivity of the synthesized materials upon sequential addition of 100 µM D-glucose (GL), 30 µM ascorbic acid (AA), 30 µM uric acid (UA), 30 µM 4-acetamidophenol (AP) and 30 µM hydrogen peroxide (H2O2). (e) Stability of Ni-based electrodes during the determination of 100 µM D-glucose

Oxidation of glucose using nickel and other transition metal catalysts involves redox reactions between metal hydroxides and their oxyhydroxides (in the case of nickel $Ni(OH)_2$/NiOOH) [66]. The mechanism of glucose electrooxidation on the surface of the nickel electrode is as follows: catalytically active NiOOH is reduced to $Ni(OH)_2$ at the expense of the hydrogen atom detached from the C1 atom of glucose, glucose in turn is oxidized to gluconolactone with subsequent hydrolysis to gluconic acid. Thus, the possible reactions occurring during the electrooxidation of glucose under alkaline conditions on the surface of Ni electrodes modified with Au and Pt can be represented as follows [66,117,119,230]:

$$Ni + 2OH^- = Ni(OH)_2 + 2\bar{e} \quad (1)$$

$$Ni(OH)_2 + OH^- = NiOOH + H_2O + \bar{e} \quad (2)$$

$$NiOOH + glucose = Ni(OH)_2 + gluconolactone \quad (3)$$

$$Au + OH^- = AuOH + \bar{e} \quad (4)$$

$$AuOH + glucose = Au + gluconolactone \quad (5)$$

$$Pt + 2OH^- = Pt(OH)_2 + 2\bar{e} \quad (6)$$

$$Pt(OH)_2 + glucose = Pt + gluconolactone \quad (7)$$

Figure 60 illustrates the possible mechanism of glucose electrooxidation on the Ni-Pt surface considering the reactions presented above.

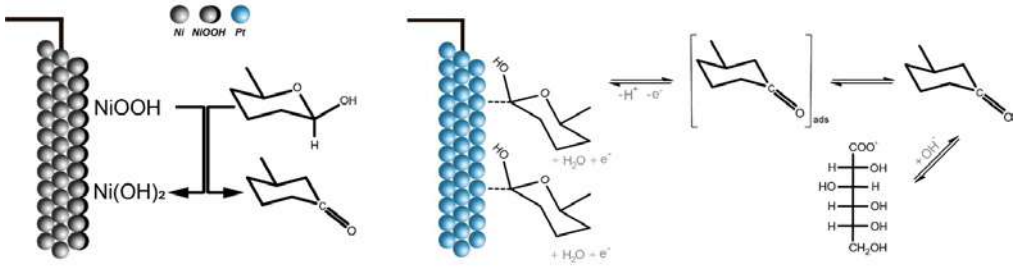

Figure 60 - Possible mechanism of glucose oxidation on the surface of Ni-Pt electrode

According to the CVs (Figure 59 b), as well as on the basis of literature data [117,119,231] and reactions (1)-(7), several potential windows can be distinguished. The window of potentials below -0.10 V with anodic peaks at -0.21 and -0.19 V for Ni-Pt and Ni-Au electrodes, respectively, corresponds to the dehydrogenation of the glucose molecule involving hydrogen at the hemiacetal carbon atom (C1). The second potential region is located between -0.10 and 0.48 V (for Ni-Pt and Ni-Au) and between -0.20 and 0.43 V (for Ni). The anodic peaks centered at 0.09, 0.08, and -0.06 V observed for Ni-Pt, Ni-Au, and Ni, respectively, correspond to the electrooxidation of the chemisorbed species. Here, the dissociation of water is accompanied by the release of hydroxide anions, which adsorb on the electrode surface, forming a catalytic hydroxide pre-monolayer (Equations (4) and (6)). The latter accelerates the electrooxidation of chemisorbed glucose by the reactions presented in equations (3), (5) and (7). In the third potential region, the anodic peaks with centers of 0.62 V (for Ni-Pt), 0.64 V (for Ni-Au), and 0.60 V (for Ni) are associated with further oxidation of glucose from solution to form gluconolactone and then gluconic acid. As for the pure Ni electrode, in alkaline medium, nickel exists in the form of hydroxide according to equation (1), which then enters the redox reaction to form catalytically active Ni(III) oxyhydroxide (equation (2)).

The analytical characteristics of the synthesized non-enzymatic nickel-based sensors are presented in Table 13. Table 14 also lists the parameters of some similar systems described in the literature. Based on the data presented, it can be concluded that Ni-Pt has a number of advantages over its comparable analogs, mainly related to its high sensitivity and low detection limit. It has been found that bimetallic sensors show a stable synergistic effect, resulting in higher electrocatalytic activity due to various electronic effects as well as the presence of a larger number of active centers [232,233]. The higher catalytic activity of the Ni-Pt electrode may also be related to the more developed morphology of this material.

Table 13 - Analytical characteristics of the electrodes studied in Section 3.2

Material	Linear range, μM	Limit of detection*, μM	Sensitivity, μA $mM^{-1}cm^{-2}$
Ni	10–300 and 300–1500	0.09 and 0.32	5953 and 1180
Ni-Au	10–1500	0.12	2542
Ni-Pt	10–300 и 300–1500	0.14 и 0.19	18570 и 2929

**Detection limit = 3σ/m, where σ is the standard deviation from linearity and m is the slope of the calibration curve.*

Table 14 - Analytical performance of nickel-based D-glucose sensors described in the literature

Material	Linear range, μM	Limit of detection*, μM	Sensitivity, μA $mM^{-1}cm^{-2}$	Reference
Ni nanowire arrays	0.5–7000	0.1	1043	[234]
Ni nanoparticles on straight multi-walled carbon nanotubes	1–1000	0.5	1438	[235]
Ni nanoparticles/porous carbon	15–6450	4.8	207.3	[236]
Au/Ni multilayer nanowire array	0.25–2000, 2000–5500	0.1	3372. 1906	[237]
AuNi nanodendrite arrays	5–15000	3	3727.7	[238]
PtNi alloy nanocatalysts on carbon	2–420	1	1795.1	[239]
Pt-Ni nanoclusters	0–15000	0.3	940	[240]
PtNi nanoparticle-graphene nanocomposites	0–35000	10	20.42	[241]

In this part of the thesis, the LIS process at the interface between the substrate and the liquid reaction medium has been studied. The main advantage of this method is identified as the direct reduction of metal ions from the precursor solution under the influence of laser radiation. It is hypothesized that the mechanism of reduction of metal ions from metal complexes under LIS is similar to the phenomena observed during laser pyrolysis of metal-organic frameworks, where the destruction of organic ligands and the subsequent formation of active reducing agents are considered crucial. However, since these processes occur at the interface between the substrate and the reactive medium, the formation of defects on the substrate due to laser irradiation is also considered important. These defect states are believed to contribute to the reduction of metal ions and the nucleation of the metal phase. This approach, based on laser-induced thermal reactions, is highlighted for its ability to facilitate

the synthesis of a wide variety of materials using simple, commercially available precursors and a single laser source of fixed wavelength. In addition, the potential for spatially selective modification of electrode materials is emphasized, opening broad prospects for the development of polymetallic systems with enhanced electrocatalytic properties. The modification of nickel electrodes with nanostructures derived from noble metals (gold and platinum) has been shown to significantly enhance the electrocatalytic activity towards D-glucose.

The following observations were made during the research:

- The processes of laser-induced synthesis at the interface between substrate and liquid reaction medium were investigated. This led to the development of methods for the synthesis of Ni electrodes and their laser-induced modification with gold (Au) and platinum (Pt) nanoparticles. It has been shown that Ni-Pt electrodes exhibit a hierarchical structure, while the surface of the Ni-Au electrode has no obvious separation between pore sizes.

- The biocompatibility and electrochemical properties of the synthesized electrodes were investigated. It was found that Ni-Au based electrodes, with a less developed surface, exhibited higher cell adhesion compared to those of Ni-Pt. Conversely, a different trend was observed in terms of electrocatalytic activity. Among the materials discussed, the Ni-Pt electrode was shown to have the best performance. For the Ni-Pt electrode, the linearity range of the calibration curve for D-glucose was determined to be between 10-300 μM and 300-1500 μM, with the sensitivity of 18,570 and 2,929 μA mM^{-1} cm^{-2}, respectively.

This chapter is based on data and graphics presented in the following publication, where the PhD candidate is the primary author [170]:

Khairullina, Evgeniia M; Tumkin, Ilya I; Stupin, Daniil D; Smikhovskaia, Alexandra V; Mereshchenko, Andrey S; Lihachev, Alexey I; Vasin, Andrey V; Ryazantsev, Mikhail N; Panov, Maxim S;

Laser-assisted surface modification of Ni microstructures with Au and Pt toward cell biocompatibility and high non-enzymatic glucose sensing,

ACS omega, 6 ,28 ,18099-18109, 2021, DOI 10.1021/acsomega.1c01880

3.3 Laser-induced synthesis at the interface between substrate and solid reaction medium

In the final part of the experimental study of the processes of laser-induced synthesis of metallic structures, special attention is paid to the study of LIS at the interface between substrate and solid reaction medium. This topic is a continuation of the study of the interaction of laser radiation with

various reaction media discussed in the previous Chapters 3.1 and 3.2. In LIS at the interface between substrate and solid reaction medium, the formation of metallic structures occurs directly under the influence of laser radiation, similar to the liquid medium. However, the chemical processes underlying this phenomenon have significant differences due to the use of metal oxide nanoparticles as precursors. In addition, the precursor film can reduce the thermal effects of laser irradiation on the substrate, which can complicate the modification of the substrate to achieve high adhesion with the synthesized material. In this regard, an important part of the work is the careful optimization of laser irradiation parameters, such as power density and scanning speed, as well as the investigation of possible ways to improve the adhesion of synthesized materials to the substrate.

Laser-induced synthesis at the interface between substrate and solid reaction medium was carried out using oxide nanoparticles as a precursor. This approach is based on the local interaction of laser radiation and a film of oxide nanoparticles, which leads to their complete or partial recovery and the formation of nanostructured electrode materials on the substrate. The target materials were Ni and Cu, the corresponding commercially available oxide nanoparticles of the aforementioned metals were used as the precursors. In order to fabricate electrodes with the required functional properties, including electrical conductivity, high adhesion and developed surface area, a fine-tuning of the laser-induced synthesis parameters is required with respect to both laser exposure parameters (power, scanning speed) and surface preparation as well as precursor composition.

The optimal precursor composition for laser-induced synthesis of electrodes at the interface between substrate and solid reaction medium was determined and is presented in Table 15. The determining parameters were viscosity and nanoparticle concentration, which allow obtaining uniform precursor films on the substrate by spincoating.

Table 15 - Precursor composition for laser-induced synthesis at the interface between substrate and solid reaction medium

Component	**CuO / NiO NP**	**PVP***	**EG****
Mass, g	3 / 1.5	0.65	1.35

** Polyvinylpyrrolidone, ** ethylene glycol*

On the example of glass-ceramic substrate, it was shown that the main parameters that determine the composition and morphology of materials during laser-induced synthesis at the interface between substrate and solid reaction medium are the laser radiation power density (P), scanning speed (v) and the distance between scanning lines (h). The ranges of variation of these parameters are presented in Table 16. The limits of the ranges were chosen taking into account previous studies on the process of laser-induced reduction of copper oxide nanoparticles [104]. Thus, by varying these parameters v and h, one

can effectively control the properties of electrode materials and create systems with different functional properties. Since this work is aimed at synthesizing electrochemically active materials and studying their properties, the determining parameters were developed morphology and low electrical resistance. Based on these requirements, optimization of v and h parameters was carried out.

Table 16 - Parameters of laser-induced synthesis at the substrate-air interface

Substrate	Scanning speed (v), mm/s	Distance between lines (h), μm	Power density (P), kW/cm^2
Glass-ceramics	1–10	5–10	45–57

Based on scanning electron microscopy data (Figure 61), it can be concluded that increasing the line spacing and scanning speed at a fixed power density of 57 kW/cm^2 leads to an insufficient thermal effect on the precursor film, resulting in the formation of nonconductiv structures with numerous defects. On the other hand, too low scanning speed promotes the formation of structures with smooth morphology due to more complete fusion of initial precursor particles under the action of laser radiation, which leads to a decrease in the surface area and available active electrocatalytic centers. Thus, the most optimal parameters are h=5 μm and v=5 mm/s at P = 57 kW/cm^2.

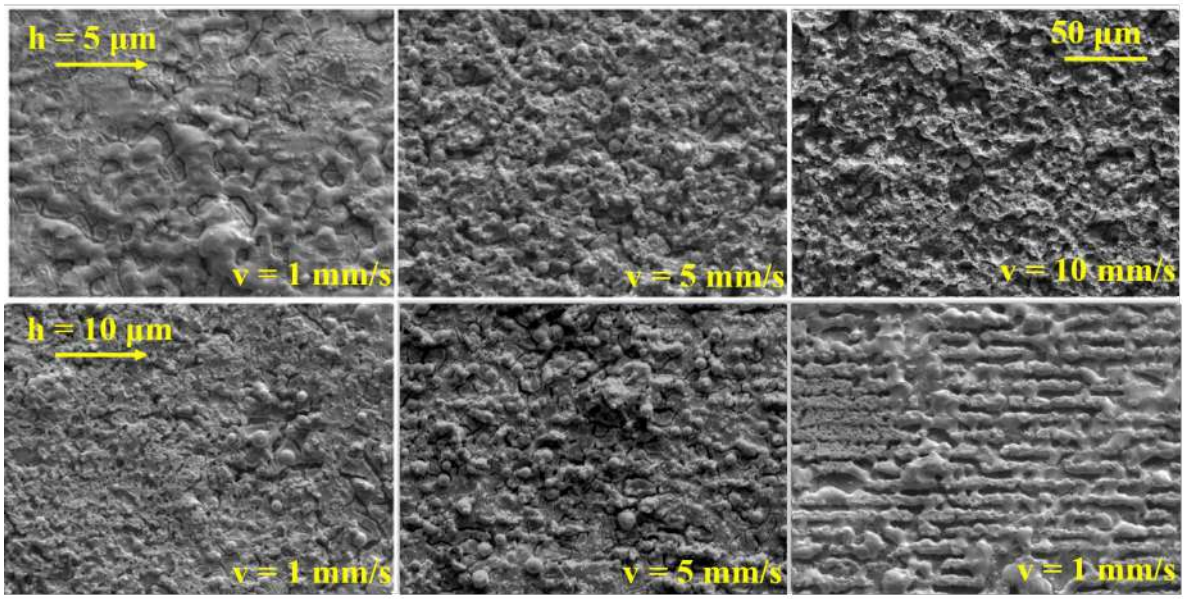

Figure 61 - SEM images of structures on the glass-ceramic surface at different scanning speeds and line spacing (corresponding h and v are indicated on the image)

In addition, it was shown that a decrease in the radiation power density to 45 kW/cm2 leads to deterioration in the morphology of the samples, including the formation of visible discontinuities due to incomplete fusion of particles and washout of the latter after synthesis (Figure 62). Thus, detailed

analysis of SEM images showed that the most optimal conditions for obtaining the structures are the following: LR power density 57 kW/cm^2, scanning speed 5 mm/s, line spacing 5 μm. The obtained materials possess a developed highly porous surface. XRD pattern showed (Figure 62 c) that the structures synthesized under optimal conditions contain metallic copper and oxide phase, which can be a product of incomplete reduction of the initial particles or formed as a result of reoxidation. Data on the composition of materials obtained by X-ray diffraction are in agreement with EDX (Figure 62 a, b). It can be concluded that the LIS process at the substrate-solid reaction medium interface favors the formation of composite structures based on copper and its oxides, which exhibit metallic conductivity. Taking into account the mechanism of glucose oxidation described in Section 1.4, copper oxide also exhibits high electrocatalytic activity with respect to this analyte, which indicates the prospect of further application of the fabricated materials as working electrodes for non-enzymatic sensors.

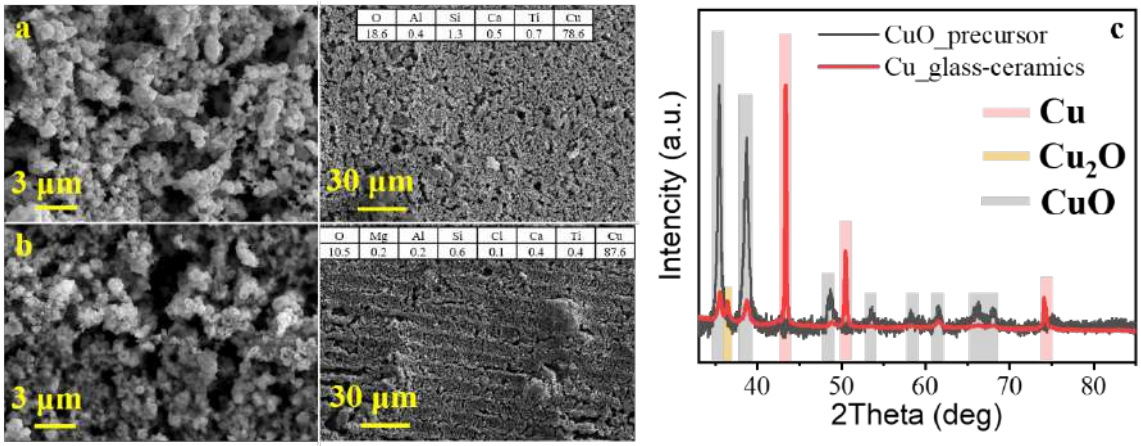

Figure 62 - SEM images and EDX analysis results (upper right corner in each panel) of Cu-Cu_xO_y structures fabricated at power densities of (a) 57 kW/cm^2 and (b) 45 kW/cm^2; (c) XRD patterns of Cu-Cu_xO_y structures and the original precursor film

Similar studies were carried out using nickel oxide nanoparticles as a precursor. Analysis of SEM images of nickel structures on the glass-ceramic surface showed that the most homogeneous metal layer is obtained also by the laser radiation power density equal to 57 kW/cm^2 (Figure 63). Elemental analysis showed that the main component of the structures is nickel, the remaining elements are related to the glass-ceramic substrate. X-ray diffraction showed the formation of metallic nickel phase with minor oxide impurities, as in the case of copper (Figure 63 e).

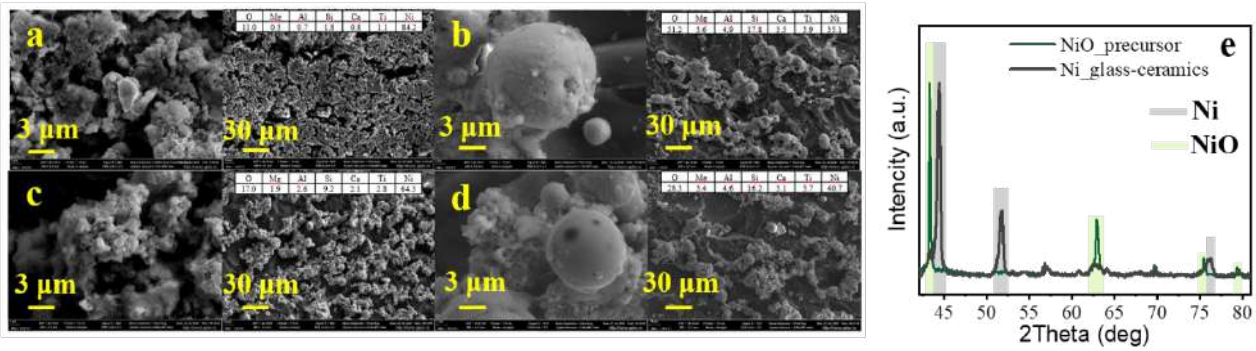

Figure 63 - SEM images and EDX analysis results (upper right corner in each panel) of Ni-NiO structures at laser power density (kW/cm^2) and scanning speed (mm/s): (a) 57 and 5; (b) 45 and 5; (c) 57 and 10; (d) 45 and 10; (e) XRD patterns of Ni-NiO structures and the original ink film

In addition, the parameters of laser-induced synthesis of electrodes on the surface of flexible polymers PET, PEN, and PI were optimized. The optimal scanning speed and line spacing, as in the case of glass-ceramics, were 5 µm and 5 mm/s, respectively. The results of SEM examination of the materials suggest that the samples have a highly developed nanostructured surface formed by sintered nanoparticles (Figure 64). The X-ray phase composition showed that the main phase of the material is metallic copper, the presence of reflexes corresponding to oxide components can be explained by incomplete reduction of the initial particles and oxidation of the surface after synthesis. As a result of the conducted studies on the surface of various substrates, a tendency to decrease the laser radiation power density required for the reduction and fusion of initial NPs to obtain conductive continuous structures was revealed. This effect can be explained by the lower thermal conductivity of polymeric materials compared to glass-ceramics (Table 17) [176].

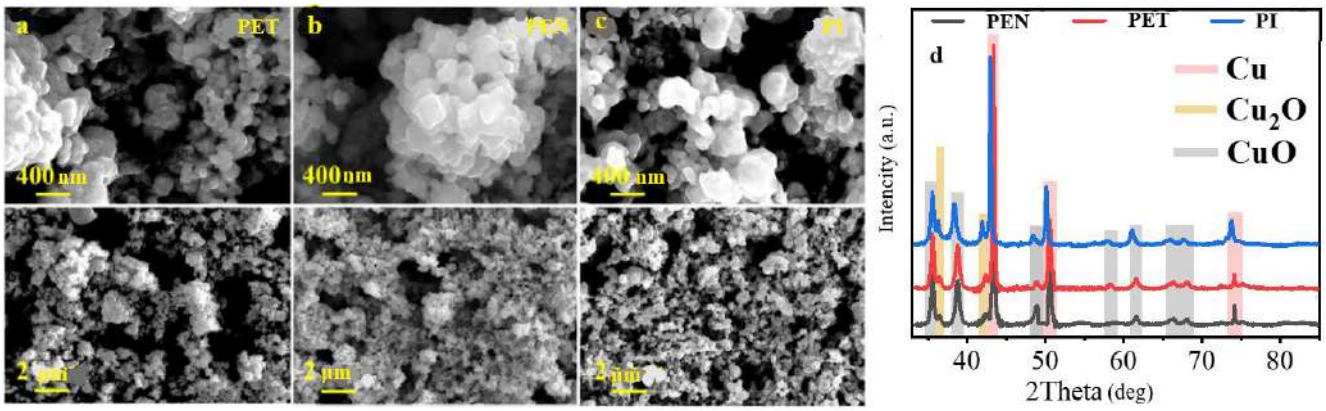

Figure 64 - SEM images of the structures on the surface of (a) PET, (b) PEN, (c) PI and (d) XRD patterns of Cu-Cu$_x$O$_y$

Table 17 - Laser exposure conditions for laser-induced synthesis at the interface between substrate and solid reaction medium on different substrates

Substrate	PET	PEN	PI	Glass-ceramic
Power density, kW/cm^2	35	38	40	57

The considered system based on ethylene glycol as a reducing agent and polyvinylpyrrolidone (PVP) as a stabilizer is a widely studied precursor for LIS at the substrate-solid reaction medium interface. At present, the mechanism of the reduction reaction is still under investigation, the following mechanism can be considered as the most probable one [242]:

$$2HO(CH_2)_2OH \xrightarrow[-2H_2O]{\Delta} 2C_2H_4O \xrightarrow{M\ (II)} C_4H_6O_2 + H_2O + M$$

In the process of ethylene glycol dehydration, acetaldehyde is formed, which can reduce copper oxide nanoparticles to copper nanoparticles.

Due to the high flexibility of the laser-induced synthesis process at the interface between the substrate and solid reaction medium, taking into account the optimized parameters, it is possible to obtain structures of any given geometry. Such structures can be used as working electrodes of non-enzymatic sensor platforms (Figure 65 a). Also in the future it is possible to create printed electrodes, where all functional electrodes are made with the help of LIS (Figure 65 b). These kinds of systems allow for rapid analysis in small volumes. The approach proposed in the study shows significant advantages compared to the traditionally used in scientific and industrial practice printed electrodes, especially in terms of flexibility and adaptability to changes in analytical tasks. The advantages of the proposed approach are particularly important in the development of portable analytical devices where the ability to rapidly change electrode parameters without significant time and cost is required.

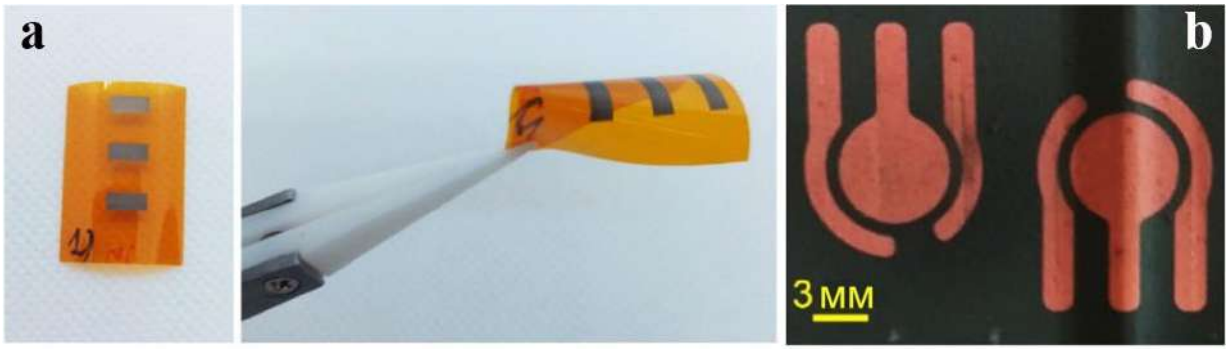

Figure 65 - Photographs of (a) Ni-NiO and (b) Cu-Cu_xO_y electrodes fabricated on the surface of polyimide (black background corresponds to the area not exposed to laser irradiation prior to the unirradiated ink removal procedure).

3.3.2 Modification of electrodes

Synthesizing colloidal nanoparticles allows producing metal particles with high control over their size and shape [243]. This control is achieved by careful selection of synthesis conditions, including the concentration of reagents, temperature, reaction time, and the choice of stabilizing agents. This approach is a powerful tool that enables the creation of new nanomaterials with unique properties for a wide range of applications, including high-performance non-enzymatic sensors. Nanoparticles with complex morphologies, including nanocages [244,245], have highly developed surfaces and an even higher relative content of surface atoms than traditional cubic or spherical particles. This shape allows access for analyte molecules to the active sites of the particles, which can lead to enhanced electrocatalytic properties towards the target analyte [246].

Thus, electrode modification with nanoparticles can significantly increase the surface area of the working electrode. This approach is intensively investigated as a way to modify a common glass-carbon electrodes [117]. However, the literature data regarding electrodes obtained by laser-induced synthesis at the substrate-solid reaction medium interface are very limited. Moreover, taking into account the range of electrode-modifier combinations that can be obtained, the deepest field of research opens up. In this work, we developed a methodology for the synthesis of gold nanoparticles with core-cage structure, which are hollow NPs with a core inside and perforated framework-like walls. The technique was developed based on scalable colloidal synthesis using cationic surfactants to stabilize the system [247]. This approach compared to the polyol method [248] avoids the use of high temperatures and the hard-to-remove stabilizer poly(vinylpyrrolidone), which can block some of the active centers. The control of the shape of the nanostructure core was achieved by regulating the reaction kinetics and using anions that promote the formation of certain crystallographic facets [249]. In particular, octahedral Au NPs were synthesized with in the presence of bromide ions, which promote the formation of crystallographic faces {111} provided that a sufficiently low concentration of reagents and room temperature is used to ensure slow growth kinetics [250]. Subsequent growth of the Ag shell leads to the formation of cubic Au@Ag nanocrystals with a centered octahedral core with vertices oriented toward the center of each face of the outer cube (Figure 66 a, b), which is ensured by the presence of chloride ions that promote the formation of {100} faces of Ag [251]. In order to create the outer Au shell, the reduction of gold from $HAuCl_4$ (Figure 66 c, d) was first carried out due to the partial dissolution of silver in view of the difference in electrochemical potentials of these metals and their ions according to equation:

$$3Ag^0 + Au^{3+} \rightarrow Au^0 + 3Ag^+$$

Finally, the remaining Ag was removed from the structure by hydrogen peroxide etching, resulting in the formation of Au nanoparticles with a core-cage structure (Figure 66 e, f). The formation of a centrally aligned octahedral core associated with one shell wall is observed, analysis of more than 1000

particles showed an 80% predominance of frameworks with a centered core, while only 20% of frameworks are formed with an angular core, i.e. a core associated with two walls. This distribution was achieved by carefully sizing the Au octahedral core and the Ag cube so that the distance between the cube surface and the octahedral core vertices was 5±1 nm, and by controlling the amount of deposited Au.

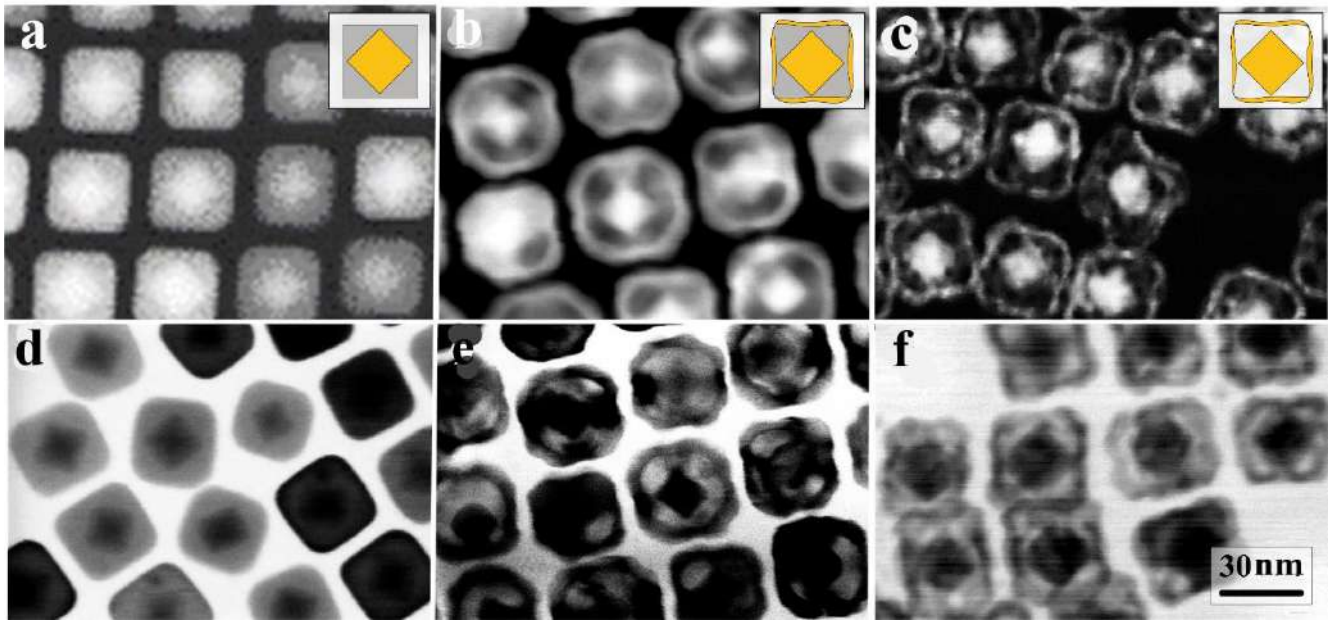

Figure 66 - TEM images of Ag nanocubes with octahedral Au core in (a) dark and (b) light field; TEM images of core-shell nanoparticles in (c) dark and (d) light field; TEM images of final Au core-cage NPs in (e) dark and (f) light field [172]

The SEM image and graphical 3D model of the nanoparticles are shown in Figure 67 a-c. The final nanoparticles have an overall size of 30±2 nm with a wall thickness of 3.5±0.4 nm and a core size of 16±2 nm (Figure 67 d-e).

Absorption spectra of colloidal solutions of nanoparticles at each synthesis step are presented in Figure 68. Octahedral Au nanoparticles show a characteristic peak at 530 nm, after the formation of the cubic Ag shell the absorption peak shifts to the blue region (430 nm) and additional shoulders appear at 350 and 384 nm, indicating the formation of the silver shell [252]. Upon subsequent deposition of gold outer cell walls with simultaneous partial dissolution of silver, the absorption spectrum broadens, which is explained by the influence of Au present on the outer surface of the resulting structure. After complete dissolution of Ag in hydrogen peroxide and formation of the final Au core-cage structure, the absorption spectrum showed two peaks with maxima at 547 nm and 824 nm. The broad absorption spectrum of the proposed particles opens prospects for their use in photoelectrocatalytic processes, where additional light exposure is used to increase the catalytic activity of the particles [253].

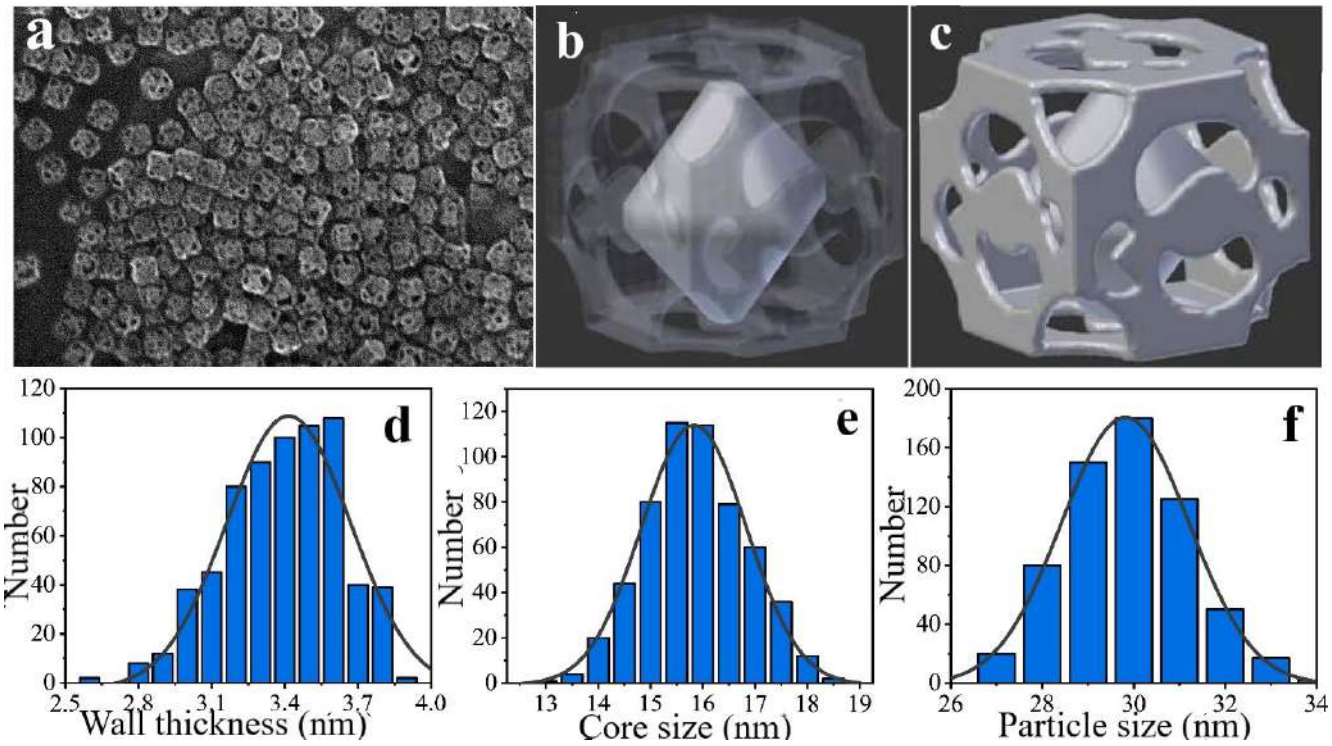

Figure 67 - (a) SEM image and (b,c) graphical model of nanoparticles; size distributions of structure elements (d) wall thickness, (e) core, (f) total particle size [172]:

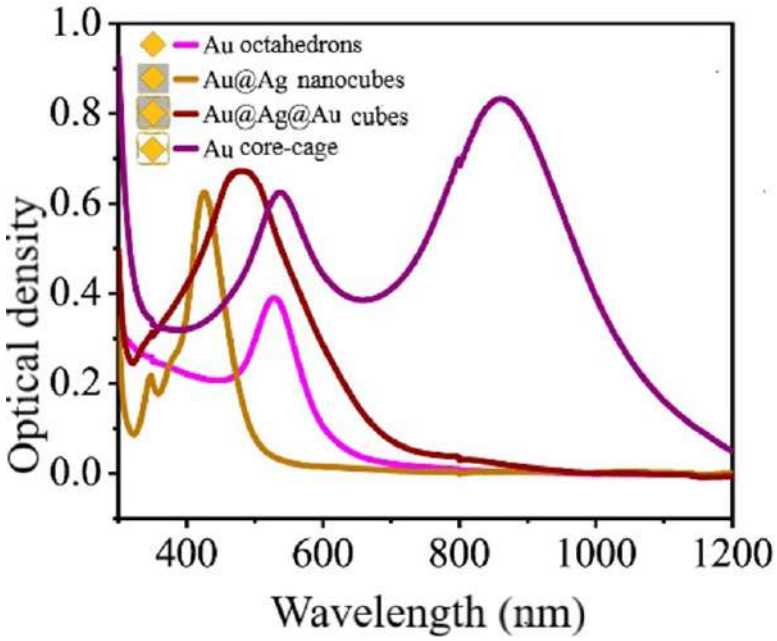

Figure 68 - Absorption spectra of core-cage nanoparticles and structures obtained at different synthesis stages [172]

To obtain bimetallic materials and enhance the electrocatalytic properties of materials fabricated by laser-induced synthesis at the interface between substrate and solid reaction medium, they were

modified with gold nanoparticles of complex morphology. Modification of Cu-Cu_xO_y electrodes was carried out by dropcasting method, for immobilization of the NPs on the electrode surface a water-alcohol solution of nafion was added to the colloidal solution of gold NPs (Figure 69). This approach does not allow to obtain an ideal uniform coating, as there is agglomeration of particles at the edges of the drop when it dries, but it was shown that using a fixed concentration of particles (controlled by optical spectroscopy) it is possible to obtain a coating with a reproducible average density of particles (Figure 70).

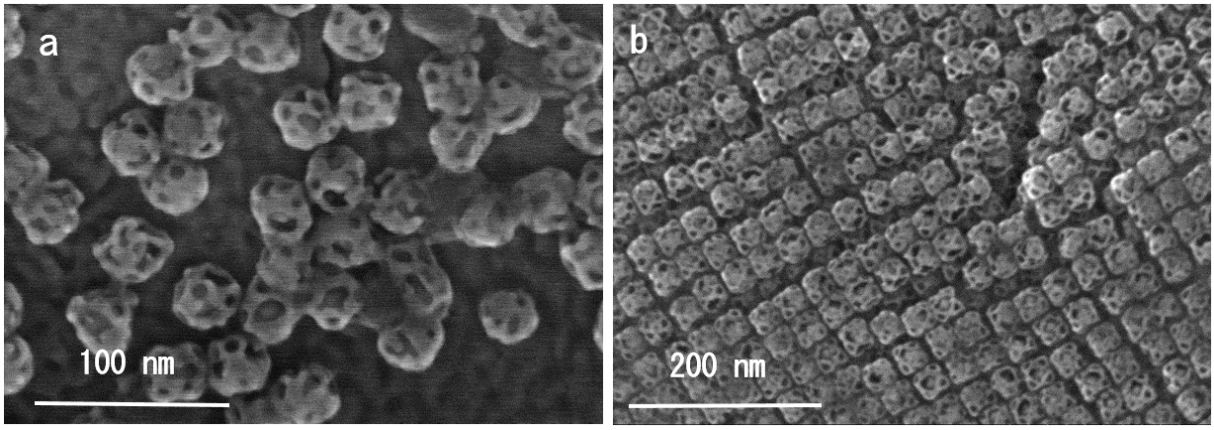

Figure 69 - SEM images of Au NPs immobilized on the surface of Cu-CuxOy electrode obtained by LIS (a) center of the electrode, (b) edge of the electrode

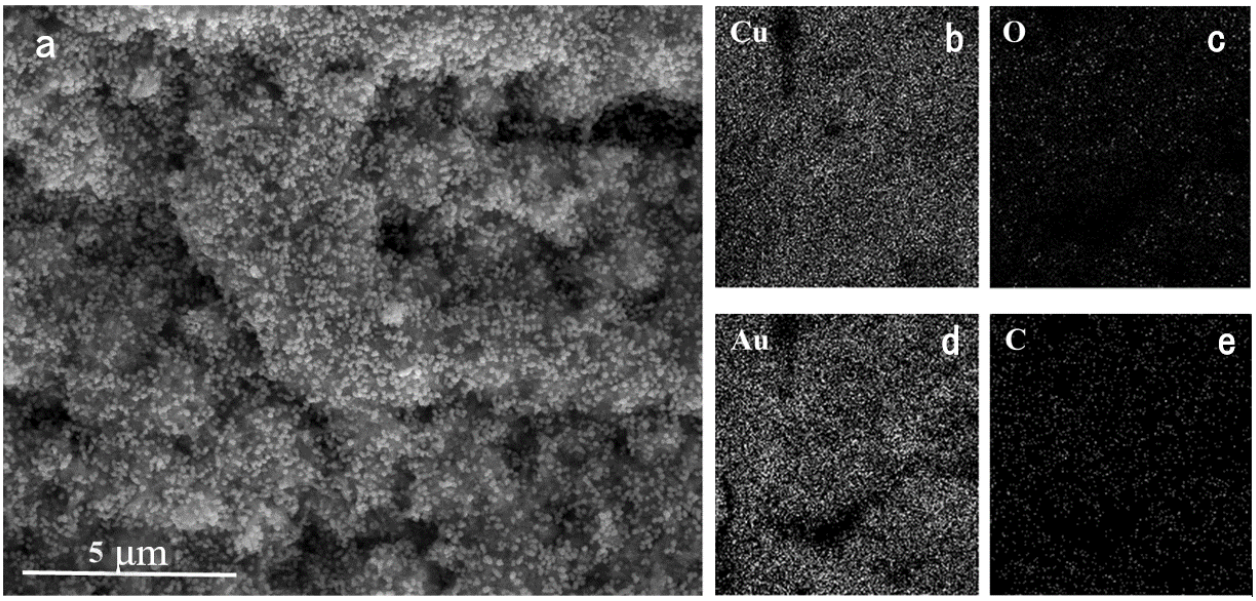

Figure 70 - SEM image and elemental mapping of the modified electrode: (a) mapping area, (b) - (e) distribution of corresponding elements over the area of the electrode

3.3.3 Study of electrocatalytic activity of synthesized materials

The electrochemical activity towards D-glucose was investigated in alkaline solution (0.1 M NaOH). The electrodes synthesized at the interface between substrate and solid reaction medium showed low adhesion to the surface of all investigated substrate materials. As can be seen from the presented CV (Figure 71) on the example of PEN substrate, the repeated measurement of the CV does not show reproducibility of the signal, the area under the curve decreases noticeably due to the electrode exfoliation (photo in the inset of Figure 71). To enhance the adhesion of the electrode to the substrate, it was proposed to use perfluorosulfonic acid polymers, which are widely used in the modification of electrodes with nanoparticles for their immobilization on the electrode surface [254,255]. In this work, the most common commercial version available under the brand name Nafion® in the form of water-alcohol mixture was used. In addition to immobilizing nanostructures on the electrode surface, the use of Nafion in electrochemical glucose sensors can help to increase the selectivity of the analysis. The Nafion film forms a membrane that allows the retention of anionic impurities. The Nafion film allows electrolyte and neutrally charged glucose to permeate through the membrane, enabling electrochemical detection while trapping negatively charged interfering agents [256,257]. 10 μl of a water-alcohol solution (0.05 wt% nafion) was applied to the surface of a 0.1 cm^2 electrode by dropcasting, then the electrode was air-dried at room temperature. Comparison of the 2nd, 5th and 10th CV cycles of the synthesized Cu-Cu_xO_y electrode on the PEN surface and the electrode coated with nafion (Figure 71 a) allowed us to conclude that the coating with the polymer composition prevents the destruction of the electrode during electrochemical measurements, which allows obtaining a stable and reproducible signal. A similar result was also obtained in chronoamperometric studies (Figure 71 b). Further, all electrodes synthesized with LIS at the interface between substrate and solid reaction medium were coated with Nafion polymer composition according to the method described above before electrochemical studies.

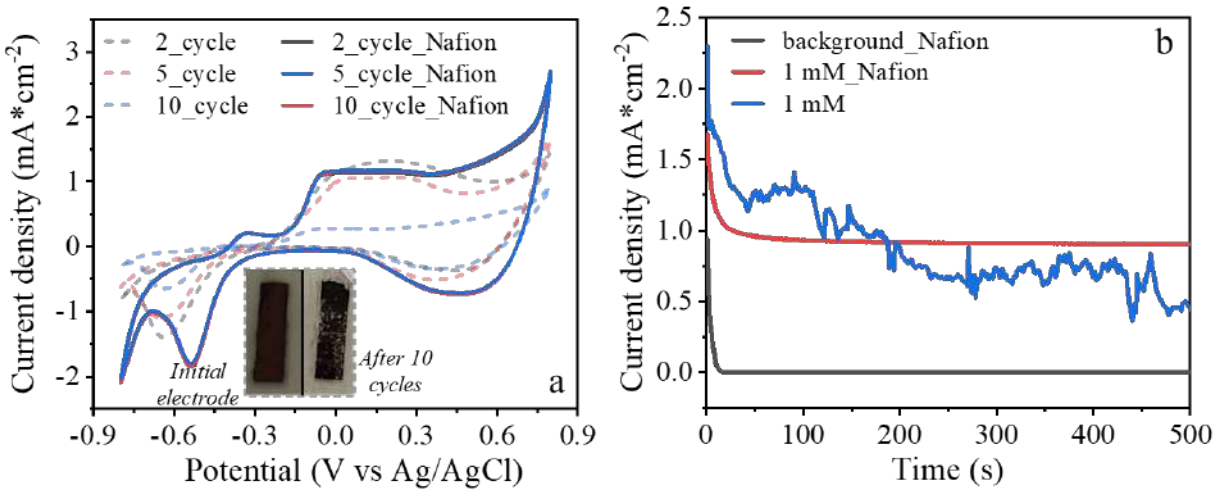

Figure 71 - (a) CV of Cu-CuxOy-PEN electrode in 0.1M NaOH: 2nd, 5th and 10th cycles untreated after LIS (dashed lines) and coated with Nafion (solid lines), inset: photos of electrode before measurements and after 10th cycle; (b) amperograms of Cu-CuxOy electrodes in 0.1M NaOH

The study of electrochemical activity of electrodes synthesized on glass ceramics at the interface between substrate and solid reaction medium is presented below. The sensing activity towards D-glucose and hydrogen peroxide was investigated by cyclic voltammetry and chronoamperometry. All of the following potentials were measured relative to a Ag/AgCl reference electrode. Figure 72 a, e shows the CVs of Cu-Cu_xO_y and Ni-NiO electrodes measured in background electrolyte and in solutions containing 1 mM D-glucose. The CV for the copper-based electrode on the glass-ceramic surface has a broad peak in the potential range from 0.35 to 0.65 V, corresponding to the anodic oxidation of glucose (Figure 72 a). In turn, the electrooxidation of glucose at the nickel electrode occurs in the potential range of 0.45-0.7 V, which shifts towards higher potentials with increasing analyte concentration (Figure 72 e). Chronoamperometry was used as an analytical method (Figure 72 c, g), from which the linear range of glucose detection, detection limit, selectivity and sensitivity for each electrode were determined. Figure 72 c, g illustrate the amperometric response to successive additions of D-glucose to 0.1 M NaOH at potentials of 0.51 V for copper and 0.6 V for nickel. Figure 72 b and e show the linear dependence of the analytical signal on the concentration of D-glucose for each material. According to these data, the linear range for non-enzymatic determination of glucose is in the range of 0.003 and 3 mM for Cu, whereas for Ni the linear range is 0.01 and 3 mM. The sensitivity of the sensor was evaluated by calculating the slopes of the calibration curves shown in Figure 72 b and f. As a result, the calculated sensitivity values for Cu and Ni are 1,110 and 2,080 $\mu AmM^{-1}cm^{-2}$, respectively. Sufficiently high values of sensitivity can be explained by the direct contact of the electrocatalytically active electrode surface with the bulk part of the electrode, since they represent a single structure in contrast to electrodes

deposited on a conductive substrate, which can lead to a decrease in the electrical conductivity of the system due to the incomplete contact of the modifier with the electrode surface.

The selectivity of the fabricated materials towards glucose determination was investigated in the presence of interfering agents such as paracetamol (AP), ascorbic acid (AA) and uric acid (UA) (Figure 72 g, h). The synthesized materials were shown to be sufficiently selective towards glucose, exhibiting a much greater analytical response to D-glucose than to other analytes.

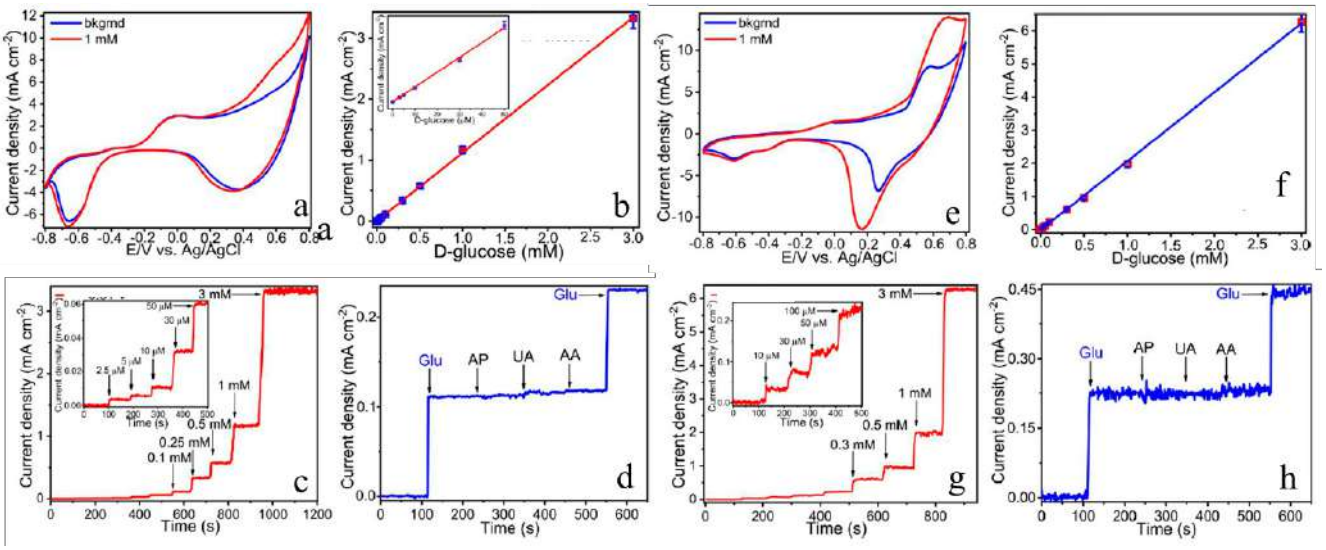

Figure 72 - CV of (a) Cu-CuxOy and (e) Ni-NiO electrodes; amperogram obtained in 0.1 M NaOH with different concentration of D-glucose for (c) Cu-CuxOy and (e) Ni-NiO electrode; linear dependence of measured current on D-glucose concentration (b) for Cu-Cu_xO_y and (f) Ni-NiO electrodes; (d), (h) amperometric response to sequential addition of 100 μM D-glucose (Glu), 20 μM 4-acetamidophenol (AP), 20 μM uric acid (UA), 20 μM ascorbic acid (AA)

In addition, the long-term stability and reproducibility of the sensor were investigated. The electrodes showed high stability over 10 days, retaining approximately 92-95% of their initial electrocatalytic activity with respect to non-enzymatic glucose detection based on a 5-electrode study. Also Cu-Cu_xO_y and Ni-NiO electrodes showed acceptable reproducibility of the analysis, with values of the relative standard deviation of the analytical response to 1 mM D-glucose for 5 measurements being in the range of 5-8%.

Also using the above methodology, the electrocatalytic properties of Cu-Cu_xO_y structures on the surface of polymeric materials such as PET, PEN, and PI were investigated (Figure 73). The electrode on PI surface showed the highest sensitivity to glucose, with all materials showing sufficient selectivity and a wide range of linearity of current dependence on analyte concentration.

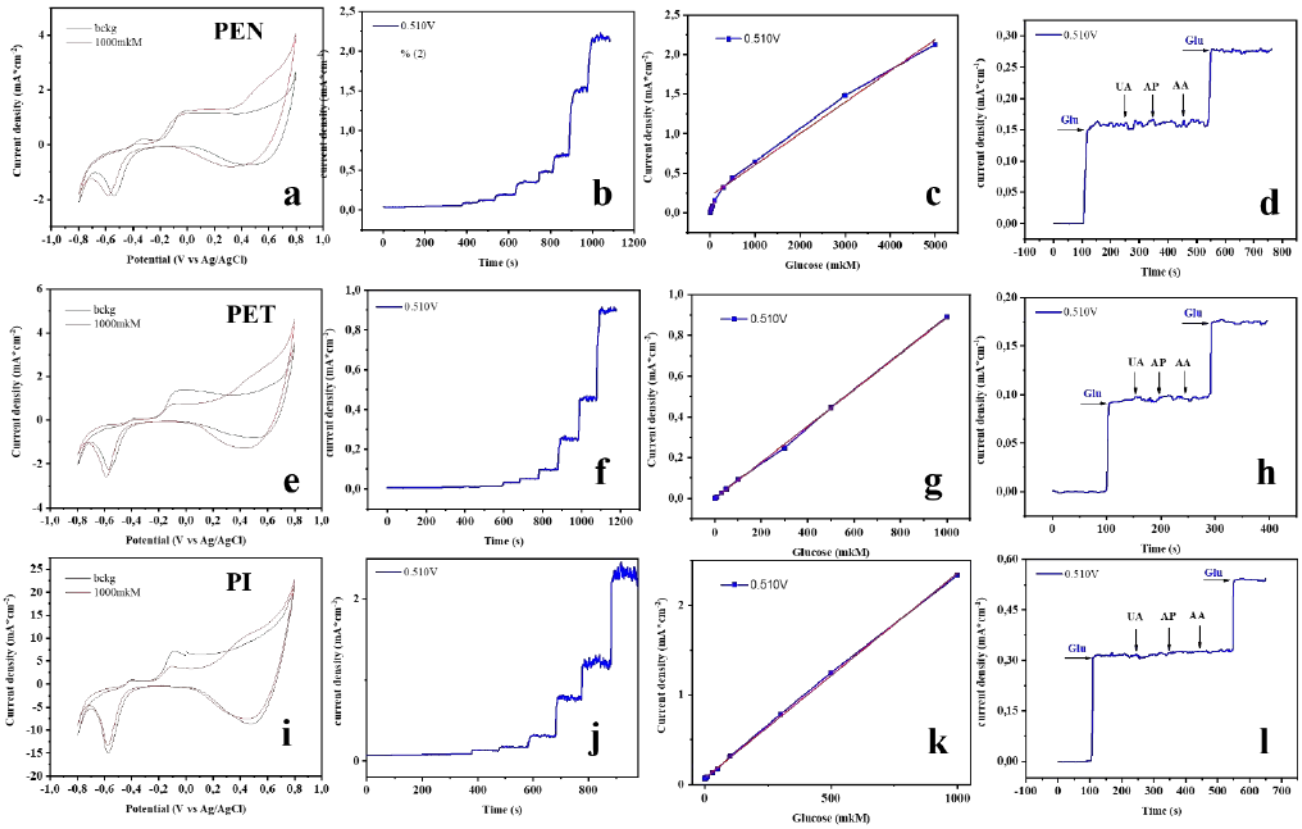

Figure 73 - Investigation of electrochemical properties of Cu-Cu_xO_y structures obtained on the surface of PEN (top row), PET (middle row) and PI (bottom row). CV (a, e, i), amperograms obtained in 0.1 M NaOH with different concentration of D-glucose (b, f, j), linear dependence of the measured current on the concentration of D-glucose (c, g, l) and amperometric response to sequential addition of 100 µM D-glucose (Glu), 20 µM 4-acetamidophenol (AP), 20 µM uric acid (UA), 20 µM ascorbic acid (AA) in 0.1 M NaOH (g, h, m)

In addition to glucose, the possibility of detecting hydrogen peroxide using the synthesized electrode at the interface between substrate and solid reaction medium was shown using Cu-Cu_xO_y on the PEN surface as an example (Figure 74). The CVs measured in phosphate buffer with hydrogen peroxide addition are shown in Figure 74 a, where the reductive peak of H_2O_2 in the potential range of -0.2 - -0.3 V is clearly visible. Chronoamperometric studies (Figure 74 b) show a proportional increase in current with the addition of given concentrations of analyte, yielding a calibration cure in the concentration range of 3-5000 µM (Figure 74 c). In addition, the electrode showed high selectivity of hydrogen peroxide detection in the presence of interfering agents such as glucose, paracetamol, and ascorbic and uric acids.

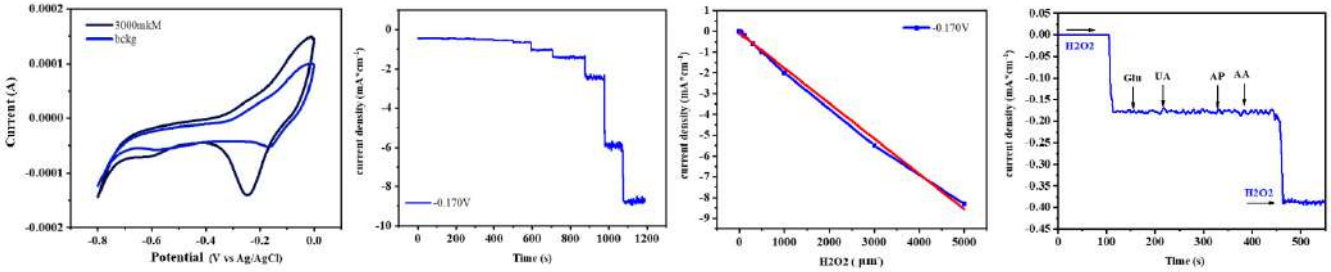

Figure 74 - CV of Cu-Cu_xO_y electrode on the surface of (a) PI in background electrolyte upon addition of H_2O_2; (b) amperometric response of Cu at different concentrations of H_2O_2; (c) linear dependence of measured current on H_2O_2 concentration, (d) amperometric response of the electrode in the study of selectivity of H_2O_2 detection

The systems obtained by modifying Cu-CuO with gold nanoparticles on the PEN surface were studied in a similar way. The CV for Cu-Cu_xO_y-Au electrodes have a shape close to that for pure copper, probably due to the relatively low content of gold in the system, but the modification of copper electrodes allowed to significantly increase the slope of the calibration curve and, consequently, the sensitivity of the analysis (Figure 75).

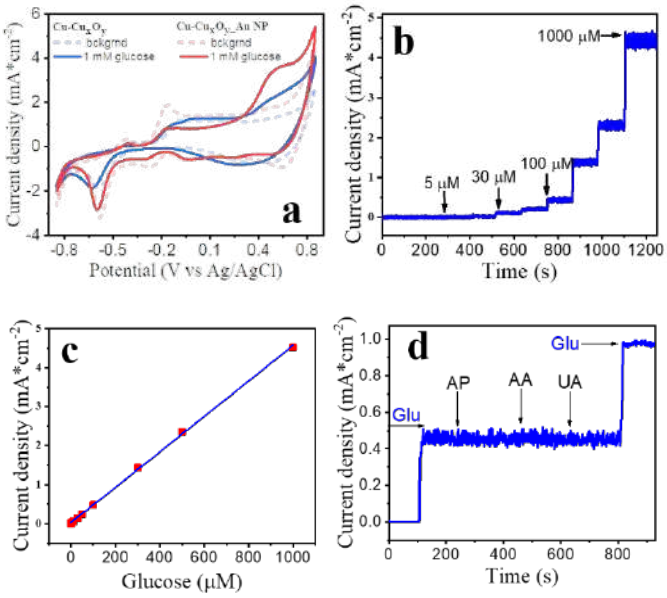

Figure 75 - (a) CV of Cu-CuxOy-Au-PEN electrode in background electrolyte when glucose is added, (b) amperometric response of Cu-CuxOy-Au-PEN electrode at different glucose concentrations, (c) linear dependence of measured current on glucose concentration, (d) amperometric response of Cu-CuxOy-Au-PEN in glucose detection selectivity study

Table 18 presents the analytical characteristics of the electrodes whose electrochemical activity was investigated in this chapter, including a systematization of sensitivity, detection limit and linear concentration range.

Table 18 - Analytical characteristics of the electrodes investigated in Section 3.3

Material	Sensitivity, $\mu A\ mM^{-1}cm^{-2}$	Linear range, µM	Limit of detection*, µM
Cu-Cu_xO_y (glass-ceramics)	1110	3–3000	0,9
Ni-NiO	2080	10–3000	2,1
Cu-Cu_xO_y PEN	1600; 396	3–100; 100–5000	0,3
Cu-Cu_xO_y-Au PEN	4510	0,5–1000	0,1
Cu-Cu_xO_y PET	888	0,5–1000	0,15
Cu-Cu_xO_y PI glucose	2290	3–1000	0,9
Cu-Cu_xO_y PI H_2O_2	1670	3–5000	1,2

**Detection limit = 3σ/m, where σ is the standard deviation from linearity and m is the slope of the calibration curve.*

In this part of the work, the main focus was on the investigation of the laser-induced physicochemical processes occurring at the interface between the substrate and the solid reaction medium and their influence on the fabrication of non-enzymatic sensors. In the presented approach, metal oxide nanoparticles were used as precursors for LIS of metal structures at the interface between substrate and solid reaction medium. The application of laser radiation leads to an increase in temperature, resulting in the reduction and sintering of nanoparticles, which in turn yields electrically conductive structures. One of the possible mechanisms for the reduction of oxide particles involves their reaction with acetaldehyde, which is itself produced during the dehydration of ethylene glycol. Optimization of the laser beam parameters, including power density, scan speed, and scan line spacing, allows a high degree of control over the morphology of the synthesized materials. This is illustrated by the creation of copper and nickel based structures.

The process of laser-induced synthesis allows the production of composite structures based on metallic copper and its oxides, characterized by metallic conductivity and high electrocatalytic activity towards glucose. Furthermore, the application of coatings, such as Nafion, significantly improves the adhesion of the electrodes to the substrate surfaces, thereby ensuring the stability and reproducibility of the analytical signal. In addition, the modification of electrodes with gold nanoparticles of complex morphology serves to further improve the electrocatalytic properties of the materials produced by laser-induced synthesis.

In the course of the conducted research were

- Methods of laser-induced synthesis of Cu-Cu_xO_y and Ni-NiO electrodes at the interface between substrate and solid reaction medium have been developed, including approaches to increase the adhesion of synthesized films, which makes it possible to use them as working electrodes of non-enzymatic sensors.

- A technique for the synthesis of gold nanoparticles of complex core-cage shape has been developed. The particles have a large surface area and many cavities accessible for small molecules. The obtained nanoparticles were used to modify transition metal-based electrode materials.

- The electrocatalytic properties of the synthesized materials towards glucose were investigated; Cu-CuxOy and Ni-NiO electrodes showed high sensitivity (1,110 and 2,080 μA mM^{-1}-cm^{-2}), low detection limit (0.91 and 2.1 μM), wide linear range (0.003-3 mM and 0.01-3 mM), and high selectivity. At the same time, modification of Cu-Cu_xO_y electrode with Au NPs allowed to significantly increase the sensitivity of the analysis and to extend the linear range of the current-analyte concentration calibration curve. Thus, laser-induced synthesis at the interface between substrate and solid reaction medium is a promising method for the preparation of materials for non-enzymatic detection of important analytes, but requires separate steps and approaches to increase the adhesion of electrodes to the substrate.

This chapter is based on data and graphics presented in the following two publications, where the PhD candidate is the primary author [171,172]:

Tumkin, Ilya I; **Khairullina, Evgeniia M**; Panov, Maxim S; Yoshidomi, Kyohei; Mizoshiri, Mizue;
Copper and nickel microsensors produced by selective laser reductive sintering for non-enzymatic glucose detection,
Materials, 14, 10, 2493, 2021, DOI: 10.3390/ma14102493

Evgeniia Khairullina, Kseniia Mosina, Rachelle M. Choueiri, Andre Philippe Paradis, Ariel Alcides Petruk, German Sciaini, Elena Krivoshapkina, Anna Lee, Aftab Ahmed, Anna Klinkova;
An aligned octahedral core in a nanocage: synthesis, plasmonic, and catalytic properties,
Nanoscale, 11, 7, 3138-3144, 2019, DOI 10.1039/C8NR09731C

3.4 Processes of laser-induced synthesis at the interface

In this study, different scenarios of controlled laser irradiation of the substrate-reaction medium system were investigated for the synthesis of electrode materials for non-enzymatic electrochemical sensors. The focus was on the fabrication of materials suitable for non-enzymatic electrodes on the

surfaces of different substrates, a crucial aspect in the development of sensor devices. This is because the conductivity and morphology of the electrode significantly influence the performance and analytical efficiency of the sensor. A key factor in determining the functionality and longevity of sensors is achieving strong adhesion between the sensor's active material and the substrate. The study focused on the interactions at the substrate-precursor interface that lead to the formation of materials with metallic conductivity and optimal adhesion to the substrate. This is essential for achieving high electrocatalytic activity and analytical signal stability. Identifying the optimal conditions for laser-induced synthesis to produce materials with the desired properties was a critical part of the research. In order to determine the parameters that are crucial for the functional properties of the resulting electrodes, three different scenarios of the laser radiation effect on the interface between the substrate and the reaction medium were investigated and analyzed from a unified position.

In the substrate-air interface LIS scenario, the substrate is directly irradiated with focused laser radiation in an air atmosphere, which is a separate synthesis step. When LIS occurs at the interface between the substrate and a liquid reaction medium, substrate activation is achieved simultaneously with laser-induced metal reduction. In these experiments, the use of precursor solutions with low concentrations of metal complexes and thus low optical density at the laser wavelength ensures that the radiation reaches the interface between the substrate and the liquid reaction medium, inducing laser-induced transformations on the substrate and` its activation. In the case of LIS at the substrate-solid interface, direct irradiation of the substrate is less likely; instead, the laser radiation interacts with the optically dense precursor layer, leading to only indirect thermal effects on the substrate due to heating of the precursor film.

Thus, 3 cases are considered in this work: direct modification of the surface in air, modifications under the precursor layer and the absence of direct interaction of laser radiation with the surface. The peculiarities of the interaction between the substrate and laser radiation and changes in the properties of the latter can have a significant impact on the functional properties of the synthesized systems. Taking into account the experimental results described above and the reduced adhesion of electrode materials obtained by the LIS method at the interface between substrate and solid reaction medium, it can be assumed that the direct interaction of laser radiation with the substrate is one of the determining factors for the formation of structures with the necessary adhesion to the surface.

Laser-induced processes encompass both changes in the chemical structure of the substrate material, including photolytic and thermal breaking of chemical bonds, and physical processes such as heating and melting. The combined effects lead to significant changes in the morphology and composition of the surface layers of the substrates.

- Change in surface morphology:

A surface with higher roughness provides more sites for mechanical adhesion to the formed structure, providing the so-called anchoring effect, increasing the overall adhesion strength. In addition, surface roughness affects wettability, which is particularly important when synthesizing metal structures in a liquid. In coating applications, increasing the surface roughness can improve the distribution of the liquid precursor over the substrate, leading to the formation of a metal film with high adhesion.

- Change in surface composition (formation of surface functional groups):

The surface of polymeric materials may contain insufficient functional groups to provide stable contact with metal films. Surface activation techniques allow the introduction of polar functional groups, thereby improving metal adhesion.

Let us take a closer look at the morphology and composition of the substrate in the context of LIS.

Surface morphology

To evaluate the morphology of the substrate after LIS, as well as the structure-substrate interface, SEM images of the cross-section of the metal structures were obtained (Figure 76).

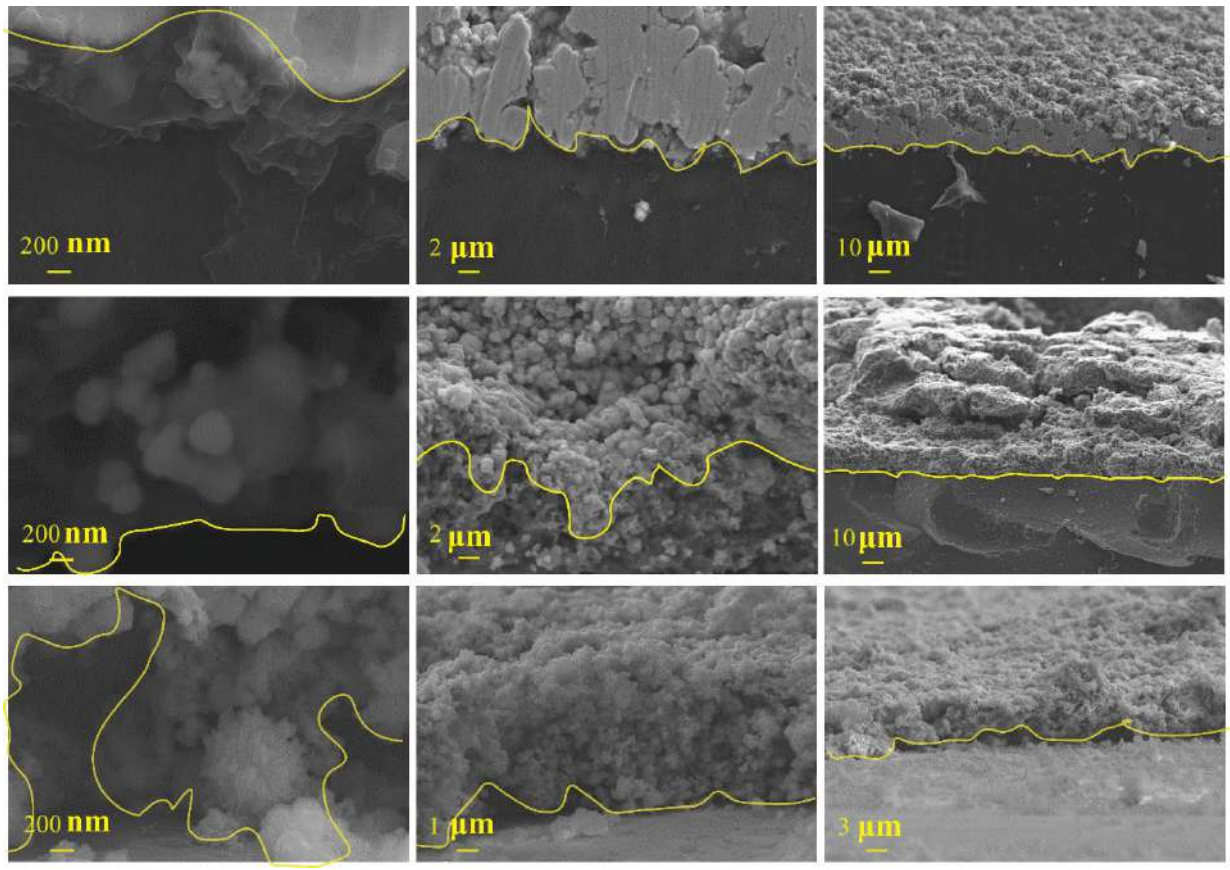

Figure 76 - SEM images of cross-sections of metal structures obtained by LIS at the substrate interface (a) air, (b) liquid reaction medium, (c) solid reaction medium

Figure 76 shows that in the case of LIS at the substrate-air interface, the copper structure and the substrate form a continuous interface, with no apparent disruption of the metal-substrate contact. For

LIS at the interface between substrate and liquid reaction medium it is also possible to note the presence of continuous contact copper - substrate, in addition, under the action of laser radiation there is a destruction of the substrate and the formation of a crater in which including the growth of the metal structure is observed. The opposite picture is observed for LIS at the interface between substrate and solid reaction medium, on SEM photographs of the cross-section of the structure can be seen the presence of many voids at the interface between the metal structure-substrate, which is the cause of insufficient adhesion, noted earlier in the study of electrocatalytic properties.

SEM images of cross sections complement the images of the substrate after interaction with laser radiation (Figure 77). For LIS at the substrate-air interface, the substrate before selective chemical deposition of copper is presented; in the case of LIS at the substrate-liquid/solid reaction medium interface, the metallic structure was dissolved in acid to investigate the surface. It can be seen from the above images that in the case of LIS at the substrate-solid reaction medium interface (Figure 77 c) there is really no significant change in the surface morphology compared to the other LIS cases considered (Figure 77 a, b).

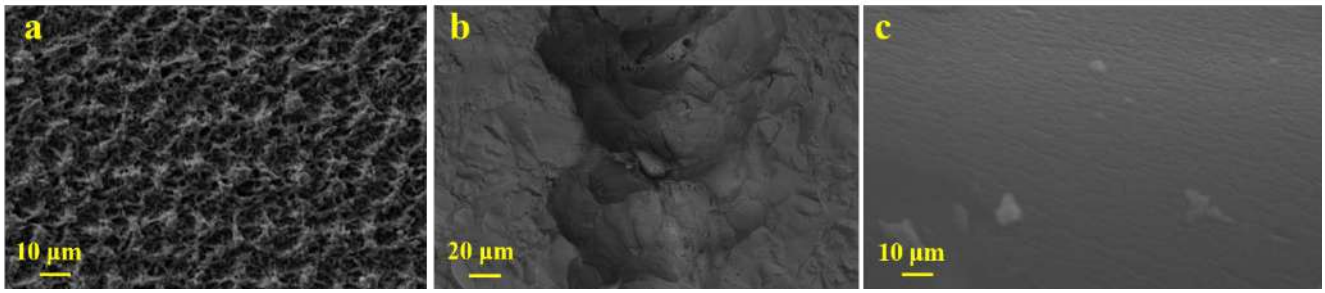

Figure 77 - SEM images of substrates after interaction with laser radiation for the LIS method at the substrate interface (a) air, (b) liquid reaction medium, (c) solid reaction medium

According to the data of the scotch test, the metal structures synthesized by the LIS method at the interface between substrate and air and substrate and liquid reaction medium demonstrate significant adhesion to the substrate (Figure 78 a, b). This conclusion is supported by the absence of visually noticeable changes in the morphology of the structures after the scotch test, indicating that the synthesized metallic structures are highly resistant to mechanical peeling. However, in the case of LIS at the substrate-solid reaction medium interface, significant delamination of the synthesized structures after the scotch test is observed (Figure 78 c). This indicates a significantly lower adhesion of the metallic structures to the substrate compared to similar structures synthesized in liquid reaction medium. This result may be due to differences in the physicochemical processes occurring at the substrate-solid reaction medium interface, which lead to the preservation of the original substrate morphology.

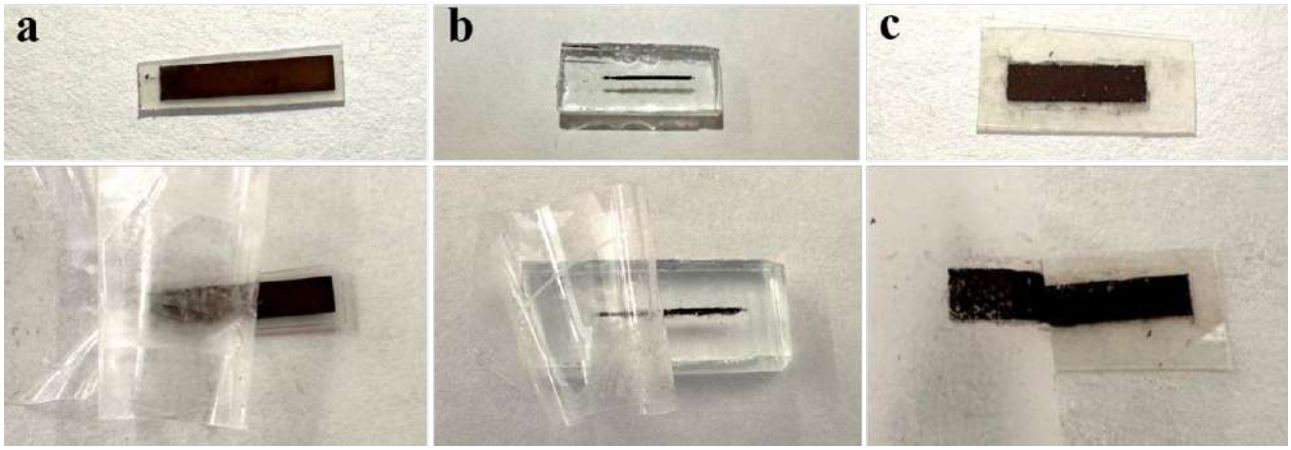

Figure 78 - Scotch test of metal structures synthesized by the LIS method at the substrate interface (a) air, (b) liquid reaction medium, (c) solid reaction medium

To confirm the influence of surface morphology on the adhesion of metallic structures, the surface of oxide glass and polyimide was modified according to optimized LIS protocols at the interface between substrate and air, followed by LIS at the interface between substrate and solid reaction medium. To evaluate the contact of the synthesized structures with the substrate, a scotch test was performed (Figure 79), the results of which showed that an increase in surface roughness leads to an increase in the adhesion of copper structures regardless of the substrate material.

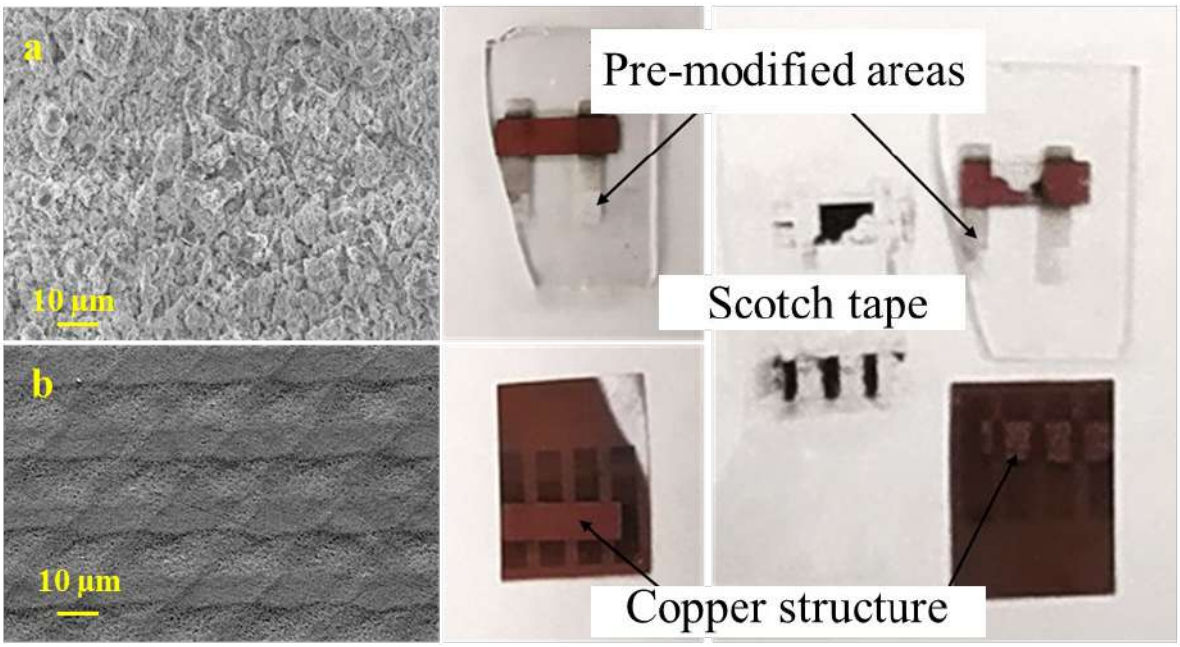

Figure 79 - SEM images of modified substrates (a) oxide glass and (b) PI, (c) copper structures before and after the scotch test

Thus, it can be concluded that modification of the substrate morphology plays a key role in determining the functional characteristics of the synthesized structures, including the improvement of adhesion. Local modification of surface morphology using laser radiation is a universal tool for improving and extending the functionality of synthesized structures, including the possibility of creating sensor-active materials on the surface of different types of substrates.

Formation of surface functional groups

As mentioned above, in addition to the change in morphology, the composition of the surface layers of the substrate can be changed under the action of laser radiation. In this case, the possible processes strongly depend on the conditions (radiation wavelength, power density, pulse duration and frequency) and the substrate material. Functional groups and defective structures formed as a result of laser exposure on the substrate can both directly participate in chemical reactions of metal reduction and participate in weak interactions with reduced metal atoms.

Let us consider the process of reduction of metallic ions with the participation of functional groups and defective structures on the substrate. For the solid substrates used in this work, such as oxide glass and glass-ceramics, a detailed understanding of the nature of activation for laser metallization was revealed by G.A. Shafeev. For solid ceramic and amorphous substrates consisting of oxides, the interaction of laser radiation with the surface can lead to the various processes resulting in the formation of active centers that facilitate electron transfer in the redox reaction. Thus, for glass and glass-ceramics, one of the main ways of surface activation is the formation of metastable oxygen vacancies at room temperature. Oxide materials are prone to oxygen loss by ablation due to a very high rate of surface cooling after interaction with laser radiationv. This effect is explained by the thermodissociation of metal oxide MeO during laser heating and since only a fraction of oxygen atoms have time to recombine due to the limitation of oxygen flux from the external environment by diffusion, this results in an increase in the Me/O ratio [23,258]. Thus, laser modification results in the formation of centers involved in the Ag^+ reduction in the case of LIS at the substrate-air interface and directly deposited metal for LIS at the substrate-liquid interface.

For polymeric materials, PET was taken as a model, PET and PEN are structurally similar, both being polymerization products of ethylene glycol and 2,6-naphthalene dicarboxylic acid and terephthalic acid for PEN and PET, respectively. In view of this, the above considerations can largely be applied equally to these substrates as they are characterized by the same functional groups (Figure 80). It has been previously shown that for the LIS method at the substrate-air interface, the ablation process plays a crucial role in surface modification since the applied power densities are above the ablation threshold [83]. The ablation mechanism for polymeric materials can be different depending on the specific chemical composition and wavelength. There are two main models of polymer ablation: photochemical

ablation, where the energy of laser photons is high enough to break the bonds of polymer molecules, and thermochemical decomposition, where the absorbed laser radiation raises the temperature of the polymer high enough to thermally break the bonds. For the laser sources used in this work, a reasonable assumption is thermochemical ablation as the dominant mechanism, since laser radiation with a wavelength of 532 nm falls within the transparency window of PET polymer. However, it should be noted that two-photon processes are possible due to the high intensity of radiation and picosecond pulse duration. In addition, the optical properties of polymers change in the process of interaction with laser radiation, namely, there is an increase in the absorption coefficient [20], which affects both the ablation thresholds and the probability of photoprocesses. According to the data obtained, supported by literature results (Figure 80), beyond the ablation threshold of XPS results for PET, an increase in the oxygen content of the surface is observed [259]. Thus, we can assume the formation of oxygen-containing functional groups (aldehyde, ketone, carboxyl) on the surface as a result of laser modification in air, which participate in the reduction of Ag+, leading to the activation of the surface with respect to further chemical metallization.

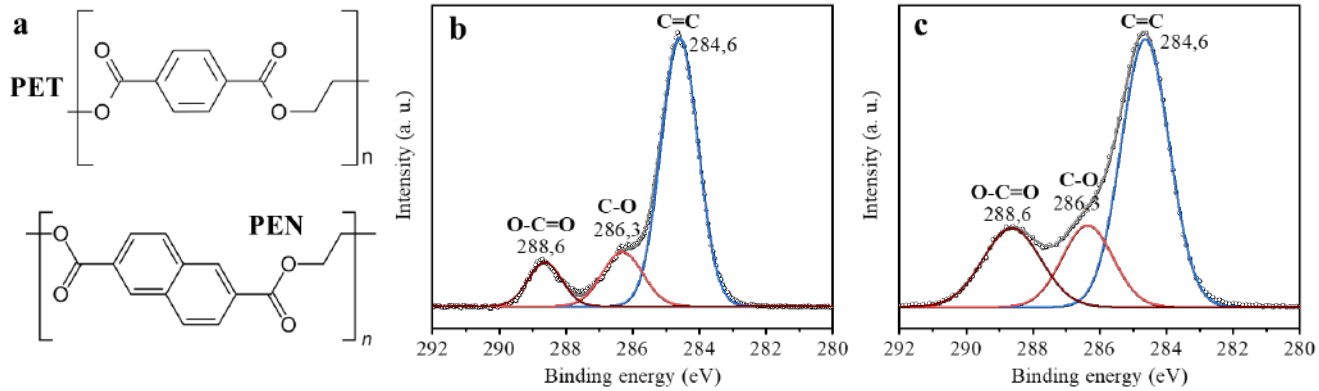

Figure 80 - (a) Structural formulas of PET and PEN. High resolution XPS spectra of C1s for (b) initial PET and (c) after laser modification in air

In addition to participating directly in the process of surface activation through the reduction of metal ions, surface groups can interact with the deposited metal atoms. In the case of polymeric materials, where the monomeric units are organic structures with different functional groups, at the early stages of metallization, the interaction of the first atoms of the reduced metal with surface groups is possible, which significantly affects the adhesion of metal structures [260]. Several types of interaction between the metal atom and the polymer surface can be distinguished (Figure 81). Oxidative attachment refers to the attachment of a metal atom to a carbon-halogen or carbon-hydrogen bond. Metals such as titanium, chromium, and aluminum are oxophilic and are capable of cleaving oxygen from ether, carbonyl, and hydroxyl groups. In some cases, metal clusters stabilized by ligands can be formed. Also

one of the interaction options is electron transfer from the transition metal to the acceptor, a prime example being the interaction of atomic Ni with tetracyanoquinodimethane. In addition, many transition metals form π-sandwich complexes. Orbital mixing processes, such as those involving the transition metals Ti, V, Cr, Cr, Zr, Nb, Mo, Hf, Ta, and W, give multilayer π-sandwich complexes with arenes. Similar complexes can be formed when these metals interact with arene substituents in polymers [260].

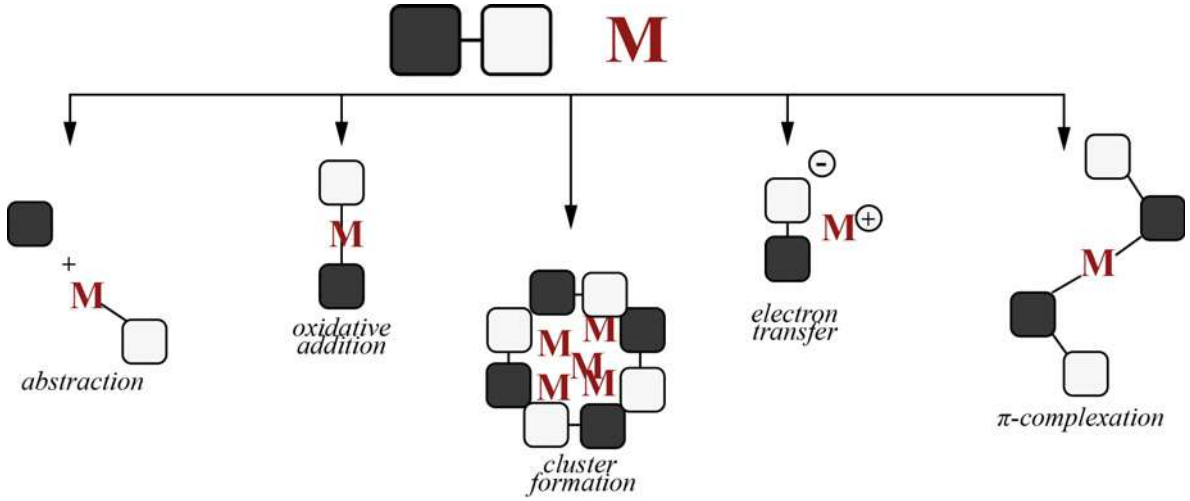

Figure 81 - Possible reactions of a metal atom with an organic molecule (monomer/substituent in a polymer) [260]

One of the possible ways to investigate the presence of such interactions is Raman spectroscopy, for which the spectra from different points of the substrate-structure interface were collected (Figure 82 and Figure 83). A detailed analysis and interpretation of the spectral data obtained during the study are presented in Table 19.

Figures 82 and 83 show the overall Raman spectra as well as individual enlarged spectral regions for a closer look at the individual peaks related to the vibrations of the carboxyl group, the π-system, and the ethylene glycol moiety. The spectral data were previously baseline corrected and normalized with respect to the 1614 cm^{-1} vibration of the aromatic ring, since this peak is the most intense and less affected by laser exposure due to the exceptional stability of the π-system.

Table 19 – Raman spectra bands assigment [261]

Wavenumber, см$^{-1}$	Assigment	Wavenumber, см$^{-1}$	Assigment
276	Ag carbonyl in-plane bending mode	1288	C(O)–O stretching
626	Ring mode C=C	1416	CH_2 bending and CCH bending
702	Ring mode C=C	1460	CH_2 bending and CCH bending
857,5	Ag mode consisting mainly of ring CC and C(O)-O stretching	1614	Ring mode 8a (in Wilson's notation)
996	O-CH2 stretching in the ethylene glycol segments	1726	Stretching C=O vibration
1094	stretching of ring CC, ester C(O)-O, and ethylene glycol CC bonds	2968	Methylene groups adjacent to oxygen atoms
1115	C(O)-O stretching and CC stretching in the ethylene glycol	3080	Aromatic C–H bonds

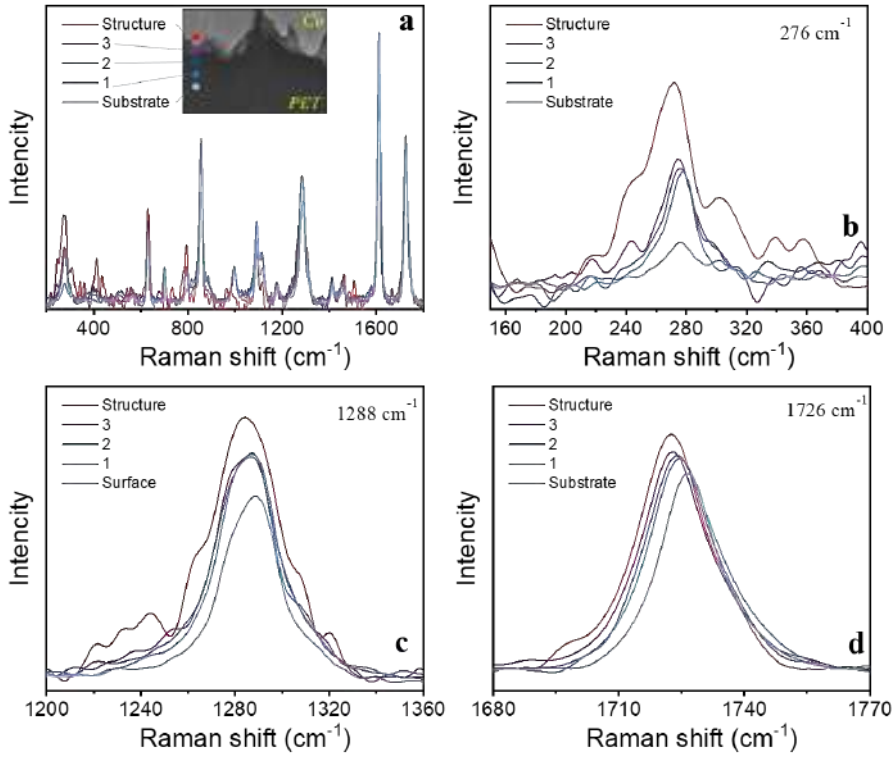

Figure 82 - Raman spectra of PET, (a) Raman spectra in a wide spectral range, (b-d) enlarged spectral ranges corresponding to vibrations of oxygen-containing groups

As a result of analyzing the spectral data, the following patterns were revealed:

- An increase of the C(O)-O peak. (1288 cm^{-1}) from the substrate to the structure, as well as its shift to the region of small wave numbers ~4-5 cm^{-1}

- The increase of the peak of C=O (1726 cm^{-1}) from the substrate to the structure, as well as its shift to the region of small wave numbers ~4-5 cm^{-1}

Examination of the bands related to the vibrations of the aromatic system and the structure of ethylene glycol revealed the following trends (Figure 83):

- Increase of the C=C peak (626 cm^{-1}) from the substrate to the structure

- Decrease in the O-CH_2 peak val. (in the ethylene glycol fragment) (996 cm^{-1}) from the substrate to the structure

- Decrease of CH_2 def., CCH def. peaks (1418 cm^{-1}, 1462 cm^{-1}) from substrate to structure

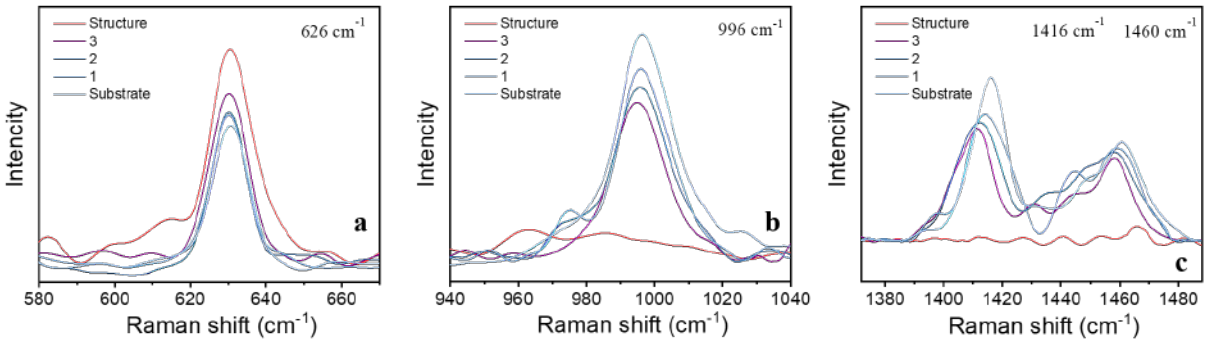

Figure 83 - Raman spectra of PET, (a-c) enlarged spectral ranges corresponding to vibrations of the aromatic system and ethylene glycol structure

Summarizing the above, it can be assumed that at the interface between the substrate and the deposited structure there is a modification of the polymer surface layers, which is accompanied by the detachment of ethylene fragments (Figure 84). The obtained data are in agreement with the literature reports on the increase in the relative oxygen content in the surface layer.

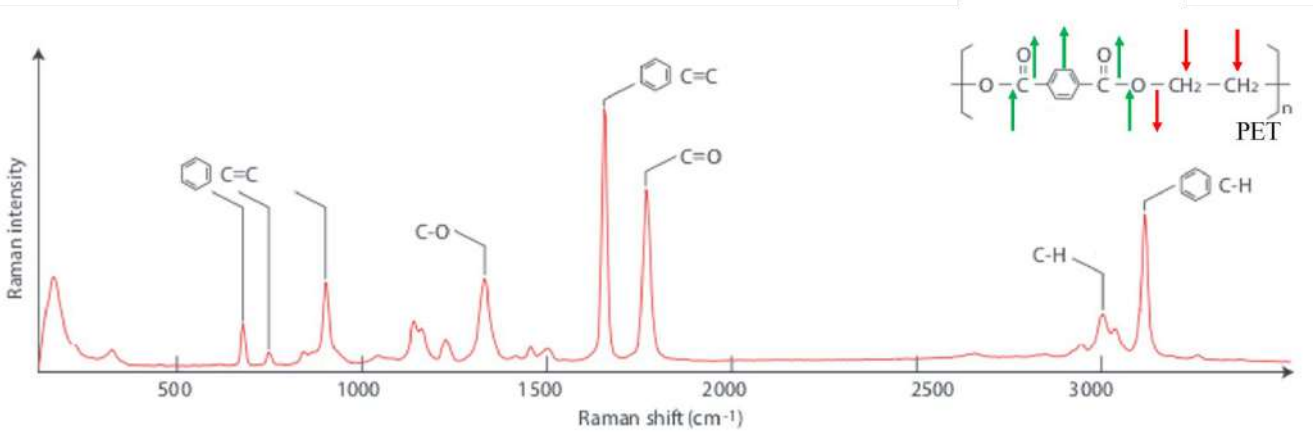

Figure 84 - Raman spectrum of PET. (Green arrows indicate the vibrations, the intensity of which increases when approaching the substrate-structure interface, red arrows indicate the vibrations, the intensity of which decreases)

As a result of Raman studies of the interface between the substrate and the synthesized structure, no new bands were detected in the spectrum compared to the spectrum of the substrate, so it is likely that the interaction between the metal and the substrate is very weak. However, it should be noted that there is a slight shift of the carbonyl group peaks in the region of small wave numbers. The small shift of the carbonyl group vibrations suggests the possibility of a weak interaction between the surface groups of the substrate and the synthesized copper structure. A. Ouhlal et al [262] evaluated the interaction between the copper atom and the carbonyl group of acetone, which was taken as a model compound (Figure 85). It was shown that in the Cu---C=O system the charge transfer mechanism (Figure 85) from Cu to carbonyl is realized, the dissociation energy is about 1.03 eV, the C=O distance slightly increases from 1.22 to 1.26 A. At the same time, the spectral band of C=O shifts from 1769 to 1556 cm^{-1}.

In addition to the carbonyl group, it is possible to interact with other structural units that are part of the monomers of the polymer substrates under study. The results of the study of the interaction between polyimide and copper atoms, on the example of model molecules PIM (phthalimide), PMDA (pyromellitic dianhydride) and PAP (4-aminophenol), which allow us to study various possible pathways of interaction with the copper atom: nitrogen atom, phenyl, imide ring and carbonyl group, showed that the most stable configurations for Cu/PIM and Cu/PMDA are those in which the copper atom is located at the carbonyl group. The binding energies of these complexes are 1.10 and 1.15 eV, respectively, indicating a rather weak interaction. At the same time, the binding energy of Cu/PAP is even smaller and equals 0.65 eV. Based on these data, we can conclude that the PMDA carbonyl group is the most likely to interact with Cu atoms [263].

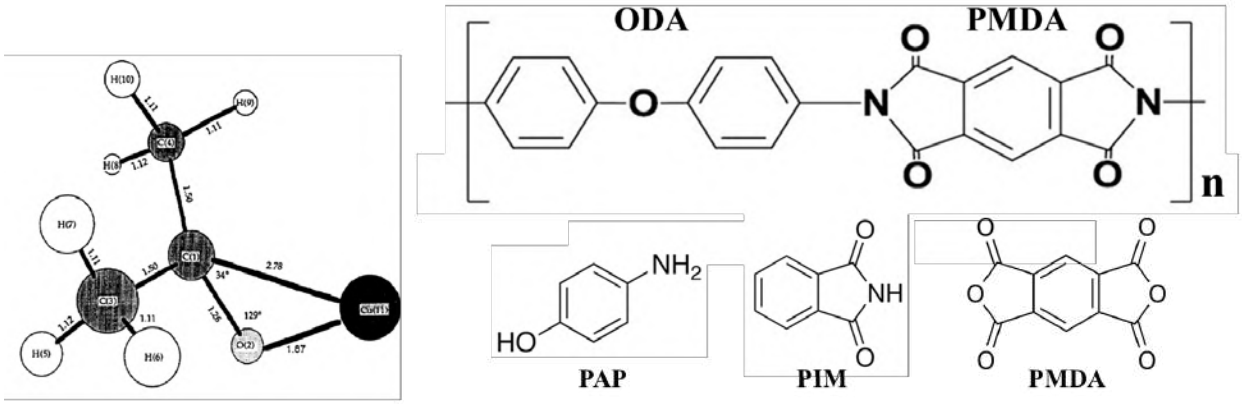

Figure 85 - (a) Computational model of Cu---C=O interaction [262], (b) structural formula of PI and model molecules

Thus, as a result of the conducted studies and analysis of literature data, it can be assumed that as a result of laser interaction with the surface of polymers there is an increase in the content of surface oxygen groups. This on the one hand contributes to the reduction of metal ions Ag^{+} for surface activation,

on the other hand can increase the adhesion of metal layers as a result of weak interactions with functional groups.

As a result of analysis and systematization of data obtained during the study of laser-induced processes at various interfaces between substrate and reaction medium, it was shown that the effect of laser radiation on the substrate plays a key role in the formation of electrode materials with high adhesion.

Laser-induced synthesis at the substrate - reaction medium interface for the fubrication of non-enzymatic sensors

In the framework of the present dissertation work, comprehensive research has been carried out to investigate laser-induced synthesis methods for the creation of non-enzymatic sensors. LIS involves laser-induced processes at the interface between the substrate and the reaction medium, including surface modification and chemical reactions for metal reduction. The main focus of the study is on the thermal effects induced by laser irradiation, which play a key role in controlling the described synthesis processes. The use of laser radiation with high power density opens new opportunities for controlled local heating of systems to high temperatures, which, in turn, makes it possible to achieve the necessary conditions for activation of chemical reactions and formation of materials with specified properties.

A detailed study of the temperature effect on the system in the process of laser-induced synthesis is a very difficult task, which is due, first of all, to the peculiarities of the synthesis process occurring at the interface between the substrate and the reaction medium, primarily in the case of solid and liquid reaction medium, since there is a precursor of complex composition, which has a significant influence on the properties of the system as a whole. In addition, it should be emphasized that the formation of metallic structures occurs under the direct influence of laser radiation. The interaction of the formed metallic structures with the LR can make a significant contribution to the heating of the system, which further complicates the consideration, for example, in the case of theoretical modeling and attempts to carry out numerical estimates of the temperature in the region of the laser focus. The complexity of the experimental study of these processes is also aggravated by their high degree of spatial localization, as well as by the variety of laser-induced processes. Nevertheless, the temperature modes of laser exposure are of crucial importance for LIS of sensor materials on the surface of flexible substrates. In all the proposed methods, sufficiently high radiation power densities are used for metal reduction or surface modification (Table 20). In the case of laser synthesis at the interface between substrate and air, the thermal impact on the substrate as a result of laser irradiation is probably not so pronounced due to the high surface scanning speed in the case of polymeric materials, which avoids their thermal destruction. In the case of LIS at the substrate-solution interface at power densities and scanning speeds necessary

for the metal ion reduction reaction, the destruction of polymer substrates is observed, which leads to the impossibility of their use. LIS in such a system could be realized only using glass or other substrates with high melting point. In the case of laser synthesis at the substrate-solid reaction medium interface, it was possible to obtain conductive metallic structures at power densities of 35-57 kW/cm^2 at medium scanning speeds; under such conditions, it is also possible to obtain structures on the surface of flexible polymers.

Table 20 - Laser exposure conditions for laser-induced synthesis at the substrate interface on different surfaces

	Substrate	**PET**	**PEN**	**PI**	**Glass-ceramics**	**Glass**
P, kW/cm^2	LIS substrate - air*	944	200	612	124	1270
	LIS substrate - liquid reaction medium**	–	–	–	–	250
	LIS substrate - solid reaction medium***	35	38	40	57	–
v, m/c	LIS substrate - air	2,0	2,0	4,0	0,1	0,2
	LIS substrate - liquid reaction medium	–	–	–	–	5*10^{-6}
	LIS substrate - solid reaction medium	0,01	0,01	0,01	0,01	–

*Laser sources used: *532 nm, 10 ps pulse duration; **532 nm, continuous wave, ***780 nm, 120 fs pulse duration*
In case of absence of experimental data in the table is "-"

Due to the versatility of LIS, which allows to carry out synthesis at different substrate-reaction medium interfaces, it has been demonstrated that each type of interface has its own unique features. These features differ significantly both in terms of experimental realization and fundamental mechanisms, as well as in terms of the functional properties of the resulting materials. A detailed discussion of the features of the techniques and the materials derived from them is presented in Table 21. Various aspects of LIS methods, including the selection of optimal laser irradiation parameters, as well as the influence of these parameters on the morphology, structure and functional properties of the synthesized non-enzymatic sensors are discussed in detail in the thesis, which allows an exhaustive analysis of LIS as a method for obtaining non-enzymatic sensors. All investigated methods allowed to create electrochemical sensors with characteristics comparable to the literature reported analogs, however, for each of the approaches it is possible to highlight their strengths and areas of application where they are most optimal.

Table 21 - Comparative characterization of techniques m

Interface Substrate -	Air	Liquid reaction medium	Solid reaction medium
Number of stages	3	1	1
Scanning speed, m/s	up to 6	$5*10^{-6}$	0.01
Sample adhesion	high	high	low
Change of substrate morphology under the action of radiation	yes	yes	no
Metallization of polymeric materials	yes	no	yes
Resistance to bending	high	–	low
Difficulty in optimizing the technique for other metals	high	low	middle

Laser-induced synthesis at the substrate-air interface requires more stages compared to LIS at the substrate-liquid/solid reaction medium interface, but this disadvantage is compensated by the very high scanning speed of the laser beam over the substrate at the modification stage and the high-throughput copper electroless plating step. This process can be scaled up significantly as it is based on a well-established chemical copper plating technology and can be realized in large volumes.

The low deposition rate is a significant disadvantage of the LIS approach at the substrate-liquid reaction medium interface. In addition, this method is limited to the use of solid substrates due to the thermal degradation of flexible polymers. However, extremely high adhesion of the structures is observed when using solid heat-resistant substrates. The combination of high adhesion and microscale allows the creation of microscale electrodes that can be integrated into various devices.

A possible limitation at the substrate-air interface is the rather high complexity of optimizing the technique for other metals, since the metallic layer is formed as a result of chemical copper plating. Chemical metallization processes have been developed for many metals, but substantial research is required to obtain polymetallic or other kinds of composite systems. Obtaining polymetallic systems can be realized much more easily using LIS at the substrate-liquid/solid reaction medium interface, since the introduction of dissimilar salts or nanoparticles into the initial precursor allows obtaining a wide range of polymetallic systems with a given composition, which is determined by the ratio of precursor components. In addition, it is important to note that LIS at the interface between substrate and air and substrate and solid reaction medium allows to fabricate non-enzymatic electrodes on the surface of flexible substrates, which is of particular practical importance. It should be separately emphasized that in the first case of synthesis at the substrate-air interface, the electrodes also have extremely high adhesion.

Thus, laser-induced synthesis is a promising approach to create electrodes for electrochemical non-enzymatic sensors with the required analytical characteristics. The high degree of versatility of the proposed method ensures the production of sensor materials meeting the requirements for various applications.

CONCLUSION

Within the framework of the thesis, the processes of laser-induced synthesis at the substrate - reaction medium interface for the fabrication of non-enzymatic sensors materials were considered. The key parameters of the laser influence on the interface between the substrate and the reaction medium, in the case of laser surface modification in air, as well as in the LIS from solid and liquid precursors for obtaining electrode materials with high electrocatalytic activity towards target analytes, were determined. The potential of using the developed materials as working electrodes for electrochemical non-enzymatic sensors was emphasized by the results presented in the study.

- Methods for laser-induced synthesis of copper structures at the substrate-air interface on the surface of both flexible and rigid substrates, including glass, glass-ceramic, PET, PEN, and PI, have been developed. The electrodes synthesized on flexible substrates were found to have high adhesion and retain functional properties under repeated bending (about 10,000 times), which emphasizes the promising potential of the proposed approach for the synthesis of non-enzymatic sensors.

- The study of the processes of laser-induced synthesis at the interface between the substrate and the liquid reaction medium led to the development of methods for the synthesis of Ni-based electrodes. It has been shown that by varying the precursor composition using the same laser source, a wide range of polymetallic systems can be obtained, as demonstrated by the sequential LIS-based synthesis of Ni-Au and Ni-Pt electrodes.

- Methods for the laser-induced synthesis of Cu-CuxOy and Ni-NiO electrodes at the interface between the substrate and the solid reaction medium have been developed. It was shown that the effect of laser radiation on the substrate through the precursor layer does not lead to a significant change in substrate morphology, which is reflected in the stability of the contact between the synthesized electrodes and the substrate.

- A wide range of approaches for surface modification of the synthesized electrodes, including galvanic replacement, electrochemical oxidation, laser-induced and synthesis of colloidal NPs, have been proposed. It has been shown that these selected approaches allow obtaining polymetallic electrodes for non-enzymatic sensors, while in many cases ensuring the preservation of the spatial selectivity of the process and the shape of the electrode set at the stage of interaction of laser-induced interaction with the reaction medium.

- The sensor properties of the fabricated materials were investigated in relation to biologically significant analytes. The significant improvement of the analytical properties of the sensors, including the increase of the sensitivity and the decrease of the detection limits, was shown to be achievable by the combination of LIS and modification of the synthesized electrodes.

ACKNOWLEDGEMENTS

The author expresses sincere gratitude to her supervisor, Doctor of Chemical Sciences, Professor Alina Anvyarovna Manshina, for her invaluable contribution to the preparation of this work. Alina Anvyarovna's profound knowledge and unwavering support at every stage of the research proved invaluable. Her determination became a support in overcoming all the difficulties that arose in the process of working on the thesis.

The author would like to express his special gratitude to the Assistant Professors of the Department of Laser Chemistry and Laser Materials Science: Ilya Igorevich Tumkin, currently representing Ruhr University Bochum, and Maxim Sergeyevich Panov for many years of fruitful cooperation. Their invaluable help in discussing methods, analyzing experimental results, and conducting experimental work deserves special thanks. The author highly appreciates their support and hopes to continue the successful cooperation in the future. The author is also grateful to the staff of the Department of Laser Chemistry and Laser Materials Science under the direction of Yuri Stanislavovich Tverjanovich for valuable advice during the investigation.

The author is also grateful to Karolis Ratautas and Gediminas Račiukaitis (Center for Physical Sciences and Technology Vilnius, Lithuania) for their invaluable help in performing the work and for the opportunity to use laser facilities for research. Deep appreciation is addressed to Mizoshiri Mizue (Nagaoka University of Technology) for the opportunity to realize research in the field of laser-induced sintering and for the high level of professionalism that contributed to the achievement of significant results. The author expresses special gratitude to Prof. Anna Klinkova (University of Waterloo) for the opportunity to open up the breathtaking world of nanoparticles with controlled shape and size.

The research was carried out using the equipment of the SPBU Research Park, including “Nanotechnology”, “X-ray Diffraction Studies”, “Optical and Laser Materials Research”, and “Physical Methods of Surface Investigation” facilities.

The author also thanks RSF and RFBR, the work was financially supported by RFBR grants № 20-53-50011 and RSF № 20-79-10075.

LIST OF ABBREVIATIONS AND SYMBOLS

LIS - laser-induced synthesis

LR - laser radiation

NPs - nanoparticles

PVP - polyvinylpyrrolidone

EG - ethylene glycol

SEM - scanning electron microscopy

EDX - Energy-dispersive X-ray spectroscopy

XPS - X-ray XPS spectroscopy

CV - cyclic voltammetry

CA - amperometry

PI - polyimide

PET - polyethylene terephthalate

PEN - polyethylene naphthalate

REFERENCES

1. Sakamoto M., Fujistuka M., Majima T. Light as a construction tool of metal nanoparticles: Synthesis and mechanism // J. Photochem. Photobiol. C Photochem. Rev. 2009. Vol. 10, № 1. P. 33–56.
2. Hong S. et al. Digital selective laser methods for nanomaterials: From synthesis to processing // Nano Today. Elsevier Ltd, 2016. Vol. 11, № 5. P. 547–564.
3. Zhao L. et al. Laser Synthesis and Microfabrication of Micro/Nanostructured Materials Toward Energy Conversion and Storage // Nano-Micro Letters. 2021. Vol. 13, № 49. 1–48 p.
4. Theerthagiri J. et al. Fundamentals and comprehensive insights on pulsed laser synthesis of advanced materials for diverse photo- and electrocatalytic applications // Light Sci. Appl. 2022. Vol. 11, № 1.
5. Ming W. et al. Recent advances in molecular dynamics of metal laser-processed nanoparticles: A review //Optics & Laser Technology. 2024. Vol. 174. P. 110618.
6. Forsythe R.C. et al. Pulsed Laser in Liquids Made Nanomaterials for Catalysis // Chem. Rev. 2021. Vol. 121, № 13. P. 7568–7637.
7. Kochemirovsky V.A. et al. Laser-induced chemical liquid phase deposition of metals: chemical reactions in solution and activation of dielectric surfaces // Russ. Chem. Rev. 2011. Vol. 80, № 9. P. 869–882.
8. Pinheiro T. et al. Direct Laser Writing: From Materials Synthesis and Conversion to Electronic Device Processing. // Adv. Mater. 2024. № 2402014.
9. Ghosh S. et al. Directed Self-Assembly Driven Mesoscale Lithography Using Laser-Induced and Manipulated Microbubbles: Complex Architectures and Diverse Applications // Nano Lett. 2021. Vol. 21, № 1. P. 10–25.
10. Ritacco T. et al. Controlling the optical creation of gold nanoparticles in a pva matrix by direct laser writing // J. Eur. Opt. Soc. 2016. Vol. 11, № 16008.
11. Nedyalkov N. et al. Laser-assisted fabrication of gold nanoparticle-composed structures embedded in borosilicate glass // Beilstein J. Nanotechnol. 2017. Vol. 8, № 1. P. 2454–2463.
12. Okinaka Y., Osaka T. Electroless deposition processes: Fundamentals and applications // Advances in electrochemical science and engineering. 2008. Vol. 3. P. 55–116.
13. Moylan C.R., Baum T.H., Jones C.R. LCVD of copper: Deposition rates and deposit shapes // Appl. Phys. A Solids Surfaces. 1986. Vol. 40, № 1. P. 1–5.
14. Park J.B. et al. Hybrid LCVD of micro-metallic lines for TFT-LCD circuit repair // Appl. Surf. Sci. 2006. Vol. 253, № 2. P. 1029–1035.
15. Mizoshiri M. et al. Femtosecond laser direct writing of Cu–Ni alloy patterns in ambient

atmosphere using glyoxylic acid Cu/Ni mixed complexes // Opt. Laser Technol. 2021. Vol. 144. P. 107418.

16. Sharif A., Farid N., O'Connor G.M. Ultrashort laser sintering of metal nanoparticles: A review // Results Eng. 2022. Vol. 16. P. 100731.
17. Borodaenko Y. et al. On-Demand Plasmon Nanoparticle-Embedded Laser-Induced Periodic Surface Structures (LIPSSs) on Silicon for Optical Nanosensing // Adv. Opt. Mater. 2022. Vol. 10, № 21. P. 2201094.
18. Bischoff K., Esen C., Hellmann R. Preparation of Dispersed Copper(II) Oxide Nanosuspensions as Precursor for Femtosecond Reductive Laser Sintering by High-Energy Ball Milling // Nanomaterials. 2023. Vol. 13, № 2693. P. 1–15.
19. Shukla P. et al. Laser surface structuring of ceramics, metals and polymers for biomedical applications: A review // Laser Surf. Modif. Biomater. Tech. Appl. 2016. P. 281–299.
20. Obilor A.F. et al. Micro-texturing of polymer surfaces using lasers: a review // Int. J. Adv. Manuf. Technol. 2022. Vol. 120. P. 103–135.
21. Mulko L., Soldera M., Lasagni A.F. Structuring and functionalization of non-metallic materials using direct laser interference patterning: A review // Nanophotonics. 2022. Vol. 11, № 2. P. 203–240.
22. Mentor K.P. Шафеев Г. А. Лазерное инициирование гетерогенных процессов в жидкой фазе: дис. д.ф-м.н: 01.04.21 / Шафеев Георгий Айратович. - М., 1999. - 233 с.
23. Shafeev G.A. Laser activation and metallisation of oxide ceramics // Adv. Mater. Opt. Electron. 1993. Vol. 2, № 4. P. 183–189.
24. Shafeev G.A. Laser-assisted activation of dielectrics for electroless metal plating // Appl. Phys. A Mater. Sci. Process. 1998. Vol. 67, № 3. P. 303–311.
25. Kochemirovsky V.A. et al. Laser-induced copper deposition from aqueous and aqueous–organic solutions: state of the art and prospects of research // Russ. Chem. Rev. 2015. Vol. 84, № 10. P. 1059–1075.
26. Tamura K. et al. Ni-based composite microstructures fabricated by femtosecond laser reductive sintering of NiO/Cr mixed nanoparticles // Jpn. J. Appl. Phys. 2017. Vol. 56, № 6. P. 2–7.
27. Nam V.B. et al. Laser digital patterning of conductive electrodes using metal oxide nanomaterials // Nano Converg. 2020. Vol. 7, № 23. P. 1–17.
28. Rahman M.K., Lee J. sol, Kwon K.S. Realization of thick copper conductive patterns using highly viscous copper oxide (CuO) nanoparticle ink and green laser sintering // J. Manuf. Process. 2023. Vol. 105. P. 38–45.
29. Bischoff K. et al. Rheological Investigation of Highly Filled Copper (II) Oxide Nanosuspensions to Optimize Precursor Particle Content in Reductive Laser-Sintering // Liquids. 2024. Vol. 4. P.

382–392.

30. Hwang E. et al. Direct Writing of Functional Layer by Selective Laser Sintering of Nanoparticles for Emerging Applications: A Review // Materials (Basel). 2022. Vol. 15, № 17.
31. Mizoshiri M., Nishitani K., Hata S. Effect of heat accumulation on femtosecond laser reductive sintering of mixed CuO/NiO nanoparticles // Micromachines. 2018. Vol. 9, № 264. P. 1–10.
32. Ha N.P., Ohishi T., Mizoshiri M. Direct writing of cu patterns on polydimethylsiloxane substrates using femtosecond laser pulse-induced reduction of glyoxylic acid copper complex // Micromachines. 2021. Vol. 12, № 493. P. 1–10.
33. Seguí Femenias Y., Angst U., Elsener B. Monitoring pH in corrosion engineering by means of thermally produced iridium oxide electrodes // Mater. Corros. 2018. Vol. 69, № 1. P. 76–88.
34. Tomková H. et al. Electrochemical sensor based on phospholipid modified glassy carbon electrode - determination of paraquat // J. Electroanal. Chem. 2018. Vol. 821. P. 33–39.
35. Swain G.M. Solid Electrode Materials: Pretreatment and Activation // Handbook of Electrochemistry. 2007. P. 111–154.
36. Ratautas K. et al. Evaluation and optimisation of the SSAIL method for laser-assisted selective electroless copper deposition on dielectrics // Results Phys. 2020. Vol. 16. P. 102943.
37. Akagündüz C.G., Soylemez E. Optimization of Laser Direct Structuring Process Parameters for Material Extrusion of Polycarbonate // Adv. Eng. Mater. 2023. Vol. 25, № 23. P. 2300907.
38. Steinert P. et al. Design of high strength polymer metal interfaces by laser microstructured surfaces // IOP Conf. Ser. Mater. Sci. Eng. 2018. Vol. 373. P. 012015.
39. Schuberth A. et al. Effect of new adhesion promoter and mechanical interlocking on bonding strength in metal-polymer composites // IOP Conf. Ser. Mater. Sci. Eng. 2016. Vol. 118. P. 012041.
40. Yulinova A. et al. Novel adhesion promoter for metal-plastic composites // Adv. Eng. Mater. 2015. Vol. 17, № 6. P. 802–809.
41. Saborowski E. et al. Determination of the strength of polymer-metal interfaces under mixed mode loading using butt-bonded hollow cylinders // Int. J. Adhes. Adhes. 2019. Vol. 89. P. 30–39.
42. Buchwalter L.P. Adhesion of polyimides to Metals and Metal Oxides // J. Adhes. Sci. Technol. 1987. Vol. 1, № 1. P. 341–347.
43. Gentle T.E. et al. Organofunctional silanes as adhesion promoters: Direct characterization of the polymer/silane interphase // J. Adhes. Sci. Technol. 1992. Vol. 6, № 2. P. 307–316.
44. Pape P.G. Adhesion Promoters: Silane Coupling Agents // Applied Plastics Engineering Handbook: Processing and Materials. 2011. Vol. 3. P. 503–517.
45. Göring M. et al. Amino Group Bearing Organic–Inorganic Hybrid Materials for Joining Aluminum Alloys and Thermoplastic Fiber-Reinforced Parts // Adv. Mater. Interfaces. 2017. Vol.

4, № 16. P. 1–12.

46. Shinde S., Sampath S. A Critical Analysis of the Tensile Adhesion Test for Thermally Sprayed Coatings // J. Therm. Spray Technol. 2022. Vol. 31, № 8. P. 2247–2279.
47. Noh J., Ha J., Kim D. Femtosecond and nanosecond laser sintering of silver nanoparticles on a flexible substrate // Appl. Surf. Sci. 2020. Vol. 511. P. 145574.
48. Cai Z., Yung K.C., Zeng X. Fabrication and adhesion performance of gold conductive patterns on silicon substrate by laser sintering // Appl. Surf. Sci. 2011. Vol. 258. P. 478–481.
49. Ji S.Y. et al. Laser patterning of highly conductive flexible circuits // Nanotechnology. 2017. Vol. 28, № 16. P. 165301.
50. Zolfaghari A., Chen T., Yi A.Y. Additive manufacturing of precision optics at micro and nanoscale // Int. J. Extrem. Manuf. IOP Publishing, 2019. Vol. 1. P. 012005.
51. Saunders J., Elbestawi M., Fang Q. Ultrafast Laser Additive Manufacturing: A Review // J. Manuf. Mater. Process. 2023. Vol. 7, № 89. P. 1–43.
52. Das A. et al. A review on critical challenges in additive manufacturing via laser-induced forward transfer // Opt. Laser Technol. 2024. Vol. 168. P. 109893.
53. Marcos Fernández-Pradas J., Serra P. Laser-induced forward transfer: A method for printing functional inks // Crystals. 2020. Vol. 10, № 8. P. 1–17.
54. Goncharova D. et al. Gold-based catalysts prepared by pulsed laser ablation: A review of recent advances // Materials Today Chemistry. 2023. Vol. 33. P. 101709.
55. Fazio E. et al. Nanoparticles engineering by pulsed laser ablation in liquids: Concepts and applications // Nanomaterials. 2020. Vol. 10, № 11. P. 1–50.
56. Zeng H. et al. Nanomaterials via laser ablation/irradiation in liquid: A review // Adv. Funct. Mater. 2012. Vol. 22, № 7. P. 1333–1353.
57. Haider A.J. et al. A comprehensive review on pulsed laser deposition technique to effective nanostructure production: trends and challenges // Opt. Quantum Electron. 2022. Vol. 54, № 488. P. 1–25.
58. Shepelin N.A. et al. A practical guide to pulsed laser deposition // Chem. Soc. Rev. Royal Society of Chemistry, 2023. Vol. 52, № 7. P. 2294–2321.
59. Gräf S. Formation of laser-induced periodic surface structures on different materials: Fundamentals, properties and applications // Adv. Opt. Technol. 2020. Vol. 9. P. 11–39.
60. Nakhoul A., Colombier J.P. Beyond the Microscale: Advances in Surface Nanopatterning by Laser-Driven Self-Organization // Laser Photonics Rev. 2024. Vol. 18, № 5. P. 2300991.
61. Edri E. et al. Laser Printing of Multilayered Alternately Conducting and Insulating Microstructures // ACS Appl. Mater. Interfaces. 2021. Vol. 13, № 30. P. 36416–36425.
62. Yang L. et al. Laser printed microelectronics // Nat. Commun. 2023. Vol. 14, № 1103. P. 1–10.

63. Lipovka A. et al. Photoinduced flexible graphene/polymer nanocomposites: Design, formation mechanism, and properties engineering // Carbon N. Y. 2022. Vol. 194. P. 154–161.
64. Rodriguez R.D. et al. Beyond graphene oxide: Laser engineering functionalized graphene for flexible electronics // Mater. Horizons. 2020. Vol. 7. P. 1030–1041.
65. Niu X. et al. Recent advances in non-enzymatic electrochemical glucose sensors based on non-precious transition metal materials: Opportunities and challenges // RSC Adv. 2016. Vol. 6, № 88. P. 84893–84905.
66. Naikoo G.A. et al. Recent Advances in Non-Enzymatic Glucose Sensors Based on Metal and Metal Oxide Nanostructures for Diabetes Management- A Review // Front. Chem. 2021. Vol. 9. P. 748957.
67. Yuan F. et al. Recent advances in inorganic functional nanomaterials based flexible electrochemical sensors // Talanta. 2022. Vol. 244. P. 123419.
68. Nugraha A.S. et al. Trimetallic Mesoporous AuCuNi Electrocatalysts with Controlled Compositions Using Block Copolymer Micelles as Templates // Small Methods. 2018. Vol. 2. P. 1800283.
69. Yang J., Han J., Jae M. Selective metallization on copper aluminate composite via laser direct structuring technology // Compos. Part B. 2017. Vol. 110. P. 361–367.
70. Lee T.H., Hwang S.M., Yoo M.J. Investigation of CuAlO2 composite dielectric properties and selective metallization by laser direct structure technology // J. Eur. Ceram. Soc. 2020. Vol. 40, № 4. P. 1390–1397.
71. Bachy B., Süß-Wolf R., Franke J. On the quality and the accuracy of the laser direct structuring, experimental investigation and optimization // J. Laser Appl. 2018. Vol. 30. P. 022006.
72. Fischer A.J., Meister S., Drummer D. Effect of fillers on the metallization of laser-structured polymer parts // J. Polym. Eng. 2017. Vol. 37, № 2. P. 151–161.
73. Xu H. et al. Laser-Induced Selective Metallization on Polymers for Both NIR and UV Lasers: Preparing 2D and 3D Circuits // Ind. Eng. Chem. Res. 2023. Vol. 62, № 1. P. 395–404.
74. Zhang J., Zhou T., Wen L. Selective Metallization Induced by Laser Activation: Fabricating Metallized Patterns on Polymer via Metal Oxide Composite // ACS Appl. Mater. Interfaces. 2017. Vol. 9, № 10. P. 8996–9005.
75. Zhang J. et al. Exposing Metal Oxide with Intrinsic Catalytic Activity by Near-Infrared Pulsed Laser: Laser-Induced Selective Metallization on Polymer Materials // Adv. Mater. Interfaces. 2017. Vol. 4, № 23. P. 1700937.
76. Zhang J. et al. Laser-Induced Selective Metallization on Polymer Substrates Using Organocopper for Portable Electronics // ACS Appl. Mater. Interfaces. 2019. Vol. 11, № 14. P. 13714–13723.
77. Xu H. et al. Fabrication of Copper Patterns on Polydimethylsiloxane through Laser-Induced

Selective Metallization // Ind. Eng. Chem. Res. 2021. Vol. 60, № 24. P. 8821–8828.

78. Xu H. et al. Autocatalytic Laser Activator for Both UV and NIR Lasers: Preparation of Circuits on Polymer Substrates by Selective Metallization // ACS Appl. Mater. Interfaces. 2022. Vol. 14, № 27.
79. Rytlewski P. et al. Laser-induced surface activation and electroless metallization of polyurethane coating containing copper(II) L-tyrosine // Appl. Surf. Sci. Elsevier B.V., 2020. Vol. 505. P. 144429.
80. Lyalin A.A. et al. Laser-assisted Etching and Metallisation of Via-Holes in Polyethylene Terephthalate // Adv. Mater. Opt. Electron. 1995. Vol. 5. P. 299–303.
81. Shafeev G., Marine W., Dallaporta H. Laser assisted metallization of polyphenylquinoxaline // Thin Solid Films. 1994. Vol. 241. P. 52–56.
82. Shafeev G.A. et al. Enhanced adherence of electroless metal deposit on SiO 2 via control of the chemical environment of the Pd seeding layer // Appl. Surf. Sci. 1995. Vol. 86. P. 387–391.
83. Ratautas K. et al. Laser-assisted selective copper deposition on commercial PA6 by catalytic electroless plating – Process and activation mechanism // Appl. Surf. Sci. 2019. Vol. 470. P. 405–410.
84. Ratautas K. Laser Assisted Selective Metallization of Polymers // 2018 13th International Congress Molded Interconnect Devices (MID). IEEE, 2018. P. 1–3.
85. Ratautas K. et al. Laser-Induced Selective Electroless Plating on PC/ABS Polymer: Minimisation of Thermal Effects for Supreme Processing Speed // Polymers (Basel). 2020. Vol. 12, № 2427. P. 1–16.
86. Panov M.S. et al. Laser-Induced Synthesis of Composite Materials Based on Iridium, Gold and Platinum for Non-Enzymatic Glucose Sensing // Materials (Basel). 2020. Vol. 13, № 3359. P. 1–11.
87. Zarzar L.D. et al. Using Laser-Induced Thermal Voxels to Pattern Diverse Materials at the Solid-Liquid Interface // ACS Appl. Mater. Interfaces. 2016. Vol. 8, № 33. P. 21134–21139.
88. Khairullina E. et al. Rapid and effective method of laser metallization of dielectric materials using deep eutectic solvents with copper acetate // J. Mater. Sci. 2023. Vol. 58, № 22. P. 9322–9336.
89. Kochemirovsky V.A. et al. The influence of non-ionic surfactants on laser-induced copper deposition // Appl. Surf. Sci. 2013. Vol. 280. P. 494–499.
90. Kordás K. et al. Laser-assisted metal deposition from liquid-phase precursors on polymers // Appl. Surf. Sci. 2001. Vol. 172, № 1–2. P. 178–189.
91. Shafeev G.A., Hoffmann P. Light-enhanced electroless Cu deposition on laser-treated polyimide surface // Appl. Surf. Sci. 1999. Vol. 138–139, № 1–4. P. 455–460.
92. Logunov L.S. et al. Influence of the ligand nature on the in situ laser- induced synthesis of the

electrocatalytically active copper microstructures // Arab. J. Chem. 2018. Vol. 11, № 5. P. 624–634.

93. Baranauskaite V.E. et al. In situ laser-induced synthesis of gas sensing microcomposites based on molybdenum and its oxides // Compos. Part B. 2019. Vol. 157. P. 322–330.
94. Gordeychuk D.I. et al. Copper-based nanocatalysts produced via laser-induced ex situ generation for homo- and cross-coupling reactions // Chem. Eng. Sci. 2020. Vol. 227. P. 115940.
95. Tumkin I.I. et al. Laser-induced deposition of nanostructured copper microwires on surfaces of composite materials // Surf. Coatings Technol. 2015. Vol. 264. P. 187–192.
96. Smikhovskaia A. V et al. In situ laser-induced synthesis of copper - silver microcomposite for enzyme-free D -glucose and L -alanine sensing // Appl. Surf. Sci. 2019. Vol. 488. P. 531–536.
97. Smikhovskaia A. V. et al. In situ laser-induced codeposition of copper and different metals for fabrication of microcomposite sensor-active materials // Anal. Chim. Acta. 2018. Vol. 1044. P. 138–146.
98. Panov M.S. et al. Talanta Non-enzymatic sensors based on in situ laser-induced synthesis of copper- gold and gold nano-sized microstructures // Talanta. 2017. Vol. 167. P. 201–207.
99. Mizoshiri M. et al. Direct writing of Cu-based micro-temperature detectors using femtosecond laser reduction of CuO nanoparticles // Appl. Phys. Express. 2016. Vol. 9. P. 036701.
100. Binh Nam V., Lee D. Highly transparent and low-voltage-driven soft actuators fabricated by laser digital patterning // Opt. Laser Technol. 2024. Vol. 168. P. 109853.
101. Kang B. et al. One-step fabrication of copper electrode by laser-induced direct local reduction and agglomeration of copper oxide nanoparticle // J. Phys. Chem. C. 2011. Vol. 115, № 48. P. 23664–23670.
102. Lee D. et al. Vacuum-free, maskless patterning of Ni electrodes by laser reductive sintering of Nio nanoparticle ink and its application to transparent conductors // ACS Nano. 2014. Vol. 8, № 10. P. 9807–9814.
103. Shin J. et al. Sensitive Wearable Temperature Sensor with Seamless Monolithic Integration // Adv. Mater. 2020. Vol. 32, № 2. P. 1905527.
104. Mizoshiri M. et al. Direct fabrication of Cu/Cu2O composite micro-temperature sensor using femtosecond laser reduction patterning // Jpn. J. Appl. Phys. 2016. Vol. 55. P. 06GP05.
105. Kefer S. et al. Tunable Bulk Polymer Planar Bragg Gratings Electrified via Femtosecond Laser Reductive Sintering of CuO Nanoparticles // Adv. Opt. Mater. 2021. Vol. 9. P. 2002203.
106. Roth G.L. et al. Fs-laser based hybrid micromachining for polymer micro-opto electrical systems // Opt. Lasers Eng. Elsevier Ltd, 2021. Vol. 137. P. 106362 Contents.
107. Lee H. et al. Enzyme-Based Glucose Sensor: From Invasive to Wearable Device // Adv. Healthc. Mater. 2018. Vol. 7, № 8. P. 1–14.

108. Guati C. et al. Progress on the influence of non-enzymatic electrodes characteristics on the response to glucose detection: A review (2016-2022) // Rev. Chem. Eng. 2024. Vol. 40, № 1. P. 123–148.
109. Dong Q., Ryu H., Lei Y. Metal oxide based non-enzymatic electrochemical sensors for glucose detection // Electrochim. Acta. 2021. Vol. 370. P. 137744.
110. He J. et al. Recent advances in perovskite oxides for non-enzymatic electrochemical sensors: A review // Analytica Chimica Acta. 2023. Vol. 1251. P. 341007.
111. Hassan M.H. et al. Recent advances in enzymatic and non-enzymatic electrochemical glucose sensing // Sensors. 2021. Vol. 21. P. 4672.
112. Thatikayala D. et al. Progress of Advanced Nanomaterials in the Non-Enzymatic Electrochemical Sensing of Glucose and H2O2 // Biosensors. 2020. Vol. 10. P. 151.
113. Gurusamy L. et al. Review of oxygen-vacancies nanomaterials for non-enzymatic electrochemical sensors application // Coordination Chemistry Reviews. 2023. Vol. 484. P. 215102.
114. Govindaraj M. et al. Current advancements and prospects of enzymatic and non-enzymatic electrochemical glucose sensors // Int. J. Biol. Macromol. 2023. Vol. 253. P. 126680.
115. H N.L.B. et al. Kinetic study of the mutarotation of D-glucose in concentrated aqueous solution by gas-liquid chromatography // Food Chem. 2001. Vol. 74. P. 119–124.
116. Largeaud F. et al. On the electrochemical reactivity of anomers: electrocatalytic oxidation of α- and β-D-glucose on platinum electrodes in acid and basic media // J. Electroanal. Chem. 1995. Vol. 397. P. 261–269.
117. Hwang D.W. et al. Recent advances in electrochemical non-enzymatic glucose sensors – A review // Anal. Chim. Acta. 2018. Vol. 1033. P. 1–34.
118. Khairullina E.M. et al. High rate fabrication of copper and copper–gold electrodes by laser-induced selective electroless plating for enzyme-free glucose sensing // RSC Adv. 2021. Vol. 11. P. 19521–19530.
119. Toghill K.E., Compton R.G. Electrochemical Non-enzymatic Glucose Sensors : A Perspective and an Evaluation // Int. J. Electrochem. Sci. 2010. Vol. 5. P. 1246–1301.
120. Zhou C. et al. Non-enzymatic electrochemical sensors based on nanomaterials for detection of organophosphorus pesticide residues // Environ. Sci. Adv. 2023. Vol. 2. P. 933–956.
121. Park S. et al. Structural and electrochemical features of 3D nanoporous platinum electrodes // Electrochim. Acta. 2010. Vol. 55, № 6. P. 2029–2035.
122. Park S., Chung T.D., Kim H.C. Nonenzymatic Glucose Detection Using Mesoporous Platinum // Anal. Chem. 2003. Vol. 75, № 13. P. 3046–3049.
123. Han J. et al. Effect of Nanoporous Structure on Enhanced Electrochemical Reaction // J. Phys.

Chem. C. 2010. Vol. 114, № 21. P. 9546–9553.

124. Luo Y. et al. Technology Roadmap for Flexible Sensors // ACS Nano. 2023. Vol. 17, № 6. P. 5211–5295.
125. Pathiraja G., Bonner C.D.J., Obare S.O. Recent Advances of Enzyme-Free Electrochemical Sensors for Flexible Electronics in the Detection of Organophosphorus Compounds: A Review // Sensors. 2023. Vol. 23. P. 1226.
126. Zhao Y. et al. Flexible and Stretchable Electrochemical Sensors for Biological Monitoring // Adv. Mater. 2023. P. 2305917.
127. Kazanskiy N.L., Khonina S.N., Butt M.A. A review on flexible wearables-Recent developments in non-invasive continuous health monitoring // Sensors Actuators A Phys. 2024. Vol. 366. P. 114993.
128. Tian H. et al. Electrochemical sensing fibers for wearable health monitoring devices //Biosensors and Bioelectronics. 2023. P. 115890.
129. Cli A. et al. Strategies for Biomolecular Analysis and Continuous Physiological Monitoring // J. Am. Chem. Soc. 2021. Vol. 143. P. 5281−5294.
130. Jin H., Abu-raya Y.S., Haick H. Advanced Materials for Health Monitoring with Skin-Based Wearable Devices // Adv. Healthc. Mater Healthc. Mater. 2017. Vol. 6, № 11. P. 1700024.
131. Huynh T., Haick H. Autonomous Flexible Sensors for Health Monitoring // Adv Mater. 2018. Vol. 30, № 50. P. 1802337.
132. Zheng X. et al. Smart biosensors and intelligent devices for salivary biomarker detection // Trends Anal. Chem. 2021. Vol. 140. P. 116281.
133. Yang C. et al. Wearable and Implantable Intraocular Pressure Biosensors : Recent Progress and Future Prospects // Adv. Sci. 2021. Vol. 8. P. 2002971.
134. Koralli P., Mouzakis D.E. Advances in Wearable Chemosensors // Chemosensors. 2021. Vol. 9, № 99. P. 1–21.
135. Manmana Y., Kubo T., Otsuka K. Recent developments of point-of-care (POC) testing platform for biomolecules // Trends Anal. Chem. 2021. Vol. 135. P. 116160.
136. Bian S. et al. Towards wearable and implantable continuous drug monitoring : A review // J. Pharm. Anal. 2021. Vol. 11, № 1. P. 1–14.
137. Yao Y. et al. Integration of interstitial fluid extraction and glucose detection in one device for wearable non-invasive blood glucose sensors // Biosens. Bioelectron. 2021. Vol. 179. P. 113078.
138. Zhou X. et al. Flexible Nonenzymatic Glucose Sensing with One-Step Laser-Fabricated Cu2O/Cu Porous Structure // Adv. Engeneering Mater. 2021. P. 2100192.
139. Glasscott M.W. et al. Electrochemical sensors for the detection of fentanyl and its analogs : Foundations and recent advances // Trends Anal. Chem. 2020. Vol. 132. P. 116037.

140. Liu Y., Pharr M., Salvatore G.A. Lab-on-Skin: A Review of Flexible and Stretchable Electronics for Wearable Health Monitoring // ACS Nano. 2017. Vol. 11. P. 9614–9635.
141. Behrent A. et al. Process-property correlations in laser-induced graphene electrodes for electrochemical sensing // Microchim. Acta. 2021. Vol. 188. P. 159.
142. Vernerová A. et al. Non-invasive determination of uric acid in human saliva in the diagnosis of serious disorders // Clin. Chem. Lab. Med. 2021. Vol. 59, № 5. P. 797–812.
143. Jarnda K. V. et al. Recent advances in electrochemical non-enzymatic glucose sensor for the detection of glucose in tears and saliva: A Review //Sensors and Actuators A: Physical. 2023. Vol. 363. P. 114778.
144. Liu T. et al. Recent Advancements in Physiological, Biochemical, and Multimodal Sensors Based on Flexible Substrates: Strategies, Technologies, and Integrations // ACS Appl. Mater. Interfaces. 2023. Vol. 15, № 18. P. 21721–21745.
145. Shin H. et al. Recent progress on wearable point-of-care devices for ocular systems // Lab Chip. 2021. Vol. 21. P. 1269–1286.
146. Zhou F. et al. Flexible electrochemical sensor with Fe/Co bimetallic oxides for sensitive analysis of glucose in human tears // Anal. Chim. Acta. 2023. Vol. 1243. P. 340781.
147. Kim J. et al. Simultaneous Monitoring of Sweat and Interstitial Fluid Using a Single Wearable Biosensor Platform // Adv. Sci. 2018. Vol. 5. P. 1800880.
148. Campbell A.S., Kim J., Wang J. Wearable electrochemical alcohol biosensors // Curr. Opin. Electrochem. 2018. Vol. 10. P. 126–135.
149. Kim J. et al. Wearable biosensors for healthcare monitoring // Nat. Biotechnol. 2019. Vol. 37. P. 389–406.
150. Kim T. et al. A 3D Printed Wearable Bioelectronic Patch for Multi-Sensing and In Situ Sweat Electrolyte Monitoring // Adv. Mater. Technol. 2021. Vol. 6. P. 2001021.
151. Xu L. et al. Advances in wearable flexible electrochemical sensors for sweat monitoring: A mini-review // Int. J. Electrochem. Sci. 2023. Vol. 18. P. 13–19.
152. Gao F. et al. Wearable and flexible electrochemical sensors for sweat analysis: a review // Microsystems Nanoeng. 2023. Vol. 9, № 1. P. 1–21.
153. Lv M. et al. A stretchable wearable sensor with dual working electrodes for reliable detection of uric acid in sweat //Analytica Chimica Acta. 2024. Vol. 1287. P. 342154.
154. Yoon H. et al. A chemically modified laser-induced porous graphene based flexible and ultrasensitive electrochemical biosensor for sweat glucose detection // Sensors Actuators B. Chem. 2020. Vol. 311. P. 127866.
155. Karuppaiah G. et al. Electrochemical sensors for cortisol detection: Principles, designs, fabrication, and characterisation // Biosensors and Bioelectronics. 2023. Vol. 239. P. 115600.

156. Sharma A. et al. Ultrasensitive electrochemical sensor for detection of salivary cortisol in stress conditions // Microchim. Acta. 2024. Vol. 191. P. 103.
157. Hong Y.J. et al. Multifunctional Wearable System that Integrates Sweat-Based Sensing and Vital-Sign Monitoring to Estimate Pre-/Post-Exercise Glucose Levels // Adv. Funct. Mater. 2018. Vol. 28, № 47. P. 1805754.
158. Zanfrognini B., Pigani L., Zanardi C. Recent advances in the direct electrochemical detection of drugs of abuse // J. Solid State Electrochem. 2020. Vol. 24. P. 2603–2616.
159. Tai L. et al. Methylxanthine Drug Monitoring with Wearable Sweat Sensors // Adv. Mater. 2018. Vol. 30, № 23. P. 1707442.
160. Mishra R.K. et al. Wearable Flexible and Stretchable Glove Biosensor for On-Site Detection of Organophosphorus Chemical Threats // ACS Sensors. 2017. Vol. 2. P. 553–561.
161. Windmiller J.R. et al. Electrochemical sensing based on printable temporary transfer tattoos // Chem. Commun. 2012. Vol. 48. P. 6794–6796.
162. Bariya M. et al. Roll-to-Roll Gravure Printed Electrochemical Sensors for Wearable and Medical Devices // ACS Nano. 2018. Vol. 12, № 7. P. 6978–6987.
163. Qin Y. et al. Inkjet Printing of a Highly Loaded Palladium Ink for Integrated, Low-Cost pH Sensors // Adv. Funct. Mater. 2016. Vol. 26, № 27. P. 4923–493.
164. Park H. et al. Laser-Based Selective Material Processing for Next-Generation Additive Manufacturing //Advanced Materials. 2023. P. 2307586. 2023.
165. Zhang T. et al. Highly Sensitive Wearable Sensor Based on (001)-Orientated TiO2 for Real-Time Electrochemical Detection of Dopamine, Tyrosine, and Paracetamol //Small. 2024. P. 2312238.
166. Cano-Raya C. et al. Chemistry of solid metal-based inks and pastes for printed electronics – A review // Appl. Mater. Today. 2019. Vol. 15. P. 416–430.
167. Lin Y.M., Yen S.C. Effects of additives and chelating agents on electroless copper plating // Appl. Surf. Sci. 2001. Vol. 178, № 1–4. P. 116–126.
168. Muench F. et al. Template-Free Electroless Plating of Gold Nanowires: Direct Surface Functionalization with Shape-Selective Nanostructures for Electrochemical Applications // ACS Appl. Mater. Interfaces. 2017. Vol. 9, № 36. P. 31142–31152.
169. Stepniowski W.J. et al. Morphology and photoluminescence of nanostructured oxides grown by copper passivation in aqueous potassium hydroxide solution // Mater. Lett. 2017. Vol. 198. P. 89–92.
170. Khairullina E.M. et al. Laser-Assisted Surface Modification of Ni Microstructures with Au and Pt toward Cell Biocompatibility and High Enzyme-Free Glucose Sensing // ACS Omega. 2021. Vol. 6, № 28. P. 18099–18109.
171. Tumkin I.I. et al. Copper and nickel microsensors produced by selective laser reductive sintering

for non-enzymatic glucose detection // Materials (Basel). 2021. Vol. 14, № 10. P. 1–11.

172. Khairullina E. et al. An aligned octahedral core in a nanocage: synthesis, plasmonic, and catalytic properties // Nanoscale. 2019. Vol. 11. P. 3138–3144.
173. Stupin D.D. et al. Adaptive Filtering to Enhance Noise Immunity of Impedance and Admittance Spectroscopy: Comparison with Fourier Transformation // Phys. Rev. Appl. 2017. Vol. 7, № 5. P. 1–11.
174. Bai S. et al. Laser-assisted reduction of highly conductive circuits based on copper nitrate for flexible printed sensors // Nano-Micro Lett. 2017. Vol. 9, № 42. P. 1–13.
175. Вейко В.П., Киеу К.К., Яковлев Е.Б. Лазерная аморфизация стеклокерамик: основные закономерности и новые возможности изготовления микрооптических элементов // Квантовая электроника. 2007. Vol. 37, № 1. P. 9298.
176. Mizoshiri M. et al. Effect of Substrates on Femtosecond Laser Pulse-Induced Reductive Sintering of Cobalt Oxide Nanoparticles // Nanomaterials. 2021. Vol. 11, № 3356. P. 1–12.
177. Dean J.A. Lange's Handbook Of Chemistry, 15th ed. // McGraw-Hill: New York. 1999. 1466 p.
178. Eslami M. et al. Study on tribological behavior of electrodeposited Cu-Si3N4 composite coatings // Mater. Des. 2014. Vol. 58. P. 557–569.
179. Wang H. et al. Synergistic enhancement of electrocatalytic CO2 reduction to C2 oxygenates at nitrogen-doped nanodiamonds/Cu interface // Nat. Nanotechnol. 2020. Vol. 15, № 2. P. 131–137.
180. Zhu H. et al. Advances in non-enzymatic glucose sensors based on metal oxides // J. Mater. Chem. B. 2016. Vol. 4. P. 7333.
181. Ngamaroonchote A. et al. Highly branched gold – copper nanostructures for non-enzymatic specific detection of glucose and hydrogen peroxide // Microchim. Acta. 2020. Vol. 187. P. 559.
182. Wang N. et al. Detection of H2O2 at the Nanomolar Level by Electrode Modified with Ultrathin AuCu Nanowires // Anal. Chem. 2015. Vol. 87. P. 457−463.
183. Huang S. et al. Electrochemical sensor for nitrite using a glassy carbon electrode modified with gold-copper nanochain networks // Microchim Acta. 2016. Vol. 183. P. 791–797.
184. Radnik J., Mohr C., Claus P. On the origin of binding energy shifts of core levels of supported gold nanoparticles and dependence of pretreatment and material synthesis // Phys. Chem. Chem. Phys. 2003. Vol. 5. P. 172–177.
185. Shen L., Zhou X., Wang A. Hydrothermal conversion of high-concentrated glycerol to lactic acid catalyzed by bimetallic CuAux (x =0.01-0.04) nanoparticles and their reaction kinetics // RSC Adv. 2017. Vol. 7. P. 30725–30739.
186. Torres-Ochoa J.A. et al. Peak-fitting of Cu 2p photoemission spectra in Cu0, Cu1+, and Cu2+ oxides: A method for discriminating Cu0 from Cu1+ // Appl. Surf. Sci. 2023. Vol. 622. P. 156960.
187. Khalakhan I. et al. On the interpretation of X-ray photoelectron spectra of Pt-Cu bimetallic alloys

// J. Electron Spectros. Relat. Phenomena. 2021. Vol. 246. P. 147027.

188. Tang A. et al. One-pot synthesis and self-assembly of colloidal copper(I) sulfide nanocrystals // Nanotechnology. 2010. Vol. 21. P. 285602.
189. Gizinski D. et al. Nanostructured Anodic Copper Oxides as Catalysts in Electrochemical and Photoelectrochemical Reactions // Catalysts. 2020. Vol. 10. P. 1338.
190. Stepniowski W.J., Misiolek W.Z. Review of Fabrication Methods , Physical Properties , and Applications of Nanostructured Copper Oxides Formed via Electrochemical Oxidation // Nanomaterials. 2018. Vol. 8. P. 379.
191. Stępniowski W.J. et al. Investigation of oxide nanowires growth on copper via passivation in NaOH aqueous solution // Surfaces and Interfaces. 2019. Vol. 14. P. 15–18.
192. Filipic G., Cvelbar U. Copper oxide nanowires: a review of growth // Nanotechnology. 2012. Vol. 23. P. 194001.
193. Ha T., Tuyen V. Phase transition of Cu2O to CuO nanocrystals by selective laser heating // Mater. Sci. Semicond. Process. 2016. Vol. 46. P. 6–9.
194. Chen L. et al. Design of Cu2O-Au composite microstructures for surface-enhanced Raman scattering study // Colloids Surfaces A Physicochem. Eng. Asp. 2016. Vol. 507. P. 96–102.
195. Mao Y. et al. Electrochemical synthesis of hierarchical Cu2O stars with enhanced photoelectrochemical properties // Electrochim. Acta. 2012. Vol. 62. P. 1–7.
196. Xu J.F. et al. Raman Spectra of CuO Nanocrystals // J. Raman Spectrosc. 1999. Vol. 30. P. 413–415.
197. Xu J.F. et al. Preparation and Characterization of CuO Nanocrystals // J. Solid State Chem. 1999. Vol. 147. P. 516–519.
198. Kang M., Gewirth A.A. Voltammetric and force spectroscopic examination of oxide formation on Cu(111) in basic solution // J. Phys. Chem. B. 2002. Vol. 106, № 47. P. 12211–12220.
199. Bogdanowicz R. et al. Ellipsometric study of oxide formation on Cu electrode in 0.1 M NaOH // J. Solid State Electrochem. 2009. Vol. 13, № 11. P. 1639–1644.
200. Gong Q. et al. Enhanced non-enzymatic glucose sensing of Cu – BTC- derived porous copper@carbon agglomerate // J. Mater. Sci. 2018. Vol. 53, № 10. P. 7305–7315.
201. Zhao J. et al. Electro-oxidation of glucose at self-assembled monolayers incorporated by copper particles // Talanta. 2006. Vol. 70. P. 449–454.
202. Giorgio M. et al. Hydrogen peroxide: A metabolic by-product or a common mediator of ageing signals? // Nat. Rev. Mol. Cell Biol. 2007. Vol. 8, № 9. P. 722–728.
203. Dhara K., Mahapatra D.R. Recent advances in electrochemical nonenzymatic hydrogen peroxide sensors based on nanomaterials: a review // J. Mater. Sci. 2019. Vol. 54. P. 12319–12357.
204. Sophia J., Muralidharan G. Amperometric sensing of hydrogen peroxide using glassy carbon

electrode modified with copper nanoparticles // Mater. Res. Bull. 2015. Vol. 70. P. 315–320.

205. Somasundrum M., Kirtikara K., Tanticharoen M. Amperometric determination of hydrogen peroxide by direct and catalytic reduction at a copper electrode // Anal. Chim. Acta. 1996. Vol. 319, № 1–2. P. 59–70.
206. Ensafi A.A., Abarghoui M.M., Rezaei B. Electrochemical determination of hydrogen peroxide using copper/porous silicon based non-enzymatic sensor // Sensors Actuators, B Chem. 2014. Vol. 196. P. 398–405.
207. Qian T. et al. Ultrasensitive dopamine sensor based on novel molecularly imprinted polypyrrole coated carbon nanotubes // Biosens. Bioelectron. 2014. Vol. 58. P. 237–241.
208. Kohila rani K. et al. Simple preparation of gold nanoparticle-decorated copper cross-linked pectin for the sensitive determination of hydrogen peroxide // Ionics (Kiel). 2019. Vol. 25. P. 309–317.
209. Alencar L.M. et al. Chemical One-step synthesis of crumpled graphene fully decorated by copper-based nanoparticles: Application in H2O2 sensing // Sensors Actuators B. Chem. 2022. Vol. 360. P. 131649.
210. Xu L. et al. Copper and molybdenum dioxide co - doped octahedral porous carbon framework for high sensitivity electrochemical detection of hydrogen peroxide // Ionics (Kiel). 2022. Vol. 28. P. 919–925.
211. Li W. et al. High catalytic performance non-enzymatic H2O2 sensor based on Cu2O@Cu9S5 yolk-shell nanospheres // Appl. Surf. Sci. 2022. Vol. 587. P. 152766.
212. Li D. et al. Hydrogen peroxide sensing using Cu2O nanocubes decorated by AgAu alloy nanoparticles // J. Alloys Compd. 2017. Vol. 690. P. 1–7.
213. Paramparambath S. et al. Nonenzymatic Electrochemical Sensor Based on CuO-MgO Composite for Dopamine Detection // IEEE Sens. J. 2021. Vol. 21, № 22. P. 25597–25605.
214. Zou J. et al. An ultra-sensitive electrochemical sensor based on 2D g-C3N4/CuO nanocomposites for dopamine detection // Carbon N. Y. 2018. Vol. 130. P. 652–663.
215. Amara U. et al. Copper oxide integrated perylene diimide selfassembled graphitic pencil for robust nonenzymatic dopamine detection // RSC Adv. 2021. Vol. 11. P. 25084–25095.
216. Huang Y. et al. Synthesis of CuO/g-C3N4 composites, and their application to voltammetric sensing of glucose and dopamine // Microchim. Acta. 2019. Vol. 186. P. 10.
217. Sundar S., Venkatachalam G. Biosynthesis of Copper Oxide (CuO) Nanowires and Their Use for the Electrochemical Sensing of Dopamine // Nanomaterials. 2018. Vol. 8. P. 823.
218. Khairullina E.M. et al. Laser-assisted surface activation for fabrication of flexible non-enzymatic Cu-based sensors // Microchim. Acta. Springer Vienna, 2022. Vol. 189, № 7.
219. Saraf S., Singh A., Desai B.G. Estimation of Porosity and Pore size distribution from Scanning Electron Microscope image data of Shale samples: A case study on Jhuran formation of Kachchh

Basin, India. // Explor. Geophys. 2019. Vol. 2019, № 1. P. 10–13.

220. Jiang H. et al. Nanoscale Laser Metallurgy and Patterning in Air Using MOFs // J. Am. Chem. Soc. 2019. Vol. 141, № 13. P. 5481–5489.
221. Tang Y.J. et al. Laser-Induced Annealing of Metal–Organic Frameworks on Conductive Substrates for Electrochemical Water Splitting // Adv. Funct. Mater. 2021. Vol. 31, № 31. P. 2102648.
222. Guo S. et al. Recent Advances in Laser-Induced Synthesis of MOF Derivatives // Adv. Mater. 2023.
223. Маньшина, А. А. Лазерно-индуцированный синтез металлических и гибридных металл/углеродных наноматериалов : дис. д. х. н.: 02.00.11 / Маньшина Алина Анвяровна. - М., 2016. - 335 с. 2016.
224. Kerner Z., Pajkossy T. On the origin of capacitance dispersion of rough electrodes // Electrochim. Acta. 2000. Vol. 46. P. 207–211.
225. Pajkossy T. Impedance of rough capacitive electrodes // J. Electroanal. Chem. 1994. Vol. 364, № 1–2.
226. Hashimoto M. et al. Matrix metalloproteases inhibition and biocompatibility of gold and platinum nanoparticles // J. Biomed. Mater. Res. - Part A. 2016. Vol. 104, № 1. P. 209–217.
227. Yang Y. et al. Catalytic Modification of Porous Two-Dimensional Ni-MOFs on Portable Electrochemical Paper-Based Sensors for Glucose and Hydrogen Peroxide Detection // Biosensors. 2023. Vol. 13, № 508. P. 1–1.
228. Zhang C. et al. Hierarchical porous Ni/NiO core-shells with superior conductivity for electrochemical pseudo-capacitors and glucose sensors // J. Mater. Chem. A. 2015. Vol. 3. P. 10519–10525.
229. El Khatib K.M., Abdel Hameed R.M. Development of Cu2O/Carbon Vulcan XC-72 as non-enzymatic sensor for glucose determination // Biosens. Bioelectron. 2011. Vol. 26. P. 3542–3548.
230. Zhou J. et al. Electrodeposition of bimetallic NiAu alloy dendrites on carbon papers as highly sensitive disposable non-enzymatic glucose sensors // Mater. Lett. 2020. Vol. 273. P. 127912.
231. Jin C., Taniguchi I. Electrocatalytic Oxidation of Glucose on Gold Nanocomposite Electrodes. 2020. Vol. 2020, № 9. P. 1298–1301.
232. Dolinska J. et al. Glucose Electrooxidation in Bimetallic Suspensions of Nanoparticles in Alkaline Media // ChemElectroChem. 2015. Vol. 2, № 8. P. 1199–1205.
233. Xu Y., Zhang B. Recent advances in porous Pt-based nanostructures: Synthesis and electrochemical applications // Chemical Society Reviews. 2014. Vol. 43, № 8. P. 2439–2450.
234. Lu L.M. et al. A nano-Ni based ultrasensitive nonenzymatic electrochemical sensor for glucose: Enhancing sensitivity through a nanowire array strategy // Biosens. Bioelectron. 2009. Vol. 25,

№ 1. P. 218–223.

235. Nie H. et al. Nonenzymatic electrochemical detection of glucose using well-distributed nickel nanoparticles on straight multi-walled carbon nanotubes // Biosens. Bioelectron. 2011. Vol. 30, № 1. P. 28–34.
236. Wang L. et al. A green and simple strategy to prepare graphene foam-like three-dimensional porous carbon/Ni nanoparticles for glucose sensing // Sensors Actuators, B Chem. 2017. Vol. 239. P. 172–179.
237. Qin L. et al. Synthesis of Ni/Au multilayer nanowire arrays for ultrasensitive non-enzymatic sensing of glucose // Sensors Actuators, B Chem. 2017. Vol. 240. P. 779–784.
238. Wang L. et al. One-step electrodeposition of AuNi nanodendrite arrays as photoelectrochemical biosensors for glucose and hydrogen peroxide detection // Biosens. Bioelectron. 2019. Vol. 142, № 1. P. 111577.
239. Sheng Q. et al. PtxNi/C nanostructured composites fabricated by chemical reduction and their application in non-enzymatic glucose sensors // Sensors Actuators, B Chem. 2014. Vol. 203. P. 588–595.
240. Zhao Y. et al. Nonenzymatic detection of glucose using three-dimensional PtNi nanoclusters electrodeposited on the multiwalled carbon nanotubes // Sensors Actuators, B Chem. 2016. Vol. 231. P. 800–810.
241. Gao H. et al. One-step electrochemical synthesis of PtNi nanoparticle-graphene nanocomposites for nonenzymatic amperometric glucose detection // ACS Appl. Mater. Interfaces. 2011. Vol. 3, № 8. P. 3049–3057.
242. Huang Y. et al. Copper circuits fabricated on flexible polymer substrates by a high repetition rate femtosecond laser-induced selective local reduction of copper oxide nanoparticles // Opt. Express. 2021. Vol. 29, № 3. P. 4453.
243. Xiao J., Qi L. Surfactant-assisted, shape-controlled synthesis of gold nanocrystals // Nanoscale. 2011. Vol. 3, № 4. P. 1383–1396.
244. McEachran M. et al. Ultrathin gold nanoframes through surfactant-free templating of faceted pentagonal silver nanoparticles // J. Am. Chem. Soc. 2011. Vol. 133, № 21. P. 8066–8069.
245. Skrabalak S.E. et al. Gold Nanocages: Synthesis, Properties, and Applications. 2008. Vol. 41, № 12. P. 1587–1595.
246. Liu M. et al. Enhanced electrocatalytic CO2 reduction via field-induced reagent concentration // Nature. Nature Publishing Group, 2016. Vol. 537, № 7620. P. 382–386.
247. Klinkova A. et al. Large-Scale Synthesis of Metal Nanocrystals in Aqueous Suspensions // Chem. Mater. 2016. Vol. 28, № 9. P. 3196–3202.
248. Skrabalak S.E. et al. Facile synthesis of Ag nanocubes and Au nanocages // Nat. Protoc. 2007.

Vol. 2, № 9. P. 2182–2190.

249. Tao A.R., Habas S., Yang P. Shape control of colloidal metal nanocrystals // Small. 2008. Vol. 4, № 3. P. 310–325.
250. Lu F. et al. Discrete nanocubes as plasmonic reporters of molecular chirality // Nano Lett. 2013. Vol. 13, № 7. P. 3145–3151.
251. Fan F.R. et al. Epitaxial growth of heterogeneous metal nanocrystals: From gold nano-octahedra to palladium and silver nanocubes // J. Am. Chem. Soc. 2008. Vol. 130, № 22. P. 6949–6951.
252. Al. M.Y. et. Au@Ag Core□Shell Nanocubes with Finely Tuned and Well-Controlled Sizes, Shell Thicknesses, and Optical Properties // ACS Nano. 2010. Vol. 4, № 11. P. 6725–6734.
253. Kale M.J., Avanesian T., Christopher P. Direct photocatalysis by plasmonic nanostructures // ACS Catal. 2014. Vol. 4, № 1. P. 116–128.
254. Özbek M.A. et al. A novel biosensor based on graphene/platinum nanoparticles/Nafion composites for determination of glucose // J. Solid State Electrochem. 2021. Vol. 25, № 5. P. 1601–1610.
255. Liu C.T. et al. A salivary glucose biosensor based on immobilization of glucose oxidase in Nafion-carbon nanotubes nanocomposites modified on screen printed electrode // Microchem. J. 2023. Vol. 191. P. 108872.
256. Chen D. et al. PVDF-Nafion nanomembranes coated microneedles for in vivo transcutaneous implantable glucose sensing // Biosens. Bioelectron. 2015. Vol. 74. P. 1047–1052.
257. Heitner-Wirguin C. Recent advances in perfluorinated ionomer membranes: Structure, properties and applications // J. Memb. Sci. 1996. Vol. 120, № 1. P. 1–33.
258. Zhao F. et al. Research on laser-assisted selective metallization of a 3D printed ceramic surface // RSC Adv. 2020. Vol. 10. P. 44015–44024.
259. Assaf Y., Kietzig A.M. Optical and chemical effects governing femtosecond laser-induced structure formation on polymer surfaces // Mater. Today Commun. 2018. Vol. 14, № January. P. 169–179.
260. Sacher E., Kowalczyk S.P. Metallization of Polymers // American Chemical Society at the International Symposium on the Metallization of Polymers. 1990. 1–531 p.
261. Rebollar E. et al. Physicochemical modifications accompanying UV laser induced surface structures on poly(ethylene terephthalate) and their effect on adhesion of mesenchymal cells // Phys. Chem. Chem. Phys. 2014. Vol. 16, № 33. P. 17551–17559.
262. Ouhlal A. et al. Chemical bonding of copper and chromium at the carbonyl group of acetone // Chem. Phys. Lett. 1993. Vol. 202, № 1–2. P. 51–56.
263. Ouhlal A., Selmani A., Yelon A. Copper/polyimide interaction: A local spin density study // J. Adhes. Sci. Technol. 1995. Vol. 9, № 7. P. 971–982.